ASSESSING THE EFFECTS OF BIAXIAL STRAIN AND CHEMICAL DOPING ON THE MAGNETIC AND ELECTRONIC PROPERTIES OF EPITAXIAL EUROPIUM MONOXIDE FILMS

A Dissertation

Presented to the Faculty of the Graduate School

of Cornell University

In Partial Fulfillment of the Requirements for the Degree of

Doctor of Philosophy

by

Alexander James Melville

January 2014

ASSESSING THE EFFECTS OF BIAXIAL STRAIN AND CHEMICAL DOPING ON THE MAGNETIC AND ELECTRONIC PROPERTIES OF EPITAXIAL EUROPIUM MONOXIDE FILMS

Alexander James Melville, Ph. D.

Cornell University 2014

The ferromagnetic semiconductor EuO, which possesses several record properties relevant to devices, has been researched in an attempt to enhance and understand this novel material, i.e., raising its Curie temperature (T_C) and developing it as a viable electronic material, by investigating three distinct research directions for EuO: chemical doping via trivalent rare-earth cations, biaxial strain via substrates with varying degrees of lattice mismatch, and preservation via application of a well-chosen capping layer.

The use of Lu^{3+} as a chemical dopant for enhancing the T_C of EuO up to 119 K was established. The spin-polarization for the Lu-doped EuO thin film was measured to be 96%, confirming its near-complete spin-polarization.

The effect of biaxial strain on T_C for EuO thin films that are commensurately strained to the substrate was explored. The use $LuAlO_3$, which imparts an asymmetric tensile strain of +0.4% strain and +1.5% strain along the [110] and [$1\bar{1}0$] EuO directions, respectively, resulted in the reduction of the T_C for commensurate EuO / $LuAlO_3$ thin films of varying thicknesses. The strain-dependence was confirmed by comparing the series to an identical series grown on the lattice-matched, i.e., unstrained, substrate yttria-stabilized

zirconia (YSZ).

Biaxial compressive strain was explored by growing EuO thin films on both single-crystal diamonds and epitaxial diamond thin films grown on silicon. Diamond is 2.2% smaller than EuO, so epitaxial integration of EuO on diamond was attempted in hopes of achieving symmetric 2.2% compressive strain. Though the EuO was epitaxial and free of extraneous phases and orientations, demonstrating the first instance of a ferromagnet epitaxially integrated with diamond, the EuO was not compressively strained, and no change in T_C was observed.

Finally, the formation of a protective Eu_2O_3 capping layer by controlled oxidation of the surface of EuO in vacuum was studied. The Eu_2O_3 was effective at preventing the degradation of the underlying EuO, as determined by the scanning tunneling electron microscopy and electron energy loss spectroscopy analysis. The analysis, in conjunction with X-ray diffraction experiments, demonstrated that the oxygen diffusion during the capping layer formation is heavily influenced by the presence of defects in the film.

BIOGRAPHICAL SKETCH

Alexander James Melville was born on March 12, 1986 in Mannheim, Germany to his parents, John Graham Melville and Manuela Melville. Moving several times during his childhood with his parents and younger sister, Vanessa Maria Melville, his family finally settled in Mechanicsburg, Pennsylvania. There, Alexander learned of his interest and aptitude for math and science in high school and chose to pursue a career in engineering. After vacillating between aerospace engineering (like his father) and materials engineering, Alexander settled on what he deemed the more “fundamental” program of materials engineering.

Alexander received his Bachelor’s degree in Materials Science & Engineering from the University of Michigan in 2007. After graduation, he began his graduate education at the Pennsylvania State University, choosing to continue studying Materials Science in the laboratory of Professor Darrell Schlom. In 2009, the lab changed affiliation to Cornell University following Professor Schlom’s acceptance of a faculty position there. During this time, Alexander re-ignited his high school relationship with Katherine Margaret Povirk and married her on November 6, 2010. She joined him at Cornell University in the Ph.D. program for Biomedical Engineering. Alexander earned his Master of Science in Materials Science & Engineering in 2011, and became a father in 2012 to Evelyn Rose Melville. While caring for his daughter, Alexander completed his research experiments and defended his dissertation work in 2013 to earn his Ph.D. in Materials Science & Engineering. Following his graduation, Alexander began working at L’Oreal USA as a Senior Scientist in their Research & Innovation Division.

“I see the holiness in the patience of the people of God: a woman who is raising children, a man who works to bring home the bread, the sick, the elderly priests who have so many wounds but have a smile on their faces because they served the Lord, the sisters who work hard and live a hidden sanctity. This is for me the common sanctity. I often associate sanctity with patience: not only patience as hypomoné, taking charge of the events and circumstances of life, but also as a constancy in going forward, day by day…This was the sanctity of my parents: my dad, my mom, my grandmother…who loved me so much.”

-- Pope Francis, August 2013 --

ACKNOWLEDGEMENTS

First of all, I'd like to express my sincerest gratitude for my advisor, Professor Darrell Schlom, for all of his advice and support during my research toward my Ph.D. degree. He gave me the opportunity to work with world-class equipment and pioneer cutting-edge research in oxide thin films. More importantly, he helped me understand the importance of focusing on a project, and that paying attention to every detail improves a product more than the sum of these details.

I also would like to thank Professors Robert B. van Dover and Kyle Shen for serving on my special committee. Their advice and direction helped shape the purpose of my dissertation.

Many other distinguished scientists deserve my thanks in building my dissertation. Notably, I'd like to thank Drs. Andreas Schmehl and Thomas Mairoser from the University of Augsburg, Dr. Jürgen Schubert from the Peter Grünberg Institute in Jülich, Germany, and Professor Jochen Mannhart from the Max Planck Institute of Stuttgart. Through collaboration with these distinguished gentlemen, we've explored many thought-experiments in several aspects of semiconductor physics. I also want to thank Professor David Awschalom, Professor Craig Fennie, Professor Stanislav Kamba, Professor David Muller, and Professor Xiaoqing Pan for their collaborations.

Of course, more thanks are due to my fellow group members. Foremost among them, Drs. Carolina Adamo and Tassilo Heeg have probably done more toward helping me obtain my Ph.D. than anyone else. They tirelessly answered my incessant (and repetitive) questions, helped me shape my experiments and papers, and made working in the lab much more fun than it had any right to be. And to Dr. Che-Hui Lee, my partner in crime, we got through it together – I couldn't do it without you! Additionally, I'd like to

thank Ross Ulbricht for teaching me patience, Dr. Charles Brooks for levity, and Daniel E. Shai for commitment. I want to thank everyone in the Schlom group during my tenure: Jessica Burton, Natalie Dawley, Dr. Rainer Held, Dr. John Heron, Dr. June Lee, Dr. Julia Mundy, Dr. Hanjong Paik, Dr. Arsen Soukiassian, Joshua Tashman, Dr. Maitri Warusawithana, and Shaobo Zhu. I also want to thank several individuals from other research groups: Dr. John Harter, Dr. Phil King, Eric Monkman, and Dr. Yuefeng Nie.

I'd be remiss if I didn't thank my family for their unyielding support these past six years. My parents, John Graham and Manuela Melville, have always believed I could do this. My wife, Katherine Margaret Melville, has struggled with me during her own graduate studies, and knows, probably better than anyone, all of the low points and high points of grad school. And, to my daughter, Evelyn Rose Melville, you time and time again won out in my personal battle of priorities. So, for you especially, I thank you in making my dissertation and degree much MUCH harder, but infinitely more worthwhile.

Finally, I have to acknowledge and thank the many sources of funding that supported me both at Penn State and Cornell University. I am grateful to Bayer for providing me with a Bayer Fellowship – and an opportunity to take a summer internship at their Pittsburgh branch. I am grateful to the Cornell Center for Materials Research program for providing me with an IGERT fellowship, and the Air Force Office of Scientific Research for funding the EuO project.

TABLE OF CONTENTS

BIOGRAPHICAL SKETCH iii
DEDICATION iv
ACKNOWLEDGEMENTS v
TABLE OF CONTENTS vii
LIST OF FIGURES viii
CHAPTER 1 1
1.1 Thesis Statement 1
1.2 EuO Background 1
1.2.1 Structure 3
1.2.2 Magnetism 6
1.2.3 Electronic Properties 9
1.2.4 Effect of Doping 11
1.2.5 Effect of Strain 14
1.3 Molecular-Beam Epitaxy 15
1.4 Adsorption-Controlled Growth 20
1.5 Contribution of the Author 23
1.6 Arrangement of Material 24
REFERENCES 27
CHAPTER 2 32
REFERENCES 44
CHAPTER 3 46
REFERENCES 61
CHAPTER 4 64
REFERENCES 82
CHAPTER 5 85
REFERENCES 100
CHAPTER 6 104
6.1 Summary 104
6.2 Future Directions 107
REFERENCES 109

LIST OF FIGURES

Figure 1-1: Ball-and-stick model of the EuO unit cell 2

Figure 1-2: Experimentally-derived phase diagram for the Eu-O system 3

Figure 1-3: Oxygen fugacity vs. temperature in the Eu-O system 5

Figure 1-4: Illustration of the overlap of orbitals in EuO and EuS 8

Figure 1-5: Resistance vs. temperature for EuO_{1-x} thin film at 0, 4 T, and 8 T applied magnetic fields. 9

Figure 1-6: Diagram of the density of states for EuO and the conduction band for EuO, both above and below the ferromagnetic transition 11

Figure 1-7: T_C vs. nominal dopant concentration for several reports of doped EuO 12

Figure 1-8: Diagram of the band structure of EuO, illustrating evidence of free electrons at varoius points in momentum space 14

Figure 1-9: Schematic of a Veeco 930 MBE system 16

Figure 1-10: Rocking curve comparison for EuO using adsorption-controlled growth conditions and flux-matched conditions 23

Figure 2-1: θ-2θ scans comparing epitaxial EuO films with 5% lanthanum-doping, 5% gadolinium-doping, and 5% lutetium-doping 37

Figure 2-2: (a) Normalized magnetization vs. temperature of t epitaxial EuO films with 5% lanthanum-doping, 5% gadolinium-doping, and 5% lutetium-doping. (b) Resistivity vs. temperature for the same three samples. 38

Figure 2-3: Comparison of X-ray photoemission intensity of the lutetium 4d core-level multiplets between 4% Lu-doped EuO, lutetium metal, and oxidized lutetium 39

Figure 2-4: Andreev reflection measurements of the contact between a niobium electrode and a 5% Lu-doped EuO sample (a) Conductance vs. voltage characteristics measured at different temperatures. The inset shows a schematic of the ramp-type junction used for differential four-point conductivity measurements. (b) Fits to the 1.8 K measurement using the Blonder-Tinkham-Klapwijk model. For comparison, fits are shown that fix P to 94%, 96%, and 98%. The inset shows the overlap of the curves near zero voltage bias to better illustrate the match of the best fit. The best fit parameters were Z = 0.9, Δ = 1.28 meV, R = 77, and P = 96%.....41

Figure 3-1: θ-2θ scans of (a) 40 nm thick EuO / YSZ and (b) 170 nm thick EuO / $LuAlO_3$ films. (c) ϕ-scan of 111 EuO diffraction peaks of the 170 nm sample.....51

Figure 3-2: The FWHM of the EuO 002 rocking curves made by rocking about both the high strain and low strain substrate axes plotted as a function of thickness of the EuO / $LuAlO_3$ films. The average FWHM (green circles) is also plotted. The arrow indicates the critical thickness for distinguishable relaxation, 69 ± 5 nm.....53

Figure 3-3: The T_C EuO / YSZ and EuO / $LuAlO_3$ as a function of thickness. The theory presented by Schiller *et al.* is displayed by the dashed green line; the mean-field approximation considering only nearest neighbors (NN) is displayed by the solid purple line, and the mean-field approximation considering both nearest neighbors and next-nearest neighbors (NNN) is displayed by the dotted black line 55

Figure 3-4: Calculated effect of biaxial strain on the T_C of EuO. The effect of changing the on-site Coulomb energy U in the density functional theory on the resulting T_C is shown by the colored data points. The inset shows that the reduction in T_C for EuO films grown commensurately on $LuAlO_3$ 57

Figure 3-5: (a) Magnetization vs. temperature for a 10 nm thick EuO film and a 170 nm thick EuO film. (b) Magnetic hysteresis curves for the 10 nm and 170 nm thick EuO thin films. 59

Figure 4-1: Diagram showing the epitaxial orientation relationship between the surface mesh of the (001) EuO film and underlying (001) diamond substrate. The top left image is the diamond surface mesh with two unit cells highlighted. The top right image corresponds to the epitaxial alignment of EuO on diamond corresponding to ~2% lattice mismatch, with two EuO unit cells highlighted. The bottom image corresponds to the epitaxial alignment of EuO on diamond with less strain, but with a near-coincident site lattice, with four EuO unit cells highlighted 69

Figure 4-2: RHEED images of a 25 nm thick EuO film grown on an epitaxial diamond film along the (a) [100] azimuth and the (b) [110] azimuth. RHEED images of a 37 nm thick EuO film grown on a single-crystal diamond along the (c) [100] azimuth and the (d) [110] azimuth. 72

Figure 4-3: (a) A θ-2θ scan of a 25 nm thick EuO film grown on an epitaxial diamond film. (b) A θ-2θ scan of a 37 nm thick EuO film grown on a single-crystal diamond. (c) Rocking curve comparison between 002 EuO and 004 diamond of the same EuO film as shown in Figure 4-3(a). (d) Rocking curve comparison between 002 EuO and 004 diamond of the same EuO film grown as shown in Figure 4-3(b). 74

Figure 4-4: (a) Azimuthal ϕ scans of a 25 nm thick EuO film grown on an epitaxial diamond film for the 111 Si, 111 Ir, 111 diamond, and 222 EuO diffraction peaks. The scans are offset for clarity. (b) An atomic model illustrates the orientation relationship between all components in the heterostructure. (c) Azimuthal ϕ scans of the 37 nm thick EuO film grown on a single-crystal diamond for the 111 diamond and 111 EuO diffraction peaks. The scans are offset for clarity. 77

Figure 4-5: Magnetization vs. of temperature of (a) a 25 nm thick EuO film grown on an epitaxial diamond film and (b) a 37 nm thick EuO film grown on a single-crystal diamond. (c) Magnetic hysteresis measurements for a 25 nm thick EuO film grown on epitaxial diamond film. (d) Magnetic hysteresis measurements for a 37 nm thick EuO film grown on single-crystal diamond 80

Figure 5-1: (a) XRD scans of a nominally 30 nm thick EuO film and a nominally 60 nm thick EuO film after exposure to 3 minutes of running water. (b) Rocking curve comparison between the 220 $YAlO_3$ substrate peak and the 002 EuO peak for the nominally 30 nm thick EuO film. (c) Rocking curve comparison between the 220 $YAlO_3$ substrate peak and the 002 EuO peak for the nominally 60 nm thick EuO film. 91

Figure 5-2: (a) HAADF image of a nominally 60 nm thick EuO film. (b) Zoomed in image of the same film in Figure 5-2(a) revealing a dark region at the substrate / film interface. An example EELS line map is also drawn on the image for reference. (c) EELS spectra for both the Eu^{2+} and Eu^{3+} signals at several points along the line shown in Figure 5-2(b). (d) Depth profile of the relative abundance of Eu^{2+} and Eu^{3+} cations as a function of position along the line shown in Figure 5-2(b), where 0 nm is within the substrate and 50 nm is within the capped region. 93

Figure 5-3: (a) Magnetization vs. temperature for a nominally 60 nm thick EuO film and a nominally 30 nm thick EuO film. (b) Magnetic hysteresis measurements at 5 K show that the same EuO films are ferromagnetic 98

CHAPTER 1

INTRODUCTION

1.1 THESIS STATEMENT

This thesis is on the development of the ferromagnetic semiconductor EuO,[1] which possesses several remarkable electronic and magnetic properties suitable for device applications. For example, it has the largest known metal-to-insulator transition (MIT), with a change in resistance of more than 13 orders of magnitude,[2] and it has the highest spin polarization (>96%)[3] of any material that has been directly integrated with conventional semiconductors, such as silicon,[4] GaAs,[5] and GaN.[4]

Although EuO has been studied for decades because of its intriguing properties, it lacks a materials technology base to effectively utilize it as an electronic material and exploit its singular properties in emerging device concepts. This thesis is dedicated to enhancing and understanding this novel material, i.e., raising its Curie temperature and developing it as a viable electronic material, by investigating three distinct research directions for EuO: chemical doping via trivalent rare-earth cations, biaxial strain via substrates with varying degrees of lattice mismatch, and preservation via application of a passivated oxide capping layer.

1.2 EUO BACKGROUND

EuO combines several interesting phenomena (e.g., ferromagnetism, a metal-to-insulator transition, and colossal magneto-resistance) in a simple rocksalt cubic

structure. So in addition to the interest in device performance, EuO is also an ideal system for investigating the fundamental science responsible for the origins of these phenomena, and how various stimuli (e.g., strain, electron concentration, temperature) affect these phenomena.

This interplay between physical properties and magnetic or electronic properties in EuO has been studied extensively since the early 1960's, but the non-trivial problem of synthesizing pure EuO with minimal oxygen vacancies has obscured the intrinsic relationship between the structure of EuO and its properties. In the following sections, EuO will be described, with specific regards to its crystal structure, magnetism, and electronic structure. Then, the primary "knobs" through which the properties of EuO can be manipulated will be discussed. And finally, the molecular-beam epitaxy thin film deposition technique and the adsorption-controlled growth regime, both of which were used to fabricate all of the EuO films in this thesis, will be described. This will provide

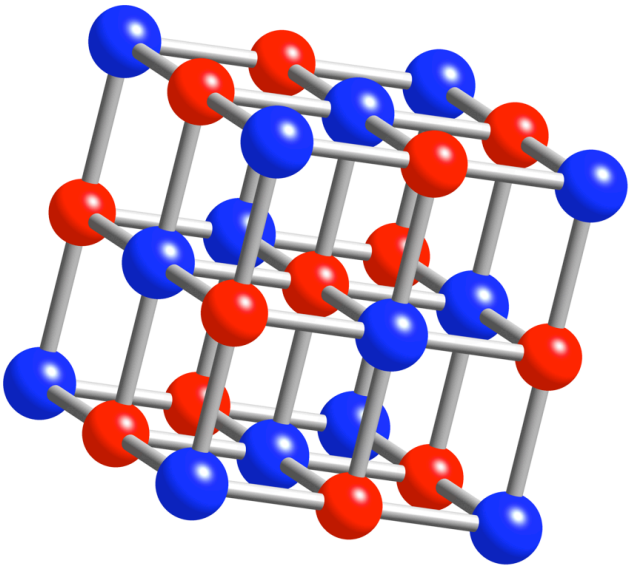

Figure 1-1: Ball-and-stick model of the EuO unit cell, illustrating that both the Eu^{2+} (blue) and O^{2-} (red) are in 6-fold coordination.

sufficient understanding of the problems and goals governing research in EuO, giving perspective to the achievements realized in the body of this thesis.

1.2.1 STRUCTURE

The structure of EuO is that of the classic NaCl rocksalt crystal structure ($Fm\bar{3}m$) as shown in Figure 1-1. The system is cubic, and the (001) plane of EuO is composed of alternating atoms, (i.e., $Eu^{2+} – O^{2-} – Eu^{2+} – O^{2-}$), giving both cations and anions 6-fold coordination.

An experimentally-derived phase diagram is shown in Figure 1-2. At high temperature (T > 1300 ºC), stoichiometric EuO does not exist, because thermodynamically-driven europium vacancies shift the stoichiometry to oxygen-rich EuO. At lower temperatures,

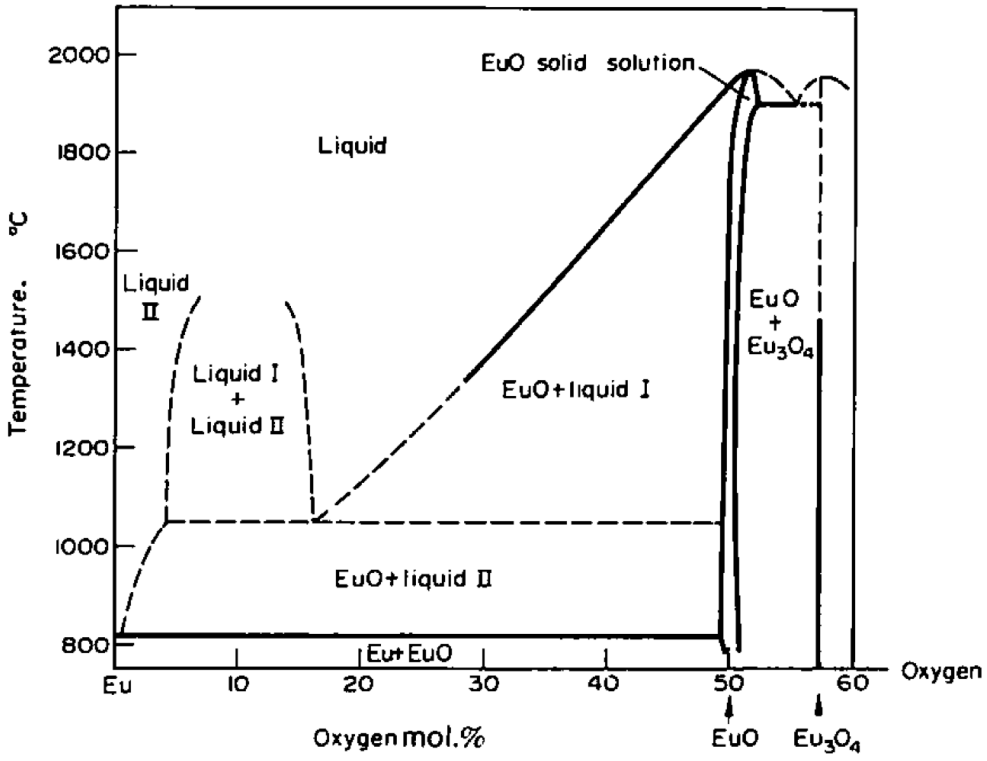

Figure 1-2: Experimentally-derived phase diagram for the Eu-O system. (Reprinted with permission from Shafer *et al.*)[6]

the structure is tolerant of 1-3% excess oxygen[6,7] before forming Eu_3O_4 or Eu_2O_3. As the temperature continues to drop, the structure becomes increasingly tolerant of excess europium, up to between 0.2% and 2% as estimated from bulk chemical and electronic measurements.[6] Above this concentration, europium metal forms as a precipitate.

EuO demonstrates a high degree of solubility with other rocksalt materials, e.g., SrO (Refs. 8,9) or BaO (Ref. 10). It can also easily accommodate replacement of the Eu^{2+} cation with trivalent cations, such as La^{3+} (Refs. 4,11,12) or Gd^{3+}.[11,13–19] It has been demonstrated that the trivalent cation, for example, Gd-doped EuO, can exceed 16% with no indication of insolubility.[20,21] The lattice constant decreases linearly with the addition of smaller cations and increases linearly with the addition of larger cations.[10,16]

In addition to Eu^{2+}, europium can exist as a metal (in vacuum or under highly reducing conditions), or it can further ionize to Eu^{3+}. Both europium metal and Eu^{2+} are easily oxidized to the more stable Eu^{3+} in the presence of oxygen or water (i.e., atmosphere). As shown in Figure 1-3, europium in the presence of oxygen forms EuO, Eu_3O_4, or Eu_2O_3 based on the activity of oxygen.[22] Europium can also be hydroxylized by water to form $Eu(OH)_3$.[23] In fact, forming the EuO compound – that is, without reducing europium to metal or oxidizing it to Eu_2O_3 – was so challenging that it remained undiscovered until the 1954,[24] where it was first discovered in solution. It was not until 1956 before EuO was isolated.[25] The instability of EuO arising from the reactivity of the Eu^{2+} is one of the key challenges that ought to be addressed for effective utilization in any practical sense.

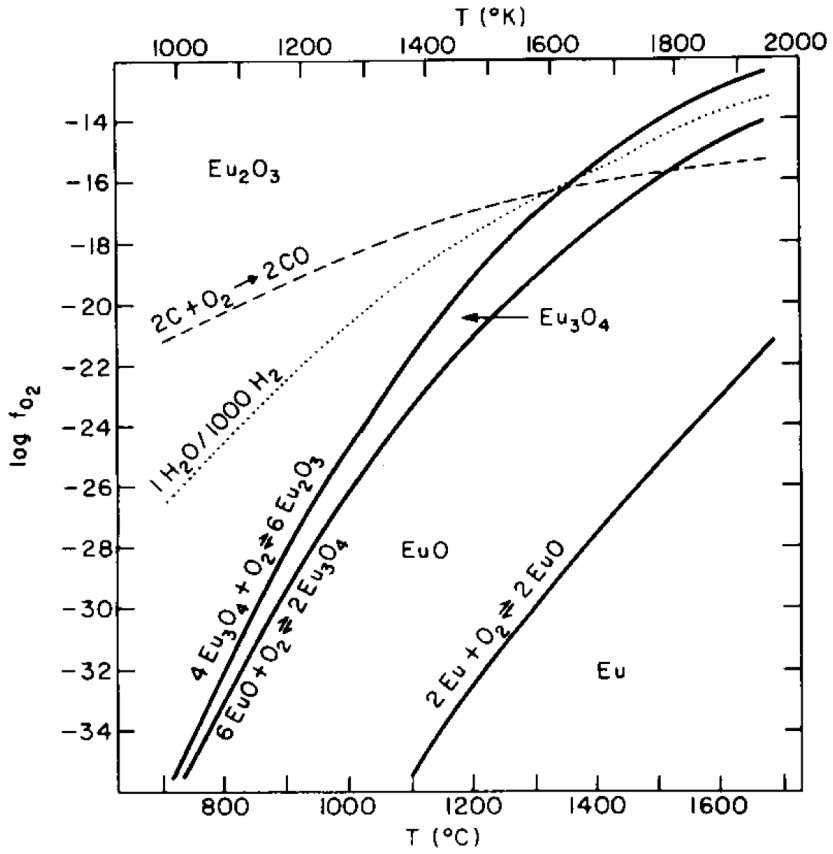

Figure 1-3: Diagram depicting the stability of various Eu_xO_y phases as a function of oxygen fugacity and temperature. (Reprinted with permission from McCarthy) [22]

Bulk EuO is passivated to an extent by the formation of Eu_2O_3 on the surface, but the passivation is poor and the EuO crystal will degrade over time. Thin film EuO, on the other hand, reacts immediately and completely as a result of how thin it is. Techniques have been employed to overcome this issue, such as depositing a protective "buffer" layer on top of the EuO, e.g., amorphous silicon,[4,20,26] aluminum,[27–29] Al_2O_3, [4,30] or by sacrificing the top layers of EuO to Eu_2O_3 in a controlled partial vacuum environment.[13,31–34]

As a result of the surface oxidation in bulk EuO and the necessary buffer layers in thin film EuO, surface probe techniques, e.g., atomic force microscopy, scanning electron

microscopy, or photoemission spectroscopy, are nearly impossible for *ex situ* measurement. In bulk EuO, these techniques may be possible immediately after polishing the surface to remove the Eu_2O_3. In thin film EuO, these techniques are possibly only by confining the films to high vacuum until the analysis is complete.[35,36] Even under ultra-high vauum, the EuO surface is oxidized in a matter of hours.[36]

1.2.2 MAGNETISM

The magnetism of EuO is rooted in the exchange interactions between the 4*f* electrons of the Eu^{2+} cation. EuO is magnetic when the electron spins from these electrons are aligned with respect to one another. Bulk EuO is most easily magnetized in the <111> directions as a result of the structure of EuO and the magnetic anisotropy constants of EuO,[37] whereas in thin films, shape anisotropy dictates that the easy axis lies in the plane of the film regardless of the magnetic anisotropy.[38] Given that Eu^{2+} has 7 4*f* electrons, i.e., 7 half-filled *f* orbitals, the maximum saturation magnetism for EuO is 7 μ_B per Eu cation, which has been experimentally verified many times.[1,4,28,39] Experiments have implied that the saturation magnetization depends heavily on the sample quality,[4,27,39] possibly as a result of an abundance of defects present in low-quality samples.

The magnetic exchange interactions in magnetic systems like EuO can be categorized as direct, superexchange, and indirect virtual exchange. Direct exchange is the effect that one magnetic moment, i.e., one centered at a Eu^{2+} cation in EuO, has on another magnetic moment. Indirect exchange is, likewise, the effect of one magnetic moment on

another, but this effect is facilitated by an intermediary particle (that does not have to be magnetic). In the case of superexchange, a magnetic moment interacts with another (its next-nearest neighbor) via the nearest neighbor, such as the classic Kramers-Anderson mechanism involving two Mn^{2+} cations and a neighboring O^{2-} anion.[40] In the case of indirect virtual exchange, a magnetic moment interacts with another (its nearest neighbor) via a virtual transfer involving intermediary orbitals, i.e., from the 4*f* orbital to a 5*d* orbital to 4*f* orbital on another cation.[41]

Direct exchange in EuO between neighboring 4*f* orbitals is minimal; the far more important interactions arise from superexchange and indirect virtual exchange. Superexchange in EuO utilizes an intermediary oxygen 2*p* orbital (primarily in the 180º-orientation given its rocksalt structure) to share spin state between neighboring Eu 4*f* electrons. Superexchange in EuO occurs via 3 mechanisms: first, the classic Kramers-Anderson mechanism; second, a more complex mechanism involving the 4*f* – 5*d* exchange interaction; and third, a cross term between the first two mechanisms.[42] Although superexchange tends to antiferromagnetic coupling (such as in the case of EuS, EuSe, and EuTe), the special blend of atomic spacing and interactions between the O 2*p* and Eu 4*f*, 5*d*, and 6*s* orbitals in EuO favors ferromagnetic coupling.[42,43] Superexchange interactions, however, account for only ~25% of the exchange energy in EuO ($J_{\text{Superexchange}} = 1.2\times10^{-6}$ eV).[43,44]

Indirect virtual exchange in EuO is responsible for most of the exchange energy ($J_{\text{Virtual exchange}} = 3.5\times10^{-5}$ eV),[44] and arises from interactions involving the 4*f* and 5*d* or 6*s*

orbitals. In this case, a 4*f* electron is virtually excited to a 5*d* or 6*s* orbital, and then interacts with the neighboring 4*f* electron.[42]

A system is ferromagnetic only when the energy saved by aligning the electron spins (magnetic exchange energy) surpasses the entropic energy cost of aligning the spins (thermal energy). In stoichiometric EuO, these terms are equal at 69 K. Below this temperature, called the Curie temperature (T_C), is the onset of magnetization, and EuO is ferromagnetic. Above this temperature, the electron spins are randomly oriented, and EuO is paramagnetic.

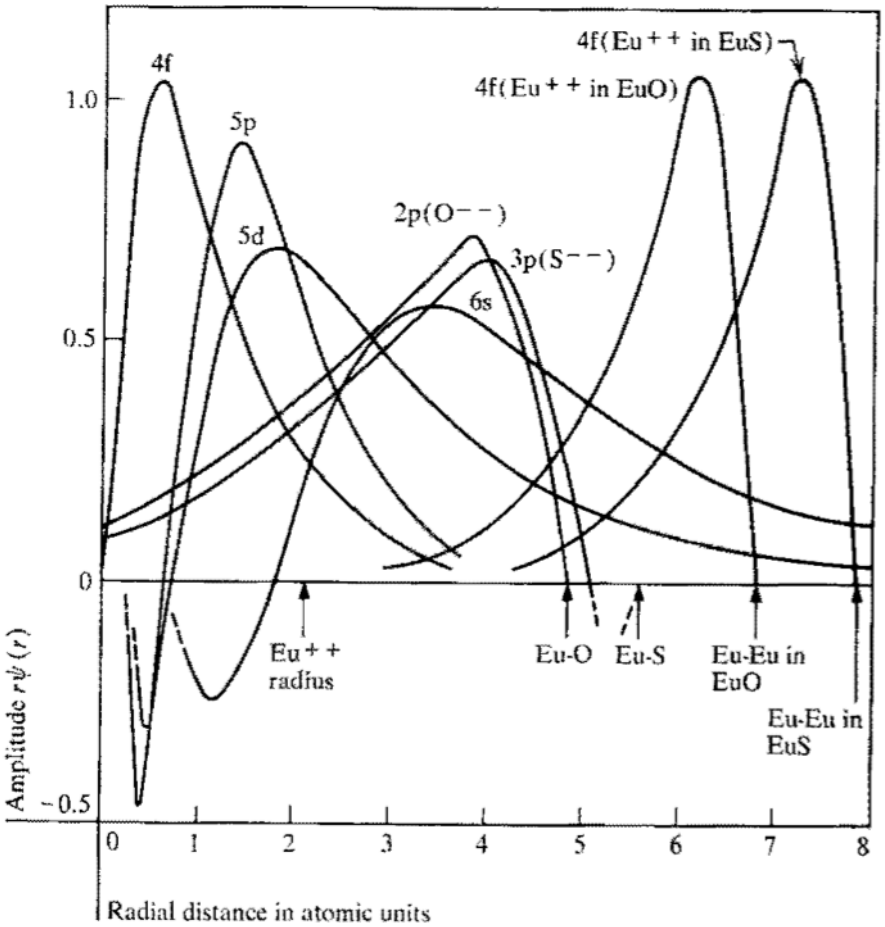

Figure 1-4: Representation of the overlap of orbitals in neighboring atoms in EuO and EuS. (Reprinted with permission from T. Kasuya, IBM J. Res. Dev. **14**, 214-223 (1970).[42]

Stronger interactions result in higher magnetic exchange energy, meaning that by enhancing the magnetic exchange energy, one can raise the T_C above its intrinsic value. The interaction strength of a material is determined in part by the overlap of the electron orbitals and is visualized in Figure 1-4 for the particular case of EuO and its homostructural chalcogenide neighbor, EuS.[42] Therefore, understanding how to manipulate the interaction of the orbitals in EuO is critical for increasing the T_C to a more practical level.

1.2.3 Electronic Properties

Stoichiometric EuO is a semiconductor with a band gap of 1.12 eV at room temperature.[45] The Fermi level sits between the valence band (formed by the Eu 4*f*

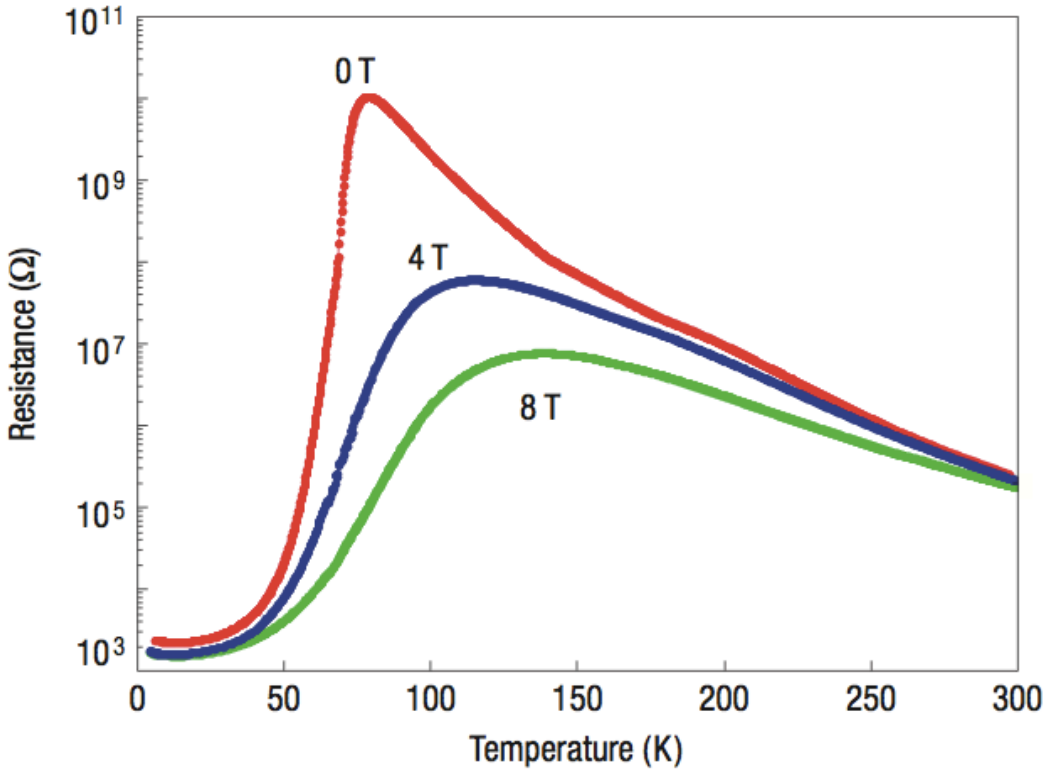

Figure 1-5: Resistance as a function of temperature for an EuO_{1-x} thin film sample with no applied field, 4 T, and 8 T. (Reprinted with permission from Schmehl *et al.*)[3]

states) and the conduction band (formed by the Eu 5*d* and 6*s* states).[46] In the electron-rich state, however, EuO exhibits a metal-to-insulator transition (MIT) spanning up to 13 orders of magnitude in bulk[2] or up to 8 orders of magnitude in thin films as pictured in Figure 1-5.[4] Figure 1-5 also illustrates the colossal magnetoresistance (CMR) of up to 6 orders of magnitude in bulk[47] or up to 5 orders of magnitude in thin films.[4] The incredible change in resistivity, both as a function of temperature and as a function of magnetic field is simply unparalleled by any other known system.

The cause of the MIT and CMR is the ferromagnetic transition in EuO. When EuO becomes ferromagnetic, the conduction band splits by 0.6 eV (Ref. 48) into a low-energy electron spin-aligned band and a high-energy electron spin anti-aligned band.[49] Any additional electrons that were previously trapped in a donor state in the band gap, as depicted in Figure 1-6, now flow into the conduction band. Therefore, electron-rich EuO is insulating in the paramagnetic state and conducting in the ferromagnetic state. As the number of electrons increases, the resistivity drops in both the ferromagnetic and paramagnetic states.[20] The decrease in resistivity in the ferromagnetic state is simply due to charge carriers in the conduction band, like any metal. The limited conductivity in the paramagnetic state is mediated by a thermally-activated hopping mechanism, and a greater density of electrons in the trap states further increases the conductivity, i.e., decreases the resistivity. In 2002, empirical evidence suggested that, due to the band-splitting, electrons in the conduction band are nearly completely spin polarized.[48] Experiments have since proven that EuO has a spin-polarization of at least 96%,[3] giving it the second highest spin-polarization of all known materials after CrO_2.[50]

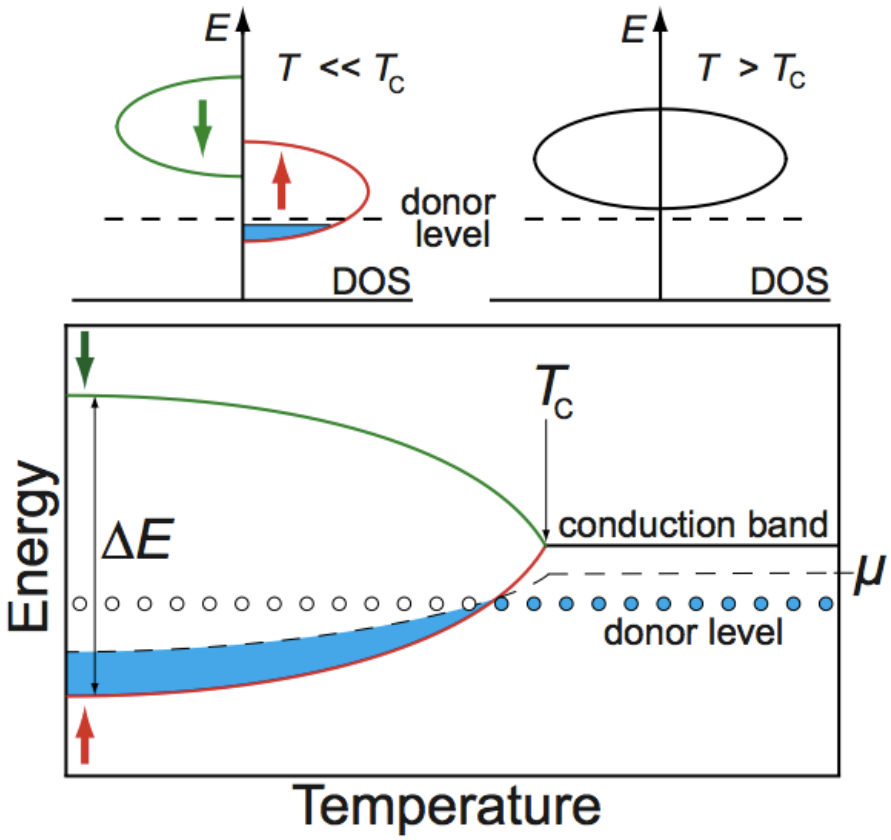

Figure 1-6: Diagram of the density of states in EuO above (top left) and below (top right) the ferromagnetic transition temperature, and a diagram of the conduction band splitting as a function of temperature (bottom). The energy level of an unspecified dopant is also illustrated "flowing" into the conduction band below the T_C. (Reprinted with permission from Mairoser *et al.*) [51]

1.2.4 Effect of Doping

Electron-rich EuO was first deliberately manufactured in 1968 by doping with RES, Eu, and RE_2O_3,[11] where RE were rare-earth elements, paving the way for future experiments. Over the next 40 years, EuO has become electron-rich in a multitude of ways, but generally in one of two ways. Electron-rich EuO is made either by deliberate Eu-rich off-stoichiometry (i.e., EuO_{1-x})[6,52–54] or by doping with trivalent cations.[4,12,19,20,51,55–58] Several trivalent cations have been used to dope EuO, such as Ag^{3+},[56] Ce^{3+},[58] Cu^{3+},[56] Fe^{3+},[56,59,60] Gd^{3+},[11,14–20,61] Ho^{3+},[11] La^{3+},[4,11,12] and Y^{3+}.[11]

In the case of Eu-rich EuO, oxygen vacancies are created to accommodate the excess electrons of the Eu, with each oxygen vacancy containing two electrons. One electron has been assumed to exist as a shallow donor, and the other to be held in a deeply trapped state.[62] In the case of trivalent cations, the single excess electron has been assumed to exist as a shallow donor.[63] These shallow donor electrons' spins can align with the neighboring 4*f* electrons, increasing the overall magnetic exchange energy in EuO.[63] As a result, the T_C of electron-rich EuO is enhanced. Experimentally, the T_C was enhanced up to 200 K in several reports,[12,15] but as shown in Figure 1−7, results in the literature are erratic regarding, first, how many excess electrons are necessary to achieve the maximum T_C enhancement, and second, how much the T_C can be enhanced.

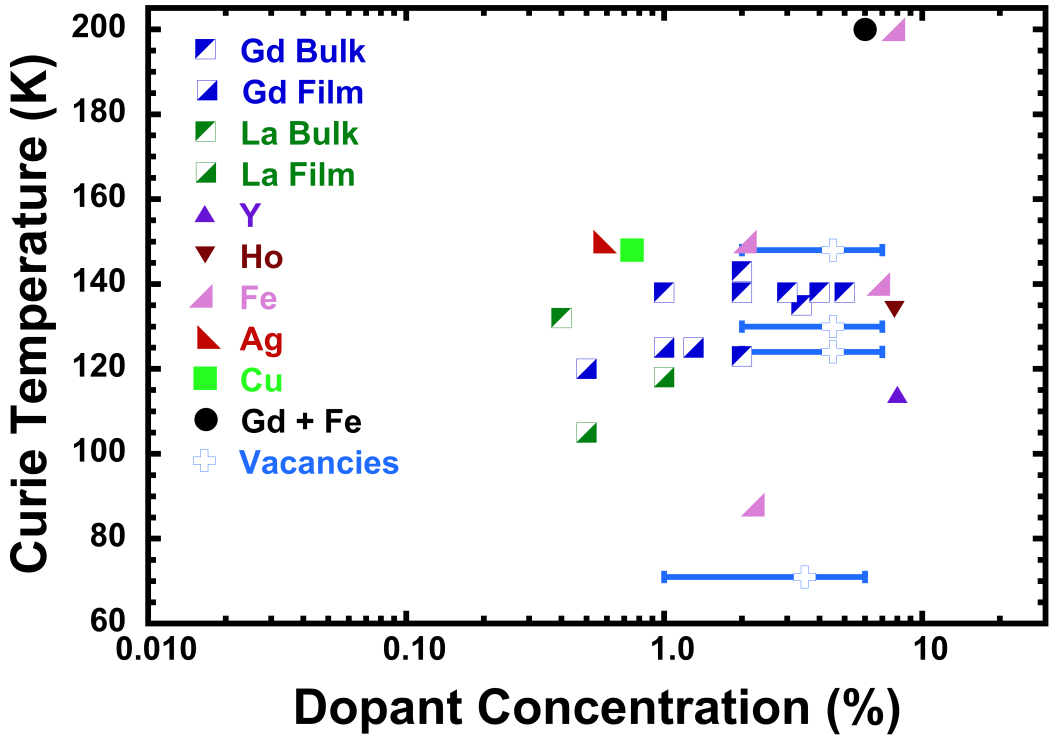

Figure 1-7: Collection of several reports of an increased T_C resulting from doped EuO, arranged by nominal dopant concentration and reported T_C.[4,11,14,16,17,54,56,57,59–61,64–66]

In many cases, the difficulty arises from simply not knowing the true electron concentration in the sample, either from an unknown amount of oxygen vacancies inherent in many growth modes or by poor control over the doping level. Furthermore, precise knowledge of the number of dopant atoms does not imply precise knowledge of the number of extra electrons. In 2010, the number of electrons in the conduction band of electron-rich EuO was far fewer than the highly controlled dopant concentration.[20] The percentage of dopants, dubbed the dopant activation, that contribute electrons to the conduction band of EuO (instead of some unknown trap state) is at most 30%.[20]

The experiment hinged upon the definitive knowledge that *only* trivalent cations contributed electrons into the system, which could only be accomplished by fabricating the EuO films in an adsorption-controlled growth regime that minimized oxygen vacancies. The adsorption-controlled growth regime is discussed in a later section of this thesis.

Further work probing the band structure of Gd-doped EuO observed electrons located at a defect level below the Fermi surface at the Γ-point of the Brillouin zone in the paramagnetic state.[36] In the ferromagnetic state, many, but not all, of these electrons migrated to the conduction band at the X-point of the Brillouin zone as illustrated in Figure 1-8. The mobile electrons corresponded to the shallow donors introduced by the Gd-doping that enter the conduction band upon cooling to the ferromagnetic state. The immobile electrons that remain trapped in a deeper energy level at the Γ-point, called deeply bound states, may be the same as the “inactive” dopants described above.[36]

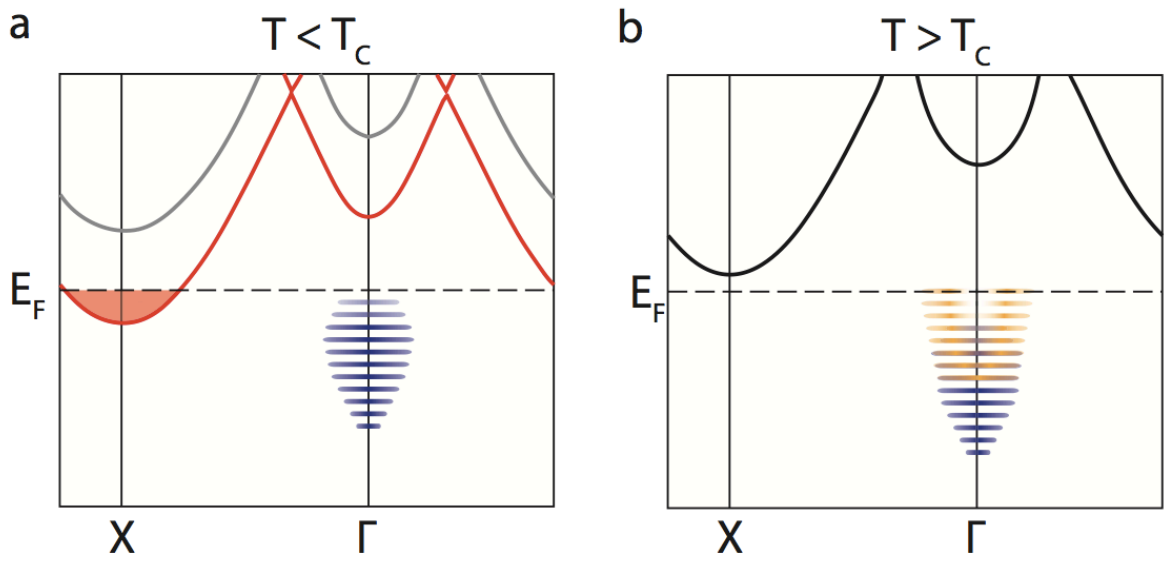

Figure 1-8: Diagram of the band structure of EuO in both (a) the ferromagnetic state and (b) the paramagnetic state. The blue region in both states depicts the trapped "deeply bound states", whereas the shallow donors travel from the conduction band at the X-point in the ferromagnetic state (red) to the Γ-point in the paramagnetic state (yellow). (Reprinted with permission from Shai *et al.*)[36]

1.2.5 Effect of Strain

As mentioned in Section 1.2.2, the strength of the orbitals' exchange interaction is determined in part by how much the orbitals overlap. It stands to reason, then, that forcing orbitals closer to each other should enhance the exchange interaction, and thus, enhance the T_C).

One common method to bring orbitals closer is to contract the lattice, e.g., apply high pressure to the system. This method has been investigated thoroughly in EuO. Early experiments on EuO single crystals demonstrated that hydrostatic pressure increased the T_C up to 125 K at 10 GPa (Ref. 67) and 200 K at 14 GPa (Ref. 68) before EuO undergoes a high-pressure transition to a mixed valence state.

In 2008, Ingle and Elfimov predicted that a similar but lesser T_C enhancement would occur as a result of biaxial compressive strain, i.e., from a commensurate EuO thin film with the exact in-plane lattice spacing of its slightly smaller substrate.[43] The reduced enhancement arises from the unconstrained out-of-plane lattice parameter of EuO, which increases due to a Poisson effect to roughly conserve volume. Ingle and Elfimov further predicted that forcing orbitals apart, e.g., biaxial tensile strain, would reduce the T_C of EuO.[43]

Prior to this thesis, EuO had been grown commensurately on $YAlO_3$, which imparts a 2% tensile strain on EuO, but no reduction in the T_C was reported.[39] A report of a 1.5 nm EuO grown on $LaAlO_3$ reported a reduction of the T_C to 45 K,[69] but this could be explained by the reduced magnetism in ultrathin EuO films.[29,70,71]

1.3 Molecular-Beam Epitaxy

Molecular-beam epitaxy (MBE) is a thin film deposition technique employed under ultra-high vacuum (UHV), where high purity materials are evaporated from effusion cells and travel as a "molecular beam," collision-free, to a heated substrate. The molecular beam description, where most molecules travel unobstructed in a line-of-sight path from the effusion cell to the substrate, is valid when the mean-free path of gas molecules in the system is much greater than the distance the molecules are traveling. A typical travel distance for MBE is on the order of one meter, while the mean-free path at a typical UHV pressure (~10^{-9} Torr), is ~10^5 m. A diagram of a Veeco 930 MBE chamber is provided in Figure 1-9.[72]

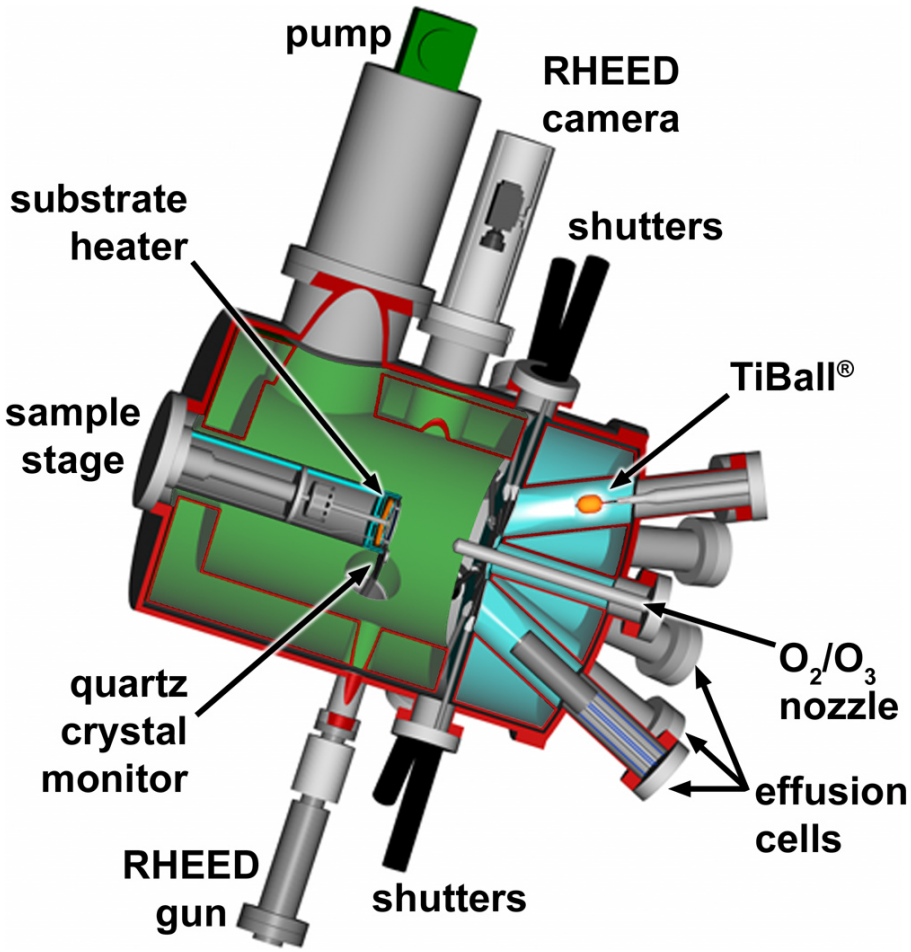

Figure 1-9: Schematic of a Veeco 930 molecular-beam epitaxy system, highlighting the relevant features for thin film growth. (Reprinted with permission from Schlom *et al.*)[72]

The Veeco 930 and Veeco Gen10 MBE systems were used in this thesis, and had been carefully designed for reactive oxide thin film growth, referring to the reaction of oxygen and metal at the surface of the substrate in order to form the oxide phase from its constituent materials.

Crucibles containing the elemental source material are housed within the effusion cells (see Figure 1-9) and are heated to a precise temperature (±0.1 ºC). The temperature of the material dictates the vapor pressure – and therefore flux – of that particular source material. The selection of elemental sources is limited only by the ability to heat a

material enough to provide a suitably high flux. That is, the flux must be sufficiently high such that the adsorption of source molecules must vastly outnumber the adsorption of gas molecules from the vacuum. For example, a flux of ~1×10^{13} atoms / $cm^2\times s$ can deposit a monolayer in about 30 seconds, while a vacuum pressure of ~1×10^{-9} Torr will deposit a monolayer in about 30 minutes. Compound sources are typically not used, since most do not evaporate congruently, creating concerns regarding the exact composition of the flux species.[72] The geometric consideration of the placement of the effusion cells relative to the substrate allow for multiple molecular beams to impinge upon the substrate simultaneously. The substrate can be fixed to deliberately create a stoichiometry gradient across the substrate,[73] or the substrate can be rotated during deposition to ensure the same stoichiometry at all points on the substrate.

An oxygen (or ozone) source is used in addition to elemental sources, and is introduced into the vacuum system by means of a piezoelectric leak valve. The background vacuum pressure is ~10^{-9} Torr, and the oxygen partial pressure should not surpass ~10^{-4} Torr, where the “molecular-beam” fails as the mean-free path diminishes.[72] In the Gen10 MBE chamber, the oxygen flux can be pointed directly at the substrate from a distance of 3.8 inches, increasing the local oxygen concentration (and gradient) at the substrate compared to the overall vacuum pressure, or the oxygen flux can be deflected at the nozzle to create a more homogenous distribution of oxygen atoms at the substrate surface. The oxygen partial pressure is controlled by monitoring the chamber pressure, which is a suitable assumption for when oxygen comprises >99% of the gaseous species in the vacuum. When lower pressure is desired, the oxygen partial

pressure is indirectly controlled by controlling the voltage to the piezoelectric leak valve or by controlling the oxygen pressure as it enters the piezoelectric leak valve.

Pneumatically controlled shutters can be inserted between each effusion cell and the substrate. Since the molecular beams travel in line-of-sight paths, these shutters, when extended, can completely block the beam. So even though multiple effusion cells are directing their molecular beams at the substrate, deposition occurs only from the effusion cells whose corresponding shutters are open. As a result, one may keep all source materials at the desired temperature – and therefore, flux – instead of heating and cooling a material every time it is used. Furthermore, changes in composition can be controlled instantly (that is, limited by the speed of the shutter as the velocities of the molecules in the molecular beam are ~10^4 m/s). Modulation doping, composition control, and multi-layered heterostructures can be accomplished simply by "shuttering" open and close the shutters to the relevant source materials. Another layer of control is established by choosing the order of the shutters opening and closing. For example, growth involving multiple molecular beams can be accomplished either by having all shutters open simultaneously (co-deposition) or by opening and closing the shutters sequentially. Sequential growths are particularly useful for layered structures (e.g., superlattices, Ruddlesden-Popper phases, high T_C cuprates, etc.).

The flux is quantified with the use of a quartz-crystal microbalance (QCM) that is positioned in front of the substrate in order to provide the most accurate flux measurement. The quartz crystal resonates at a different frequency as atoms collect on

its surface and add to the mass of the crystal, and this change in frequency over time is used to calculate the mass accumulation rate,[74] which can then be converted to a flux given the density and molecular weight of a material. To balance the speed of growth with source material depletion, the flux is typically in the range of ~1-3×10^{13} atoms / cm^2×s. The growth rate, then, is approximately one monolayer per minute.

Reflection high-energy electron diffraction (RHEED) is a tool commonly found in MBE systems, and it allows for *in situ* observation of the film surface during growth. An electron beam is directed at a variably shallow angle at the substrate, and the diffracted beam is collected at a phosphor screen on the opposite side, as depicted in Figure 1-9. The angle is sufficiently shallow that only the first few monolayers are probed by the RHEED.[75] As such, RHEED is acutely responsive to changes in the surface of the thin film, conferring a huge amount of information to the viewer. RHEED patterns can be used to distinguish the epitaxial quality of a thin film, whether single-crystalline, polycrystalline, or amorphous.[75] They can also be used to identify the structure and crystallographic orientation of a film.[75] RHEED patterns can be used to identify the morphology and growth mode of a film.[75] RHEED patterns can also be used to monitor the adsorption of a single monolayer, giving strict control over the thickness and signaling when to shutter the sources for abrupt heterostructure changes.[76] This is especially true given the relatively slow growth rate, since users have nearly a full minute per monolayer to react and respond to the incoming information.

MBE is the most sophisticated growth technique for thin films by virtue of the many

technologies that work in tandem. The precise flux control of the source materials, the relatively slow growth rate, the clean UHV environment, and the ability to monitor and react to the film in real time are the key ingredients that directly generate the unparalleled control in composition, stoichiometry, and doping along the growth direction.

1.4 ADSORPTION-CONTROLLED GROWTH

Simply having the machinery to create precisely controlled compositions is insufficient. An understanding of the kinetics and surface morphology at the substrate surface is critical in controlling the composition. This is especially true in systems composed of multiple elements, e.g., GaAs,[77] $PbTiO_3$,[78] and $Eu_{1-x}Gd_xO$,[20] because each element has a unique sticking coefficient, vapor pressure, and reactivity.

In systems where one component has a high vapor pressure in a certain "growth window",[79] adsorption-controlled growth can be employed. In an adsorption-controlled growth regime, the volatile, high vapor pressure component is provided in excess, and the non-volatile components limits the reaction on the substrate. The excessive volatile component desorbs. The key is finding and identifying suitable materials systems and the specific growth window for these systems.

The advantages of the adsorption-controlled growth technique are the ease with which these films are grown, the high fidelity in stoichiometry, and the high quality. The disadvantage of the adsorption-controlled growth technique is that this regime is

typically only possible for materials containing a constituent having a high vapor pressure. Hardware limitations, such as maximum substrate temperatures or minimum partial pressures, preclude this technique from more widespread use.

The concept of an adsorption-controlled growth regime was first applied in 1958 to polycrystalline GaAs[80] and later applied to the growth of epitaxial GaAs in UHV conditions.[77] GaAs is grown in excess As_2 or As_4 gas using gallium to limit the reaction. Excess As_2 or As_4 gas desorbs. Insufficient temperature, however, reduces the vapor pressure of arsenic enough to nucleate arsenic on the substrate.[77] In 1998, the concept of adsorption-controlled growth was expanded for the growth of $PbTiO_3$.[78] In the case of $PbTiO_3$, excess lead flux and oxygen gas are utilized, and titanium limits the growth of $PbTiO_3$. Lead first reacts with oxygen at the substrate surface to form PbO. If titanium is available and reacts with oxygen to form TiO_2, then PbO reacts with it to form $PbTiO_3$. Excess PbO desorbs. Here, an intermediary product becomes the desorbing material. Insufficient O_2 partial pressure, however, fails to oxidize the lead, so only TiO_2 remains on the substrate, as the lead will also desorb.

In the case of EuO, it would seem that the volatility of EuO in excess oxygen precludes such a technique. In previous MBE growth of EuO, great care was taken to balance the oxygen flux with the europium flux – so called “flux-matched” growth – yet precise stoichiometry control remained difficult. A local or temporary abundance of oxygen results in regions of Eu_2O_3 or Eu_3O_4. Likewise, a local or temporary dearth of oxygen results in regions of europium metal or EuO_{1-x}. The formation of EuO_{1-x} is particularly

problematic because it is a source of electron-doping oxygen vacancies, whose quantity is difficult to measure or reliably reproduce.

The adsorption-controlled growth regime in EuO was first utilized in 2002, when Steeneken witnessed the lack of a MIT in EuO thin films as growth temperature was increased.[81] In the case of EuO, the desorbing species are europium metal and oxygen. Only the oxide products remain on the substrate, since they have a much lower vapor pressure compared to the metal (e.g., $P_{EuO} = 10^{-10}$ Torr at 550 ºC and $P_{Eu} = 10^{-3}$ Torr at 550 ºC). This was not acknowledged as an adsorption-controlled growth, however, until 2006, when Ott employed the technique to control the stoichiometry,[18] and 2008, when Ulbricht proved that it was adsorption-controlled by demonstrating the dependence of EuO growth rate on the oxygen partial pressure when applying an overabundance of europium.[39]

In the adsorption-controlled growth regime for EuO, when the oxygen flux limits the growth of EuO, unreacted europium atoms simply desorb from the surface instead of being incorporated into the EuO lattice and being accompanied by oxygen vacancies. Furthermore, if the europium flux is set much larger than the oxygen flux, then the formation of Eu_2O_3 is also precluded since the local oxygen fugacity is too low (refer to Figure 1-3). Thus, the adsorption-controlled growth regime enabled scientists to grow high-quality EuO for the first time as shown in Figure 1-10, which directly compares the rocking curve of an EuO thin film grown in the adsorption-controlled growth regime to a rocking curve of an EuO thin film grown using flux-matched conditions.

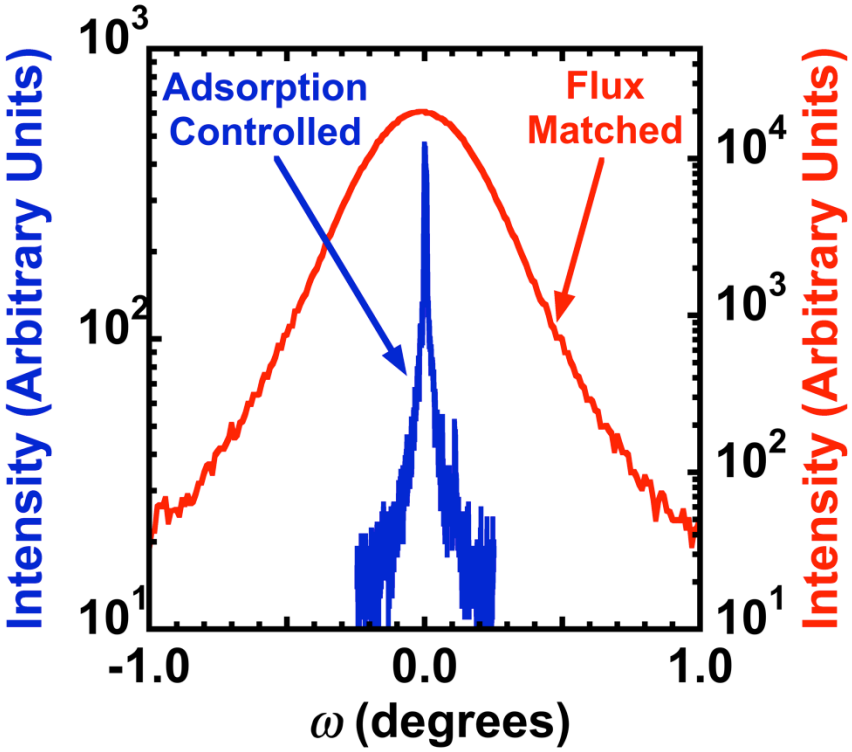

Figure 1-10: Rocking curve comparison between an EuO film grown in an adsorption-controlled growth regime (blue) and an EuO film grown under flux-matched conditions (red). (Adapted with permission from Schmehl *et al.*)[4]

The advancement of EuO deposition science allowed for more sensitive probes into the physics underpinning EuO, since they simply were not possible with prior defect-laden EuO_{1-x} thin films. The oxygen vacancies or local inclusions of europium metal or Eu_2O_3 that plagued EuO since its discovery in the 1950's are no longer a concern. Since then, numerous studies have led to a greater understanding of EuO.[20,26,36,51]

1.5 Contribution of the Author

The remaining chapters of this dissertation consist of articles submitted to or published in refereed journals. The author's role in these works was the fabrication of the EuO thin films using reactive oxide MBE; the structural characterization of said films via X-ray

diffraction and atomic force microscopy; the magnetic characterization using a superconducting quantum interference device (SQUID) magnetometer; and, the electronic characterization by patterning contacts and test structures onto the films and then characterizing the films using a Keithley 2400 SourceMeter. For some films, the magnetic and electronic characterization was performed by Drs. Andreas Schmehl and Thomas Mairoser, collaborators from the University of Augsburg in Germany.

1.6 Arrangement of Material

This dissertation describes the investigation of the properties of EuO when doped with trivalent rare-earth cations (Chapter 2) or biaxially strained by the substrate (Chapters 3-4), and also the investigation of the application and efficiency of an Eu_2O_3 capping layer for EuO (Chapter 5).

The specific arrangement of the contents are as follows:

Chapter 2: This chapter describes the use of Lu^{3+} as a novel dopant cation for EuO. It characterizes the effects of this dopant on the magnetic and electronic properties of EuO, and compares them to the effects caused by the La^{3+} and Gd^{3+} dopants commonly used in EuO literature. Finally, the spin-polarization of Lu-doped EuO is demonstrated to be >96%, the largest spin-polarization value for EuO ever reported.

Chapter 3: This chapter describes the use of a novel substrate, $LuAlO_3$, as

a template for EuO, which, due to the lattice mismatch, imparts a +1% biaxial tensile strain on EuO. The critical thickness for EuO films grown on $LuAlO_3$ was established to be 69 nm. The effect of strain was extracted by growing a thickness series of identical EuO films on both yttria-stabilized zirconia (YSZ), which is lattice-matched to EuO and imparts no strain, and $LuAlO_3$. The reduction in T_C for EuO thin films under biaxial tensile strain was demonstrated, matching theoretical predictions.

Chapter 4: This chapter describes the growth of epitaxial EuO on diamond substrates. Although these films could not be commensurately grown on EuO, and therefore did not show an enhanced T_C, they represent the first integration of a ferromagnet with diamond, and they also pave the way for future epitaxial oxide growth on diamond. The optimal growth conditions are established and compared for EuO grown on both diamond films on silicon and on single-crystal diamonds. Although the epitaxy is confirmed, the structural quality is reduced compared to EuO films grown on oxide substrates. So while the EuO thin films on diamond are still ferromagnetic with a T_C of 69 K, the saturation magnetization is also reduced as compared to higher quality EuO thin films.

Chapter 5: This chapter describes the application of a passivated Eu_2O_3 capping layer for EuO by oxidizing the topmost EuO layers. The Eu_2O_3 capping layer was performed for both commensurate and incommensurate

thin films grown on $YAlO_3$, and the oxygen was found to diffuse further into the incommensurate sample. The effectiveness of the incommensurate capping layer was analyzed with scanning tunneling electron microscopy (STEM) and electron energy loss spectroscopy (EELS) to structurally and chemically confirm the presence of Eu_2O_3 at only the surface of EuO. Small amounts of Eu_2O_3 were seen at the interface between EuO and the substrate in the incommensurate sample, and were attributed either to an anomalous growth feature or enhanced oxygen diffusion down stress-related defect channels, which could also have been responsible for the deeper penetration of oxygen during the capping process compared to the commensurate film. Magnetic characterization of both the commensurate and incommensurate films presented no significant differences, and both thin films had magnetic properties that were similar to other high-quality EuO thin films.

Chapter 6: This chapter summarizes the accomplishments of the Chapters 2-5, highlighting the major achievements. It also considers directions for future work in the EuO system, based on the results of this thesis.

REFERENCES

[1] B. T. Matthias, R. M. Bozorth, and J. H. Van Vleck, Phys. Rev. Lett. **7**, 160–161 (1961).

[2] G. Petrich, S. Von Molnár, and T. Penney, Phys. Rev. Lett. **26**, 885–888 (1971).

[3] A. Melville, T. Mairoser, A. Schmehl, D. E. Shai, E. J. Monkman, J. W. Harter, T. Heeg, B. Holländer, J. Schubert, K. M. Shen, J. Mannhart, and D. G. Schlom, Appl. Phys. Lett. **100**, 222101 (2012).

[4] A. Schmehl, V. Vaithyanathan, A. Herrnberger, S. Thiel, C. Richter, M. Liberati, T. Heeg, M. Röckerath, L. F. Kourkoutis, S. Mühlbauer, P. Böni, D. A. Muller, Y. Barash, J. Schubert, Y. Idzerda, J. Mannhart, and D. G. Schlom, Nat. Mater. **6**, 882–887 (2007).

[5] A. G. Swartz, J. Ciraldo, J. J. I. Wong, Y. Li, W. Han, T. Lin, S. Mack, J. Shi, D. D. Awschalom, and R. K. Kawakami, Appl. Phys. Lett. **97**, 112509 (2010).

[6] M. W. Shafer, J. B. Torrance, and T. Penney, J. Phys. Chem. Solids **33**, 2251–2266 (1972).

[7] R. G. Bedford and E. Catalano, J. Solid State Chem. **3**, 112–124 (1971).

[8] G Brauer and N Schultz, J. Less-Common Met. **13**, 213–218 (1967).

[9] B. Stroka, J. Wosnitza, E. Scheer, H. v. Löhneysen, W. Park, and K. Fischer, Phys. B Condens. Matter **39**, 39–43 (1992).

[10] V. Vaithyanathan and D. G. Schlom, *unpublished*.

[11] M. W. Shafer and T. R. McGuire, J. Appl. Phys. **39**, 588–590 (1968).

[12] H. Miyazaki, H. J. Im, K. Terashima, S. Yagi, M. Kato, K. Soda, T. Ito, and S. Kimura, Appl. Phys. Lett. **96**, 232503 (2010).

[13] K. Y. Ahn and J. C. Suits, IEEE Trans. Magn. **3**, 453–455 (1967).

[14] S. von Molnár and M. W. Shafer, J. Appl. Phys. **41**, 1093–1094 (1970).

[15] K. Y. Ahn, J. Appl. Phys. **43**, 231–232 (1972).

[16] A. A. Samokhvalov, B. A. Gizhevskii, and M. I. Simonova, Sov. Phys. - Solid State **14**, 230–231 (1972).

[17] A. Mauger, C. Godart, M. Escorne, J. C. Achard, and J. P. Desfours, Le J. Phys. **39**, 1125–1133 (1978).

[18] H. Ott, S. Heise, R. Sutarto, Z. Hu, C. Chang, H. Hsieh, H.-J. Lin, C. Chen, and L. Tjeng, Phys. Rev. B **73**, 094407 (2006).

[19] R. Sutarto, S. Altendorf, B. Coloru, M. Moretti Sala, T. Haupricht, C. Chang, Z. Hu, C. Schüßler-Langeheine, N. Hollmann, H. Kierspel, J. Mydosh, H. Hsieh, H.-J. Lin, C. Chen, and L. Tjeng, Phys. Rev. B **80**, 085308 (2009).

[20] T. Mairoser, A. Schmehl, A. Melville, T. Heeg, L. Canella, P. Böni, W. Zander, J. Schubert, D. Shai, E. Monkman, K. Shen, D. G. Schlom, and J. Mannhart, Phys. Rev. Lett. **105**, 257206 (2010).

[21] J. An, S. Barabash, V. Ozolins, M. van Schilfgaarde, and K. Belashchenko, Phys. Rev. B **83**, 064105 (2011).

[22] G. J. McCarthy, J. Am. Ceram. Soc. **57**, 502 (1974).

[23] J. L. G. Fierro, *Metal Oxides: Chemistry and Applications*, p. 298, CRC Press: Boca Raton, FL (2006).

[24] G Brauer, R Müller, and K H Zapp, Zeitschrift Für Anorg. Und Allg. Chemie **280**, (1954).

[25] H. A. Eick, N. C. Baenziger, and L. Eyring, J. Am. Chem. Soc. **78**, 5147–5149 (1956).

[26] T. Mairoser, F. Loder, A. Melville, D. G. Schlom, and A. Schmehl, Phys. Rev. B **87**, 014416 (2013).

[27] J. Lettieri, V. Vaithyanathan, S. K. Eah, J. Stephens, V. Sih, D. D. Awschalom, J. Levy, and D. G. Schlom, Appl. Phys. Lett. **83**, 975–977 (2003).

[28] R. Sutarto, S. Altendorf, B. Coloru, M. Moretti Sala, T. Haupricht, C. Chang, Z. Hu, C. Schüßler-Langeheine, N. Hollmann, H. Kierspel, H. Hsieh, H.-J. Lin, C. Chen, and L. Tjeng, Phys. Rev. B **79**, 205318 (2009).

[29] M. Müller, G.-X. Miao, and J. S. Moodera, J. Appl. Phys. **105**, 07C917 (2009).

[30] T. Santos and J. Moodera, Phys. Rev. B **69**, 241203 (2004).

[31] K. Y. Ahn and G. S. Almasi, IEEE Trans. Magn. **5**, 944–949 (1969).

[32] K. Y. Ahn, J. Appl. Phys. **40**, 3193–3195 (1969).

[33] G. S. Almasi and K. Y. Ahn, J. Appl. Phys. **41**, 1258–1259 (1970).

[34] G. Street, IEEE Trans. Magn. **8**, 45–47 (1972).

[35] H. Miyazaki, T. Ito, S. Ota, H. Im, S. Yagi, M. Kato, K. Soda, and S. Kimura, Phys. B Condens. Matter **403**, 917–918 (2007).

[36] D. E. Shai, A. Melville, J. W. Harter, E. J. Monkman, D. Shen, A. Schmehl, D. G. Schlom, and K. M. Shen, Phys. Rev. Lett. **108**, 267003 (2012).

[37] Köbler, *Vibrationsmagnetometer, Faradaywaage, SQUID und Meßbeispiele*, in *Magnetismus von Festkörpern und Grenzflächen*, Chapter 3, Jülich: Jülich Research Center (1993).

[38] M. Getzlaff, in *Fundamentals of Magnetism,* p. 89-115, New York, New York: Springer (2008).

[39] R. W. Ulbricht, A. Schmehl, T. Heeg, J. Schubert, and D. G. Schlom, Appl. Phys. Lett. **93**, 102105 (2008).

[40] P. W. Anderson, Phys. Rev. **79**, 350–356 (1950).

[41] T. Kasuya, A. Yanase, and T. Takedat, Solid State Commun. **8**, 1543–1546 (1970).

[42] T. Kasuya, IBM J. Res. Dev. **14**, 214–223 (1970).

[43] N. Ingle and I. Elfimov, Phys. Rev. B **77**, 121202 (2008).

[44] A. Mauger and C. Godart, Phys. Rep. **141**, 51–176 (1986).

[45] P. Wachter, CRC Crit. Rev. Solid State Mater. Sci. **3**, 189–241 (1972).

[46] S. J. Cho, Phys. Rev. B **1**, 4589 (1970).

[47] Y. Shapira, S. Foner, and TB Reed, Phys. Rev. B **8**, 2299 (1973).

[48] P. Steeneken, L. Tjeng, I. Elfimov, G. Sawatzky, G. Ghiringhelli, N. Brookes, and D.-J. Huang, Phys. Rev. Lett. **88**, 047201 (2002).

[49] J. Feinleib, WJ Scouler, JO Dimmock, J. Hanus, TB Reed, and CR Pidgeon, Phys. Rev. Lett. **22**, 1385–1388 (1969).

[50] A. Anguelouch, A. Gupta, Gang Xiao, D. Abraham, Y. Ji, S. Ingvarsson, and C. Chien, Phys. Rev. B **64**, 180408 (2001).

[51] T. Mairoser, A. Schmehl, A. Melville, T. Heeg, W. Zander, J. Schubert, D. E. Shai, E. J. Monkman, K. M. Shen, T. Z. Regier, D. G. Schlom, and J. Mannhart, Appl. Phys. Lett. **98**, 102110 (2011).

[52] K. Y. Ahn and M. W. Shafer, J. Appl. Phys. **41**, 1260–1262 (1970).

[53] C. Llinares, J. P. Desfours, J. P. Nadai, C. Godart, A. Percheron, and J. C. Achard, Phys. Status Solidi **25**, 185–192 (1974).

[54] M. Barbagallo, N. Hine, J. Cooper, N.-J. Steinke, A. Ionescu, C. Barnes, C. Kinane, R. Dalgliesh, T. Charlton, and S. Langridge, Phys. Rev. B **81**, 235216 (2010).

[55] K. Y. Ahn, Appl. Phys. Lett. **17**, 347–349 (1970).

[56] K. Lee and J. C. Suits, Phys. Lett. **34A**, 141–142 (1971).

[57] K. Lee and J. C. Suits, IEEE Trans. Magn. **7**, 391 (1971).

[58] P. Liu, J. Tang, J. A. Colón Santana, K. D. Belashchenko, and P. A. Dowben, J. Appl. Phys. **109**, 07C311 (2011).

[59] T. R. McGuire, G. F. Petrich, B. L. Olson, V. L. Moruzzi, and K. Y. Ahn, J. Appl. Phys. **42**, 1775–1777 (1971).

[60] K. Y. Ahn, K. N. Tu, and W. Reuter, J. Appl. Phys. **42**, 1769–1770 (1971).

[61] T. Matsumoto, K. Yamaguchi, M. Yuri, K. Kawaguchi, N. Koshizaki, and K. Yamada, J. Phys. Condens. Matter **16**, 6017–6028 (2004).

[62] J. B. Torrance and M. W. Shafer, Phys. Rev. Lett. **29**, 1168–1171 (1972).

[63] A. Yanase and T. Kasuya, J. Phys. Soc. Japan **25**, 1025–1042 (1968).

[64] H. Miyazaki, T. Ito, H. Im, K. Terashima, S. Yagi, M. Kato, K. Soda, and S. -I. Kimura, Jpn. J. Appl. Phys. **48**, 055504 (2009).

[65] Y. Capiomont, N. V. Dang, O. Massenet, and B. K. Chakraverty, Solid State Commun. **10**, 679–683 (1972).

[66] O. Massenet, Y. Capiomont, and N. V. Dang, J. Appl. Phys. **45**, 3593–3599 (1974).

[67] D. B. McWhan, P. C. Souers, and G. Jura, **143**, 385–389 (1966).

[68] V. G. Tissen and E. G. Ponyatovskil, JETP Lett. **46**, 361–364 (1987).

[69] R. W. Ulbricht, *Growth of EuO Thin Films by Molecular Beam Epitaxy*, The Pennsylvania State University, Doctoral Dissertation (2009).

[70] R. Schiller and W. Nolting, Solid State Commun. **110**, 121–125 (1999).

[71] M. Barbagallo, T. Stollenwerk, J. Kroha, N.-J. Steinke, N. Hine, J. Cooper, C. Barnes, A. Ionescu, P. Monteiro, J.-Y. Kim, K. Ziebeck, C. Kinane, R. Dalgliesh, T. Charlton, and S. Langridge, Phys. Rev. B **84**, 075219 (2011).

[72] D. G. Schlom, L.-Q. Chen, X. Q. Pan, A. Schmehl, and M. A. Zurbuchen, J. Am. Ceram. Soc. **91**, 2429–2454 (2008).

[73] M. P. Warusawithana, C. Richter, J. A. Mundy, P. Roy, J. Ludwig, S. Paetel, T. Heeg, A. A. Pawlicki, L. F. Kourkoutis, M. Zheng, M. Lee, B. Mulcahy, W. Zander, Y. Zhu, J. Schubert, J. N. Eckstein, D. A. Muller, C. S. Hellberg, J. Mannhart, and D. G. Schlom, Nat. Commun. **4**, 2351 (2013).

[74] C. K. O'Sullivan and G. G. Guilbault, Biosens. Bioelectron. **14**, 663–670 (1999).

[75] A. Ichimiya and P. I. Cohen, *Reflection High Energy Electron Diffraction*, Cambridge University Press: Cambridge, United Kingdom (2004).

[76] J. H. Haeni, C. D. Theis, and D. G. Schlom, J. Electroceramics **4**, 385–391 (2000).

[77] J. R. Arthur, J. Appl. Phys. **39**, 4032 (1968).

[78] C Theis and D. G. Schlom, J. Cryst. Growth **174**, 473–479 (1997).

[79] D. G. Schlom, J. H. Haeni, J. Lettieri, C. D. Theis, W. Tian, J .C. Jiang, and X. Q. Pan, Mater. Sci. Eng. B **87**, 282–291 (2001).

[80] K. G. Günther, Naturwissenschaften **45**, 415–416 (1958).

[81] PG Steeneken, *New Light on EuO Thin Films*, Rijksuniversiteit Groningen, Doctoral Dissertation (2002).

CHAPTER 2

LUTETIUM-DOPED EUO FILMS GROWN BY MOLECULAR-BEAM EPITAXY

Originally published in Applied Physics Letters, Volume 100, 222101 (2012)

A. Melville,[1] T. Mairoser,[2] A. Schmehl,[2] D.E. Shai,[3] E.J. Monkman,[3] J.W. Harter,[3] T. Heeg,[1] B. Holländer,[4] J. Schubert,[4] K.M. Shen,[3,5] J. Mannhart,[6] and D.G. Schlom[1,5]

[1]*Department of Materials Science and Engineering, Cornell University, Ithaca, New York 14853, USA*

[2]*Zentrum für elektronische Korrelationen und Magnetismus, Universität Augsburg, Universitätsstraße 1, D-86159 Augsburg, Germany*

[3]*Laboratory of Atomic and Solid State Physics, Department of Physics, Cornell University, Ithaca, New York 14853, USA*

[4]*Peter Grünberg Institute, PGI 9-IT, JARA-FIT, Research Centre Jülich, D-52425 Jülich, Germany*

[5]*Kavli Institute at Cornell for Nanoscale Science, Ithaca, New York, 14853, USA*

[6]*Max Planck Institute for Solid State Research, D-70569 Stuttgart, Germany*

The effect of lutetium doping on the structural, electronic, and magnetic properties of epitaxial EuO thin films grown by reactive molecular-beam epitaxy is experimentally investigated. The behavior of Lu-doped EuO is contrasted with doping by lanthanum and gadolinium. All three dopants are found to behave similarly despite differences in

electronic configuration and ionic size. Andreev reflection measurements on Lu-doped EuO reveal a spin-polarization of 96% in the conduction band, despite non-magnetic carriers introduced by 5% lutetium doping.

The ferromagnetic half-metal europium oxide (EuO) has potential for spin-based devices like spin-injectors based on its >90% spin-polarization[1] or optical devices based on its giant magneto-optic Kerr effect[2] and a Faraday rotation of 8.5×10^5 deg/cm in a field of 2 T.[3] Its low Curie temperature (T_C = 69 K),[4] however, impedes the incorporation of EuO into devices.

The T_C of EuO can be increased by doping it with electrons. The interaction between the Eu *f*-electrons and the dopant electrons enhances the ferromagnetic exchange energy[4,5] and results in an increased T_C. To date this has been accomplished through the use of trivalent cations including iron,[6–8] lanthanum,[1,9,10] gadolinium,[11–17] and holmium.[9] Alternatively the T_C can be increased by deliberately making oxygen-deficient EuO such that the resulting oxygen vacancies donate an electron.[6,18–22] In the cation-doped EuO films an unknown and uncontrolled concentration of oxygen vacancies is often included, which may be responsible for the disparate results for the dependence of T_C on cation doping. For example, in films doped with gadolinium, the maximum reported T_C varies between 120 K (Ref. 15) and 170 K.[14] Films doped with lanthanum have a maximum reported T_C between 118 K (Ref. 1) and 200 K.[10] Likewise, for films doped with iron, the reported T_C varies between 88 K and 200 K.[6,7] For Gd-doped films grown in an adsorption-controlled regime, however, the Curie temperatures are consistent and similar,[15,16] conceivably due to a minimized amount of oxygen vacancies realized in this particular growth regime.[23] In this Letter we report the behavior of an unexplored dopant for EuO, lutetium, which enhances the T_C in epitaxial films grown in an adsorption-controlled regime. We contrast the magnetic and electronic properties of

EuO doped with lanthanum, gadolinium, and lutetium when grown under identical adsorption-controlled growth conditions.

Doped EuO thin films were grown directly on (110) $YAlO_3$ substrates via reactive oxide molecular-beam epitaxy (Veeco 930 and Gen10) in an adsorption-controlled growth regime at a substrate temperature of 350°C to ensure high crystalline quality and stoichiometric films.[17,23] Pure oxygen gas was introduced during growth to a background oxygen partial pressure of 1×10^{-9} Torr above the base pressure of the vacuum system. In the adsorption-controlled regime, the oxygen flux limits the EuO growth rate if the incident flux of europium metal is greater than the effective oxygen flux. The adsorption-controlled growth regime and the growth rate of EuO were determined by measuring the areal density of Eu atoms in calibration EuO samples using Rutherford backscattering spectrometry (RBS).[23] Each film was nominally 35 nm thick, but the uncertainty in the exact oxygen flux during each growth corresponds to roughly 10% variability in the EuO growth rate and therefore the thickness. Europium and the dopant were codeposited from separate effusion cells. Prior to growth, the europium flux was calibrated using a quartz crystal microbalance (QCM) to a flux of 1.1×10^{14} atoms/ (cm^2□s). This flux was 100% higher than the rate at which europium was incorporated into the EuO film. The lanthanum, gadolinium, and lutetium fluxes were calibrated by a QCM to correspond to 4% doping of the EuO for the films characterized by *in situ* X-ray photoelectron spectroscopy (XPS) measurements and 5% for the films characterized *ex situ*.

Several films were transferred under ultra-high vacuum immediately after growth into an

analysis chamber for XPS characterization using Mg K_α radiation (1253.6 eV). The remaining films were capped with 20 nm of amorphous silicon to protect the films from further oxidation during their *ex situ* characterization. Structural characterization was performed using four-circle X-ray diffraction (XRD) utilizing Cu K_α radiation. The T_C was determined using superconducting quantum-interference-device (SQUID) magnetometry. The films were measured in zero field after applying a demagnetization routine at 300 K to minimize the spurious magnetic fields originating from parts of the SQUID.[16] At this temperature the EuO is in the paramagnetic state without oriented ferromagnetic domains. Bridges were patterned into the doped EuO films using photolithography in combination with *in situ* ion etching and sputter deposition.[16] Bridges 1 mm × 0.1 mm in size were used for four-point resistivity measurements from 4 K to 300 K and Hall measurements at 4 K, and bridges 50 μm × 250 μm in size were used across a ramp-type junction between superconducting niobium and metallic Lu-doped EuO for differential four-point conductivity measurements for Andreev reflection from 1.8 K to 12 K.

The effect of the three dopants on the crystallinity of the epitaxial doped EuO films was assessed by XRD. Figure 2-1 shows the θ-2θ XRD patterns of typical EuO films doped with 5% lanthanum, gadolinium, or lutetium. All samples exhibit only 00ℓ EuO peaks in addition to the substrate peaks. XRD rocking curves show the full width at half maximum (FWHM) of the EuO 002 peaks to be 0.16 ± 0.01° for all samples. These data indicate that the doped EuO samples are structurally indistinguishable by XRD.

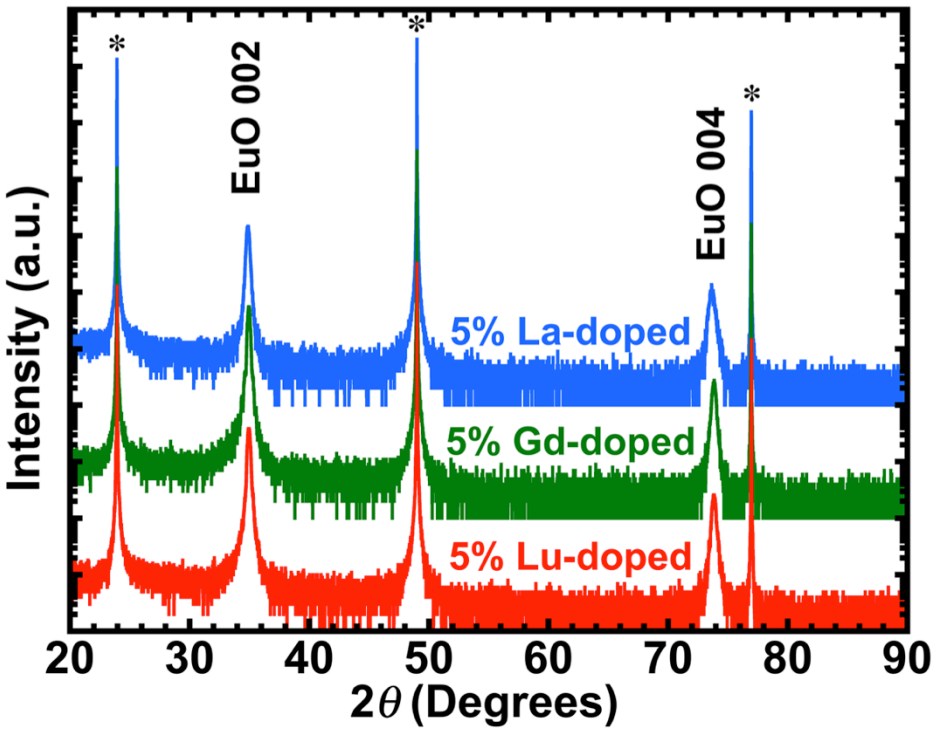

Figure 2-1: *θ*-2*θ* scans comparing epitaxial EuO films with 5% lanthanum-doping (blue), 5% gadolinium-doping (green), and 5% lutetium-doping (red). All three films are phase-pure with no indication of dopant insolubility. The curves are offset for clarity and the substrate peaks are marked with asterisks.

SQUID magnetometry reveals the T_C of the 5% doped films to be similar. La-doped EuO has T_C = 116 K; Gd-doped EuO has T_C = 122 K; and Lu-doped EuO has T_C = 119 K as seen in Figure 2-2(a). The observed kink in the Lu-doped EuO (and to a lesser extent, the La-doped EuO) could be consistent with clustering of dopants in the film.[10] The temperature dependence of the resistivity for the same samples is shown in Figure 2-2(b). Hall measurements for these samples reveal that Gd-doped EuO has the highest carrier concentration with $n = 5 \times 10^{20}$ cm^{-3} followed by both the La- and the Lu-doped EuO with carrier concentrations of $n = 2.1 \times 10^{20}$ cm^{-3} and $n = 1.8 \times 10^{20}$ cm^{-3}, respectively. The difference in T_C and carrier concentration is within the accuracy of our doping level control, the accuracy of the film thickness, and the strong dependence of dopant activation on substrate temperature.[1]

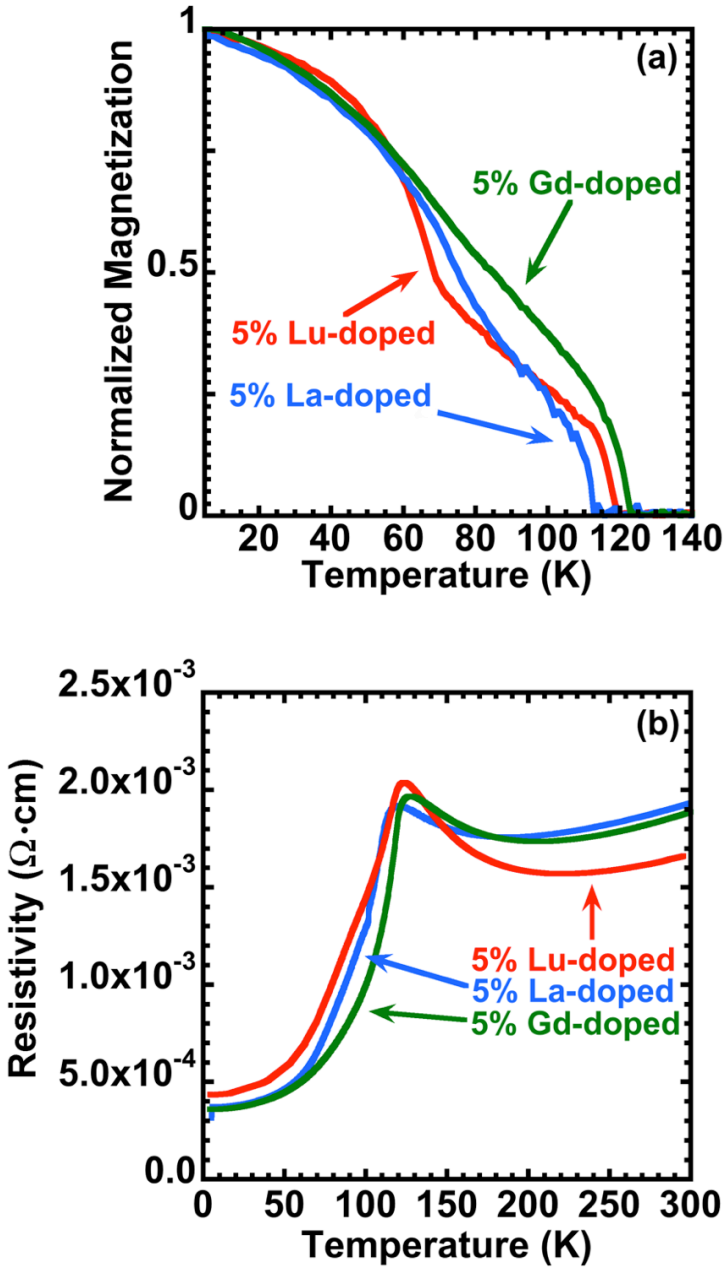

Figure 2-2: (a) Normalized magnetization as a function of temperature of the same three samples studied in Figure 2-1. All three dopants increase the T_C to approximately the same value at 5% doping concentration. (b) Resistivity as a function of temperature for the same three samples. Doped EuO exhibits reduced resistivity and a reduced metal-to-insulator transition compared to undoped EuO. The change in resistivity is comparable regardless of dopant choice.

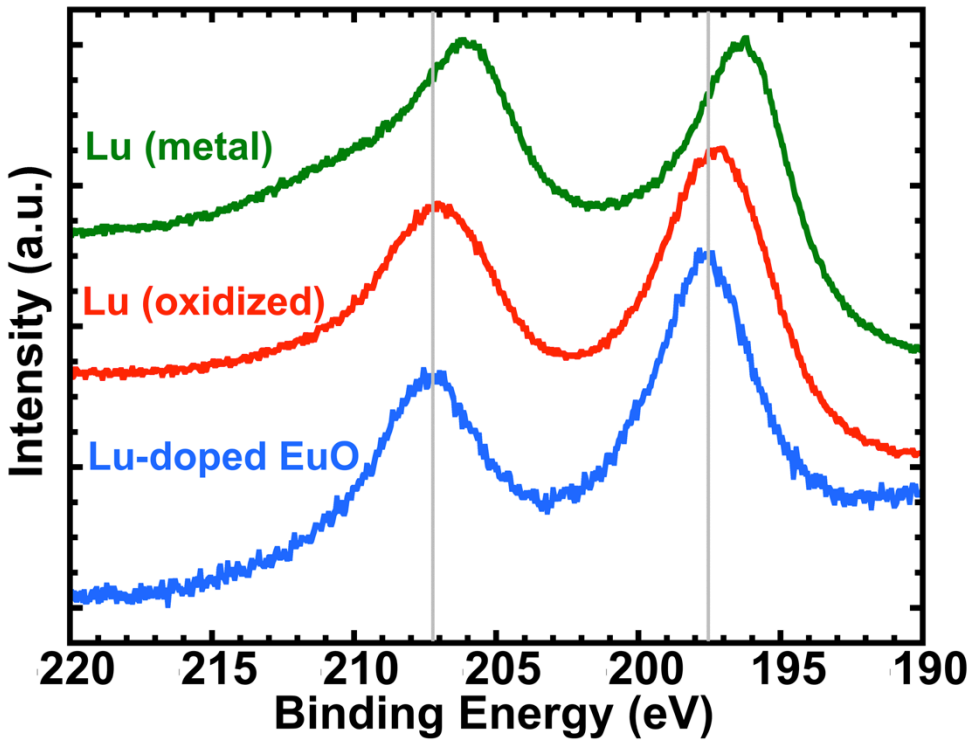

Figure 2-3: Comparison of X-ray photoemission intensity of the lutetium 4d core-level multiplets between 4% Lu-doped EuO (blue), lutetium metal (green), and oxidized lutetium (red). The dashed lines are guides for the eye to highlight the similarity in peak position between the 4% Lu-doped EuO and the oxidized lutetium.

XAS was used to verify the 3^+ oxidation state of the gadolinium in the Gd-doped EuO films[17] and XPS was used to verify the 3^+ oxidation state of the lanthanum and lutetium in the La- and Lu-doped EuO films, respectively. XAS and XPS were also used to confirm that the oxidation state of Eu is nearly completely Eu^{2+}, with a small amount of Eu^{3+} attributed to surface oxidation in uncapped samples as documented in the Supplementary Information of Ref. 16. Figure 2-3 shows the XPS intensity of the lutetium 4d core-level multiplets for the lutetium in Lu-doped EuO, lutetium metal, and Lu_2O_3. Lutetium metal was deposited at room temperature in vacuum by MBE, and Lu_2O_3 was formed by keeping the lutetium metal in vacuum with a background pressure of 2×10^{-9} Torr for at least one hour. Comparing the peak positions to the literature[24] confirmed that the lutetium in the Lu-doped EuO film was indeed 3^+ as expected. A

similar process was followed for identifying the oxidation state of lanthanum in the La-doped EuO. From the free carrier concentration, oxidation state, and the doping concentration, it is evident rare-earth dopant ions inject far less than one mobile electron into the EuO conduction band. The dopant activation is less than 40%, in agreement with results for Gd-doped EuO,[16] pointing to the possible ubiquity of the challenge of achieving high dopant activation in EuO. All samples have comparable resistivity curves, reduced dopant activation, and fairly similar carrier concentrations.

Differential conductance measurements were performed on 5% Lu-doped EuO and are shown in Figure 2-4. Since Andreev reflection is suppressed at the interface between a material with high spin-polarization and a superconducting material, a drop in conductivity across the Lu-doped EuO / Nb interface for energies less than the superconducting gap of the niobium film at temperatures below the superconducting critical temperature is expected. By fitting the drop in conductance to the Blonder-Tinkham-Klapwijk model[25] that has been modified specifically for non-negligible series resistance in spin-polarized ferromagnetic semiconductor devices,[26–28] one can extract the spin-polarization value. The best fit is in accordance with a spin-polarization of 96%, which is in agreement with previous reports of the near-complete spin-polarization of EuO.[1] The high spin-polarization despite 5% doping of nonmagnetic atoms is critically important, as it shows that EuO retains its high spin-polarization in the presence of a dopant which significantly boosts its T_C. This is not so surprising given that doped EuO is a half-metal due to the spin-splitting of the conduction band,[29–31] so the carriers are spin-polarized anyway despite the nature of the dopant.

Figure 2-4: Andreev reflection measurements of the contact between a niobium electrode and the same 5% Lu-doped sample studied in Figures 2-1 and 2-2. (a) Conductance vs. voltage characteristics were measured at different temperatures. Below the superconducting gap of the niobium electrode the conductance diminishes because Andreev reflection is forbidden for an interface between a 100% spin-polarized material and a superconductor. The inset shows a schematic of the ramp-type junction used for differential four-point conductivity measurements. (b) Fits to the 1.8 K measurement using the Blonder-Tinkham-Klapwijk model are in accordance with a spin-polarization of 96% (green). For comparison, fits are shown that fix P to 94% (blue) and to 98% (red). The inset shows the overlap of the curves near zero voltage bias to better illustrate the match of the best fit. The best fit parameters were Z = 0.9, Δ = 1.28 meV, R = 77, and P = 96%.

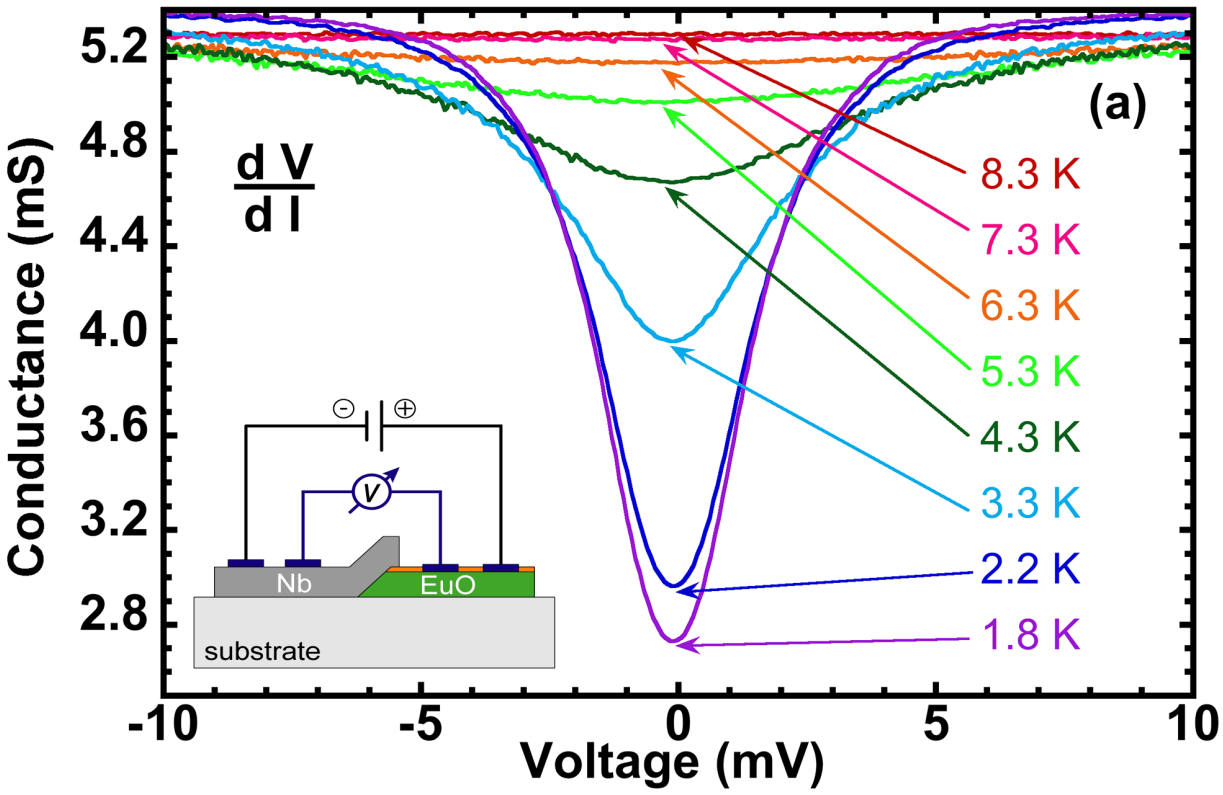
(a)
dV/dI
Conductance (mS)
5.2
4.8
4.4
4.0
3.6
3.2
2.8
8.3 K
7.3 K
6.3 K
5.3 K
4.3 K
3.3 K
2.2 K
1.8 K
Nb
EuO
substrate
V
-10
-5
0
5
10
Voltage (mV)

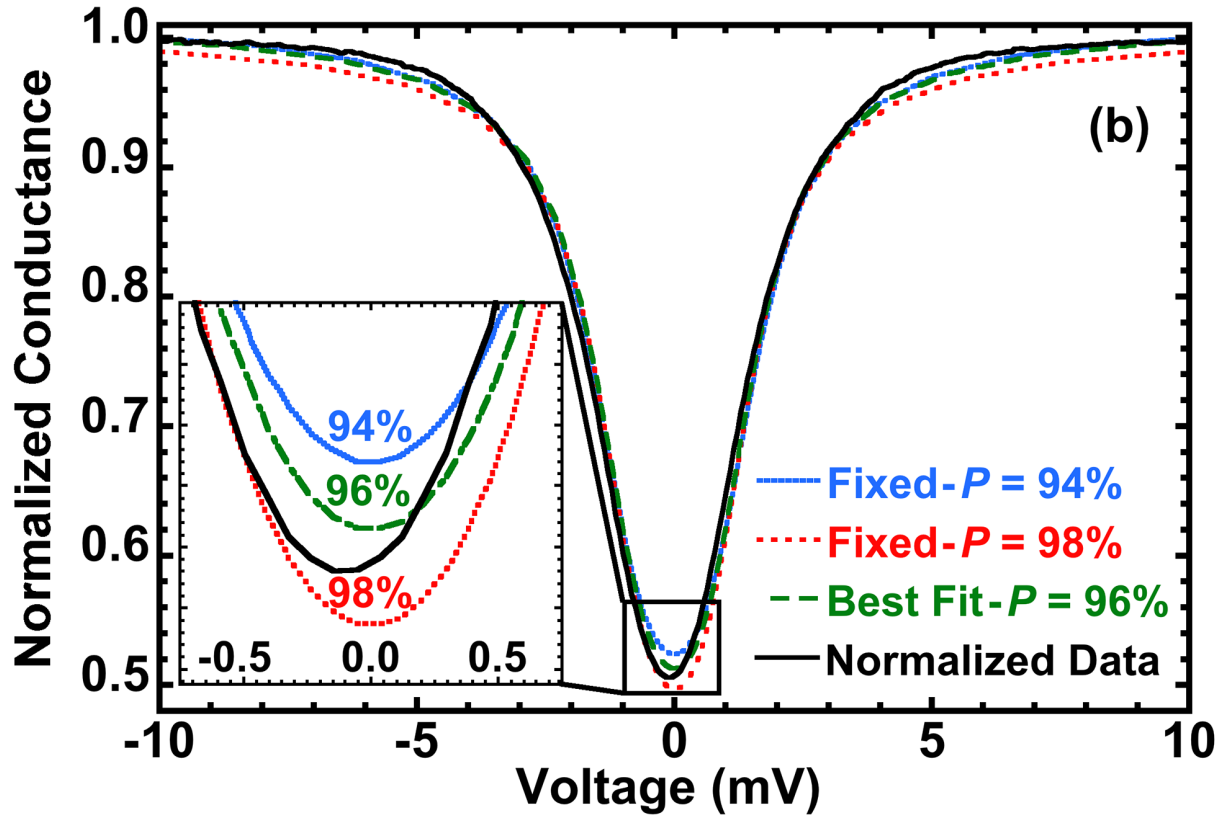
(b)
Normalized Conductance
1.0
0.9
0.8
0.7
0.6
0.5
94%
96%
98%
-0.5
0.0
0.5
Fixed-P = 94%
Fixed-P = 98%
Best Fit-P = 96%
Normalized Data
-10
-5
0
5
10
Voltage (mV)

In summary, we have explored the properties of Lu-doped EuO. Lutetium donates electrons to EuO in the same fashion as lanthanum and gadolinium dopants. Furthermore, EuO retains near-complete spin-polarization (P = 96%) despite being heavily doped with the non-magnetic ion Lu^{3+}.

The work at Cornell was supported by the AFOSR (Grant No. FA9550-10-1-0123), the NSF MRSEC program by cooperative agreement 1120296, and NSF DMR-0847385, and a Cottrell Scholars Award (20025). The work in Augsburg was supported by the DFG (Grant No. TRR 80) and the EC (oxIDes). AM gratefully acknowledges support from the NSF IGERT program (NSF Award DGE-0654193) and by the IMI Program of the National Science Foundation under Award No. DMR 0843934. EJM acknowledges NSERC for PGS support.

REFERENCES

[1] A. Schmehl, V. Vaithyanathan, A. Herrnberger, S. Thiel, C. Richter, M. Liberati, T. Heeg, M. Röckerath, L. F. Kourkoutis, S. Mühlbauer, P. Böni, D. A. Muller, Y. Barash, J. Schubert, Y. Idzerda, J. Mannhart, and D. G. Schlom, Nat. Mater. **6**, 882–887 (2007).

[2] J. C. Suits and K. Lee, J. Appl. Phys. **42**, 3258–3260 (1971).

[3] K. Y. Ahn and M. W. Shafer, J. Appl. Phys. **41**, 1260–1262 (1970).

[4] T. R. McGuire and M. W. Shafer, J. Appl. Phys. **35**, 984–988 (1964).

[5] F. Holtzberg, T. R. McGuire, and S. Methfessel, Phys. Rev. Lett. **13**, 18–21 (1964).

[6] K. Lee and J. C. Suits, Phys. Lett. **34A**, 141–142 (1971).

[7] T. R. McGuire, G. F. Petrich, B. L. Olson, V. L. Moruzzi, and K. Y. Ahn, J. Appl. Phys. **42**, 1775–1777 (1971).

[8] K. Y. Ahn, K. N. Tu, and W. Reuter, J. Appl. Phys. **42**, 1769–1770 (1971).

[9] M. W. Shafer and T. R. McGuire, J. Appl. Phys. **39**, 588–590 (1968).

[10] H. Miyazaki, H. J. Im, K. Terashima, S. Yagi, M. Kato, K. Soda, T. Ito, and S. Kimura, Appl. Phys. Lett. **96**, 232503 (2010).

[11] S. von Molnár and M. W. Shafer, J. Appl. Phys. **41**, 1093–1094 (1970).

[12] A. A. Samokhvalov, B. A. Gizhevskii, and M. I. Simonova, Sov. Phys. - Solid State **14**, 230–231 (1972).

[13] A. Mauger, C. Godart, M. Escorne, J. C. Achard, and J. P. Desfours, Le J. Phys. **39**, 1125–1133 (1978).

[14] H. Ott, S. Heise, R. Sutarto, Z. Hu, C. Chang, H. Hsieh, H.-J. Lin, C. Chen, and L. Tjeng, Phys. Rev. B **73**, 094407 (2006).

[15] R. Sutarto, S. Altendorf, B. Coloru, M. Moretti Sala, T. Haupricht, C. Chang, Z. Hu, C. Schüßler-Langeheine, N. Hollmann, H. Kierspel, J. Mydosh, H. Hsieh, H.-J. Lin, C. Chen, and L. Tjeng, Phys. Rev. B **80**, 085308 (2009).

[16] T. Mairoser, A. Schmehl, A. Melville, T. Heeg, L. Canella, P. Böni, W. Zander, J. Schubert, D. Shai, E. Monkman, K. Shen, D. G. Schlom, and J. Mannhart, Phys. Rev. Lett. **105**, 257206 (2010).

[17] T. Mairoser, A. Schmehl, A. Melville, T. Heeg, W. Zander, J. Schubert, D. E. Shai, E. J. Monkman, K. M. Shen, T. Z. Regier, D. G. Schlom, and J. Mannhart, Appl. Phys. Lett. **98**, 102110 (2011).

[18] K. Lee and J. C. Suits, IEEE Trans. Magn. **7**, 391 (1971).

[19] Y. Capiomont, Nguyen-Van-Dang, O. Massenet, and B. K. Chakraverty, Solid State Commun. **10**, 679–683 (1972).

[20] O. Massenet, Y. Capiomont, and N. Van Dang, J. Appl. Phys. **45**, 3593–3599 (1974).

[21] H. Miyazaki, T. Ito, H. Im, K. Terashima, S. Yagi, M. Kato, K. Soda, and S. -I. Kimura, Jpn. J. Appl. Phys. **48**, 055504 (2009).

[22] M. Barbagallo, N. Hine, J. Cooper, N.-J. Steinke, A. Ionescu, C. Barnes, C. Kinane, R. Dalgliesh, T. Charlton, and S. Langridge, Phys. Rev. B **81**, 235216 (2010).

[23] R. W. Ulbricht, A. Schmehl, T. Heeg, J. Schubert, and D. G. Schlom, Appl. Phys. Lett. **93**, 102105 (2008).

[24] W. C. Lang, B. D. Padalia, L. M. Watson, D. J. Fabian, and P. R. Norris, Faraday Discuss. Chem. Soc. **60**, 37–43 (1975).

[25] G. E. Blonder, M. Tinkham, and T. M. Klapwijk, Phys. Rev. B **25**, 4515–4532 (1982).

[26] S. Upadhyay, A. Palanisami, R. N. Louie, and R. A. Buhrman, Phys. Rev. Lett. **81**, 3247–3250 (1998).

[27] R. J. Soulen Jr., Science (80-.). **282**, 85–88 (1998).

[28] I. I. Mazin, Phys. Rev. Lett. **83**, 1427–1430 (1999).

[29] S. Von Molnár, IBM J. Res. Dev. **14**, 269–275 (1970).

[30] M. R. Oliver, J. O. Dimmock, and T. B. Reed, IBM J. Res. Dev. **14**, 276–278 (1970).

[31] P. Steeneken, L. Tjeng, I. Elfimov, G. Sawatzky, G. Ghiringhelli, N. Brookes, and D.-J. Huang, Phys. Rev. Lett. **88**, 047201 (2002).

CHAPTER 3

EFFECT OF FILM THICKNESS AND BIAXIAL STRAIN ON THE CURIE TEMPERATURE OF EUO

Originally published in Applied Physics Letters, Volume 102, 062404 (2013)

A. Melville,[1] T. Mairoser,[2] A. Schmehl,[2] T. Birol,[3] T. Heeg,[4] B. Holländer,[4] J. Schubert,[4] C. J. Fennie,[3] and D.G. Schlom[1,5]

[1]*Department of Materials Science and Engineering, Cornell University, Ithaca, New York 14853, USA*

[2]*Zentrum für elektronische Korrelationen und Magnetismus, Universität Augsburg, Universitätsstraße 1, 86159 Augsburg, Germany*

[3]*School of Applied and Engineering Physics, Cornell University, Ithaca, New York 14853, USA*

[4]*Peter Grünberg Institute, PGI 9-IT, JARA-FIT, Research Centre Jülich, D-52425 Jülich, Germany*

[5]Kavli *Institute at Cornell for Nanoscale Science, Ithaca, New York, 14853, USA*

The effects of film thickness and epitaxial strain on the magnetic properties of commensurate EuO thin films grown on single crystalline (001) yttria-stabilized zirconia (YSZ) and (110) $LuAlO_3$ substrates are presented. Magnetic measurements show a

reduction in the Curie temperature (T_C) for EuO / YSZ films thinner than ~10 nm. Additionally, the EuO / $LuAlO_3$ films exhibit a systematically lower T_C than the corresponding EuO / YSZ films. This further reduction in T_C is attributed to the effect of biaxial tensile strain arising from lattice mismatch: 0.0% for EuO / YSZ and +1.0% for EuO / $LuAlO_3$.

Europium oxide (EuO) has a rocksalt structure (a = 5.144 Å)[1] with Eu^{2+} cations whose half-filled 4*f* orbital is responsible for a large ferromagnetic response below its Curie temperature (T_C) of 69 K.[2] This pronounced ferromagnetism induces a metal-to-insulator transition spanning up to 13 orders of magnitude in resistivity[3] and spin-polarization of 96%,[4] as a result of conduction band splitting by 0.6 eV.[5,6] This makes EuO exceptional and of interest for spintronic applications.

The low bulk T_C restricts the utilization of EuO in device applications, so overcoming this limitation is one of the key challenges yet to be addressed. Theoretical predictions indicate that the T_C can be manipulated by injecting electrons into the system[7] or by straining the crystal.[8] The added electrons enhance the T_C by filling the spin-polarized conduction band, thus adding to the magnetic exchange energy of the system. In fact, doping with 3^+ cations like lanthanum,[9–11] gadolinium,[9,12–15] or oxygen vacancies[3,9,16–18] is a common technique for injecting electrons, increasing the T_C up to a maximum reported value of 200 K.[11,19] The strain-induced T_C manipulation is driven by altering the distance between the magnetic 4*f* electrons relative to the bulk spacing. Increasing this distance leads to a reduced T_C, while reducing this distance causes an enhanced T_C. In thin films biaxial strain can be achieved via commensurate, epitaxial growth to a well-chosen substrate with a specific lattice mismatch.

In this Letter we contrast the dependence of the magnetic properties on thickness in a series of strain-free epitaxial EuO films with that of +1% biaxially-strained epitaxial EuO films to determine the effect of strain on T_C. The unstrained films were grown on (001)

9.5 mol % yttria-stabilized cubic zirconia (YSZ). YSZ is nearly lattice-matched to EuO with a lattice constant of 5.140 Å.[20] The epitaxial orientation relationship is cube-on-cube with (001) EuO || (001) YSZ and [100] EuO || [100] YSZ. For comparison, strained EuO films were grown on (110) $LuAlO_3$. $LuAlO_3$ is an orthorhombic perovskite similar to $YAlO_3$, and the (110) surface has a rectangular surface net with in-plane lattice constants of 7.379 Å along the [$1\bar{1}0$] direction and 7.300 Å along the [001] direction.[21] The expected epitaxial orientation relationship is (001) EuO || (110) $LuAlO_3$ with [$1\bar{1}0$] EuO || [001] $LuAlO_3$ and [110] EuO || [$1\bar{1}0$] $LuAlO_3$, with a linear lattice mismatch of +0.4% and +1.5% along the EuO [110] and [$1\bar{1}0$] directions, respectively.

All films were grown in a Veeco Gen10 molecular-beam epitaxy chamber with a chamber background pressure of ~2×10^{-9} Torr. The EuO films on YSZ were grown at a substrate temperature of 400ºC after annealing the substrates at 650ºC in an oxygen background partial pressure of 3×10^{-7} Torr prior to growth to form a well-ordered surface.[22] For films thicker than 10 nm, the EuO films on $LuAlO_3$ were grown at 550°C.[23] For films thinner than 10 nm, the EuO films on $LuAlO_3$ were grown at 400ºC, to match the growth conditions to the films grown on YSZ. All films were grown within an adsorption-controlled growth regime.[23] During growth oxygen was introduced yielding a chamber background pressure of less than 1×10^{-8} Torr. The incident flux of europium atoms was calibrated to 1.1×10^{14} atoms / (cm^2 s) using a quartz crystal microbalance, approximately 20% higher than the EuO growth rate, which had been determined earlier from areal density measurements of the europium content of calibration samples using Rutherford backscattering spectrometry (RBS). Growth under europium-excess

conditions is key to the adsorption-controlled deposition of EuO. The samples were capped with 30 nm of amorphous silicon or 100 nm of aluminum immediately after growth to prevent further oxidation during *ex situ* characterization. A series of films with thicknesses varying from 1.5 nm to 170 nm (as measured by RBS) were grown both on YSZ and $LuAlO_3$ substrates. Structural measurements were made using a four-circle X-ray diffractometer (XRD) equipped with Cu K_α radiation. Magnetic measurements were performed using superconducting quantum interference device (SQUID) magnetometry. SQUID measurements to determine TC were made in zero applied field for all samples.[24]

The θ-2θ scan of a 40 nm thick EuO film grown on YSZ, Figure 3-1(a), exhibits only peaks at 2θ = 34.9º and 73.8º, consistent with the growth of phase-pure epitaxial EuO. The complete overlap of film and substrate peaks occurs because EuO and YSZ both have face-centered cubic lattices with nearly identical parameters (a_{YSZ} = 5.140 Å[20] and a_{EuO} = 5.144 Å[1]). These features were observed for all EuO / YSZ films. The θ-2θ scan of a 170 nm thick EuO / $LuAlO_3$ film is shown in Figure 3-1(b) and reveals only substrate peaks and 00ℓ EuO peaks, as did all EuO / $LuAlO_3$ films included in this study, indicating that these samples are also phase-pure within the resolution of our XRD measurements. Figure 3-1(c) shows a ϕ-scan of the 111 off-axis EuO peaks of the same film studied in Figure 3-1(b), which, together with the θ-2θ scan, confirm the epitaxy of EuO on $LuAlO_3$ with an orientation relationship of [110] (001) EuO || [1$\bar{1}$0] (110) $LuAlO_3$.

Figure 3-1: θ-2θ scans of (a) 40 nm thick EuO / YSZ and (b) 170 nm thick EuO / $LuAlO_3$ films. Both scans reveal phase-pure EuO with no indication of Eu metal, Eu_3O_4, or Eu_2O_3, and are characteristic of all EuO films grown in this study. (c) ϕ-scan of 111 EuO diffraction peaks of the same film studied in Figure 3-1(b) at χ = 35.3° showing the epitaxial relationship of EuO on $LuAlO_3$ to be $[1\bar{1}0](001)$ EuO || [001](110) $LuAlO_3$. χ = 90° aligns the diffraction vector perpendicular to the plane of the substrate. ϕ = 45° is aligned to be parallel to the [001] in-plane direction of the (110) $LuAlO_3$ substrate. (Ref. 38).

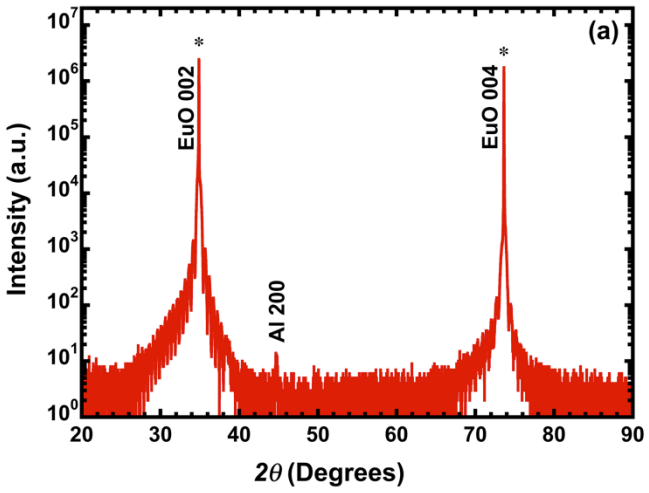
(a)
EuO 002
Al 200
EuO 004
Intensity (a.u.)
2θ (Degrees)

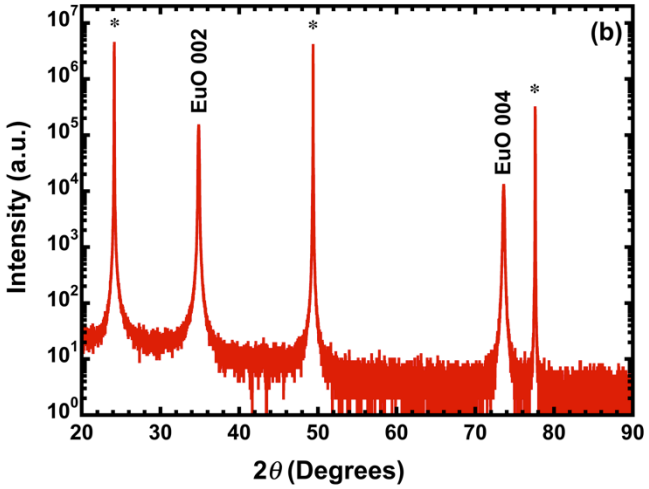
(b)
EuO 002
EuO 004
Intensity (a.u.)
2θ (Degrees)

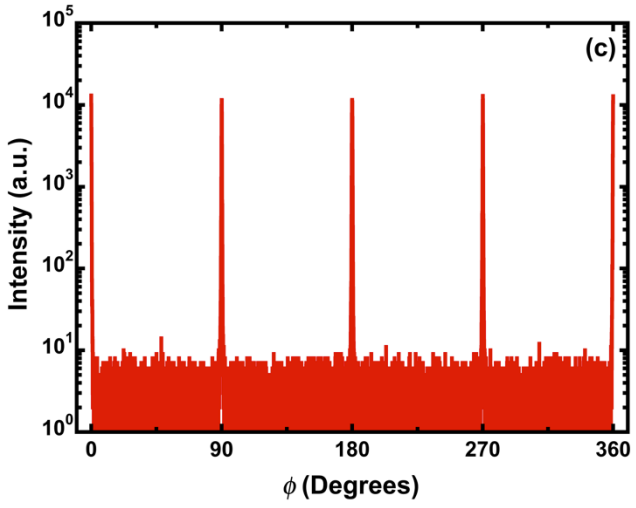
(c)
Intensity (a.u.)
ϕ (Degrees)

The interplanar spacings of the (110) and ($1\bar{1}0$) planes of a strained EuO film were calculated from the measured θ-2θ positions of multiple reflections from the (001), (111), and ($1\bar{1}1$) planes of a 10 nm thick film. The lattice spacing along [110] EuO was 3.694 ± 0.005 Å and the lattice spacing along [$1\bar{1}0$] EuO was 3.652 ± 0.005 Å, which match the $d_{2\bar{2}0}$ and d_{002} interplanar spacings of the $LuAlO_3$ substrate within experimental error. The out-of-plane spacing was 5.123 ± 0.005 Å, which agrees with the expected value (5.122 Å) based on the biaxial strain and the elastic constants of EuO.[25] These results indicate that the EuO films up to 10 nm in thickness are commensurately strained to the underlying substrate.

Rocking curves of the 002 EuO diffraction peak were taken by rocking the substrate

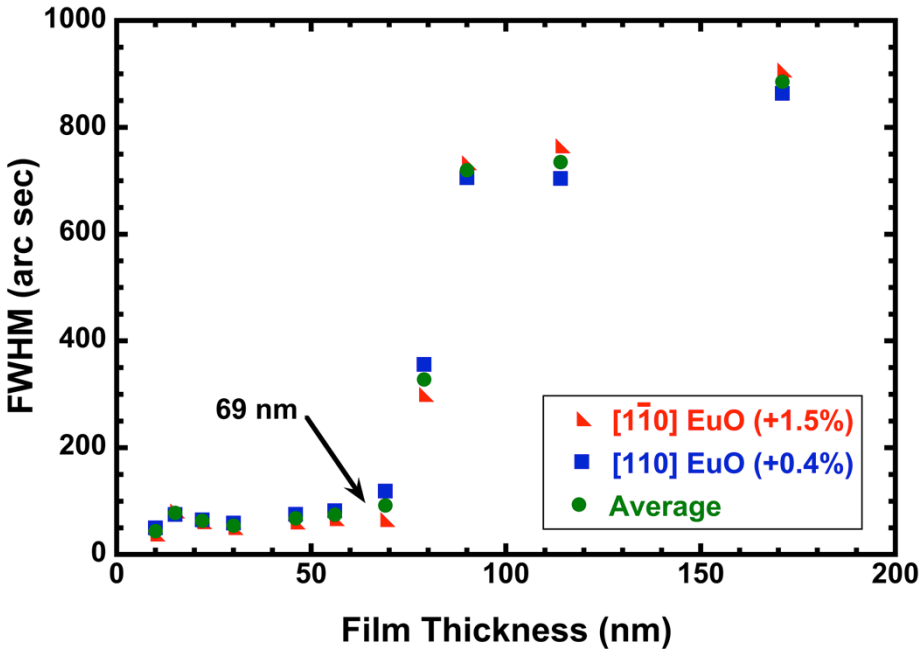

Figure 3-2: The FWHM of the EuO 002 rocking curves made by rocking about both the [110] high strain (red triangles) and [110] low strain (blue squares) substrate axes plotted as a function of thickness of the EuO / $LuAlO_3$ films. The average FWHM (green circles) is also plotted. The arrow indicates the critical thickness for distinguishable relaxation, 69 ± 5 nm.

along its [1$\bar{1}$0] and [001] axes because the film strain is different along these two substrate directions. In Figure 3-2, the full width at half maximum (FWHM) of the EuO films along these directions is plotted as a function of film thickness. The FWHM of the substrates ranged from 25 to 37 arc sec. The FWHM for the thin films was as low as 38 arc sec, with a dramatic increase in FWHM for films thicker than 69 nm. This broadening of the rocking curve is attributed to film relaxation via the introduction of stress-reducing defects, e.g., dislocations.[26–28] The critical thickness for the onset of observable relaxation in epitaxial EuO on (110) $LuAlO_3$ using our growth conditions is thus 69 ± 5 nm. This is nearly twice the critical thickness reported for EuO films grown commensurately under similar growth conditions on (110) $YAlO_3$ (38 nm),[23] which has an average lattice mismatch that is nearly twice that of $LuAlO_3$ (+1.8%). Additionally, the onset of relaxation for EuO / $LuAlO_3$ is the same along both the [1$\bar{1}$0] and [001] in-plane directions of the substrate, despite a difference in in-plane strain of more than 1%. This indicates that the relaxation mechanism for the two directions is coupled.

Figure 3-3 compares the Curie temperatures of these epitaxial EuO films as a function of thickness on both YSZ and $LuAlO_3$ substrates. The YSZ series explores the effect of film thickness in unstrained epitaxial EuO. The T_C is reduced below a film thickness of ~10 nm, which is expected because of too few neighboring magnetic atoms[29,30] and consistent with other reports that describe a reduced T_C below a thickness of 4-10 nm in polycrystalline EuO films.[30–32] Furthermore, the reduction in T_C matches both the prediction of the theory by Schiller *et al.*,[29] and mean-field approximation considering nearest neighbors and next-nearest neighbors for films thicker than 5 nm.[30,32] These calculations are plotted alongside the data in Figure 3-3.

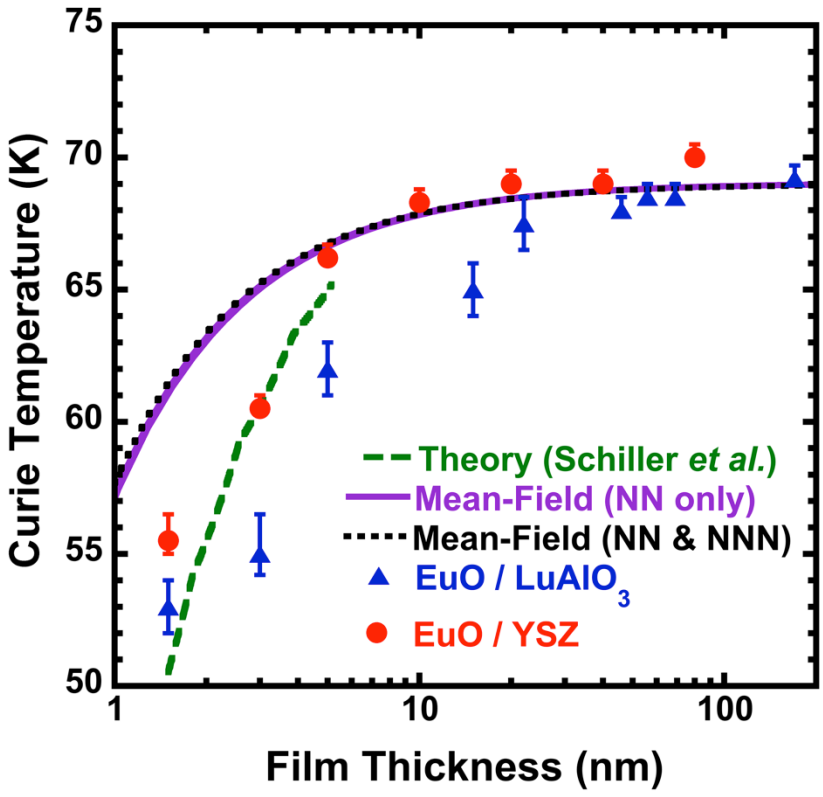

Figure 3-3: The Curie temperature as a function of film thickness is compared for EuO / YSZ (red circles) and EuO / $LuAlO_3$ (blue triangles). The T_C is reduced below the bulk T_C of 69 K for films thinner than 10 nm for EuO / YSZ as a result of size effects. The T_C of EuO / $LuAlO_3$ is lower than the T_C of EuO / YSZ for films below the critical thickness for relaxation on $LuAlO_3$, about 69 nm. Films thicker than this exhibit a T_C that asymptotes to the bulk T_C of unstrained EuO (69 K). The theory presented by Schiller *et al.* (Ref. 29) is displayed by the dashed green line; the mean-field approximation considering only nearest neighbors (NN) is displayed by the solid purple line (Ref. 32), and the mean-field approximation considering both nearest neighbors and next-nearest neighbors (NNN) is displayed by the dotted black line (Ref. 30).

To predict the effect of biaxial strain on the T_C of an epitaxial (001) EuO film commensurately grown on a (110) $LuAlO_3$ substrate, we performed first principles calculations using density functional theory (DFT) as implemented in VASP.[33] The generalized gradient approximation[34] together with an on-site Coulomb energy (GGA+U) formalism was used in order to better take into account the localized nature of the *f* electrons. An external pressure was applied during the relaxation of the crystal

structure in order to correct for the overestimation of volume by GGA. The pressure required was determined by calculations for bulk EuO with cubic symmetry. The pressure value obtained from these calculations was applied during subsequent calculations in which biaxial strain was imposed on the EuO and its in-plane lattice constants were kept fixed, but the out-of-plane one was allowed to relax.

Our calculations cover the biaxial strain range ±2.0%, since EuO is predicted to undergo a structural phase transition at large values of biaxial strain, which is beyond the scope of this work.[35] We confirmed the absence of a structural phase transition within our strain range by calculating the frequencies of both the zone center and the zone boundary phonon modes. Furthermore, high pressure (and with it the corresponding change in lattice parameter) leads to a fluctuating electron configuration between $4f^7 5d^0$ and $4f^6 5d^1$ in EuO and causes a downturn in T_C above 14 GPa.[36,37] The details of such dynamic fluctuations are beyond the reach of standard DFT+U calculations. The strain range we consider, however, is sufficiently far from both electron configuration and structural transitions such that our calculations should predict the correct trend of T_C.

In order to calculate the exchange constants precisely, we built 32 atom supercells for each biaxial strain value and fit energies of 8 different spin configurations to an Ising model. Calculations for cubic EuO indicated that 3rd and 4th nearest neighbor exchange couplings are negligible, so we ignored them in our calculations of EuO under biaxial strain. In order to get an estimate of T_C, we used a mean-field model. As expected from DFT and mean field approximations, T_C is grossly overestimated by our calculations;

further, T_C depends on the exact value of U chosen. As we are interested in the change in T_C with strain, in Figure 3-4 we present T_C / T_{C0}, i.e., the ratio of the Curie temperature under biaxial strain to that in bulk. The calculations were performed for a range of reasonable U values, the results of which are denoted with different colors and shapes in Figure 3-4. The calculated change in T_C for different U overlap well, indicating that the result is robust and physically meaningful. T_C decreases with increasing biaxial strain, which is consistent with Ref. 8.

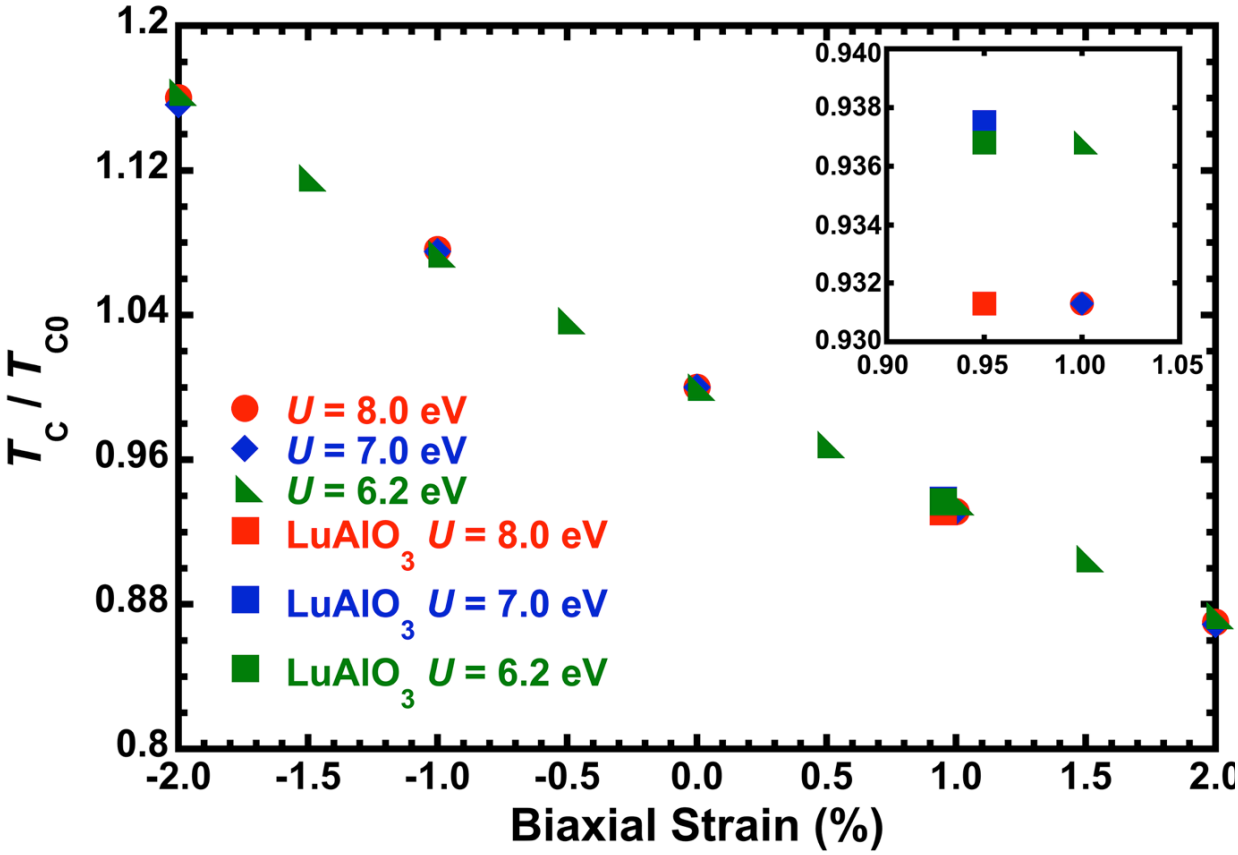

Figure 3-4: Calculated effect of biaxial strain on the T_C of EuO. The effect of changing the on-site Coulomb energy U in the density functional theory on the resulting T_C is shown by the colored data points. The squares represent the specific case of the biaxial strain imparted by a (110) $LuAlO_3$ substrate on a commensurate epitaxial (001) EuO film. The inset shows that the reduction in T_C for EuO films grown commensurately on $LuAlO_3$ is ~6%.

In order to explore the effect of the anisotropic strain induced by the (110) $LuAlO_3$ substrate (+0.4% and +1.5% along perpendicular in-plane directions in a commensurate (001) EuO film), we also calculated the exchange constants and the resultant T_C for the anisotropic boundary conditions corresponding specifically to $LuAlO_3$. The ratio of the resultant Curie temperature to that of bulk is presented as the squares at 0.95% strain in Figure 3-4. The fact that these squares lie in-line with other points, all calculated with isotropic in-plane biaxial strain, indicates that the anisotropy of the substrate surface does not lead to an important difference, and that T_C is decreased by the same amount as it would be on a substrate with an isotropic surface and the same average lattice constant. The calculated decrease in T_C for commensurate (001) EuO on (110) $LuAlO_3$ is about 6%, which corresponds to ~4 Kelvin with respect to bulk. We emphasize that our standard DFT calculations utilize periodic boundary conditions, corresponding to a film that is infinite in all dimensions, such that finite-size effects are not considered.

These calculations match, within the error bars, the T_C of the commensurate EuO / $LuAlO_3$ films that are unaffected by finite-size effects, that is, films thicker than 10 nm. Furthermore, the T_C of all commensurate EuO / $LuAlO_3$ films are consistently reduced relative to the T_C of the EuO / YSZ films. For example, a 1.5 nm EuO film on YSZ has a T_C of 56 ± 1 K, while a 1.5 nm EuO film on $LuAlO_3$ has a T_C of 53 ± 1 K. EuO / $LuAlO_3$ films thicker than 69 nm are partially relaxed and as the strain diminishes, the T_C recovers to that of bulk EuO (69 K). As the only difference between these films is the strain imparted by epitaxial misfit from the different substrates, the T_C reduction is attributed to the imposed biaxial tensile strain, which is in agreement with our

calculations and the literature.[8]

Figure 3-5(a) shows the onset of magnetization for a fully commensurate EuO film (10 nm thick) and a fully relaxed EuO film (170 nm thick) on $LuAlO_3$. The T_C of the 10 nm

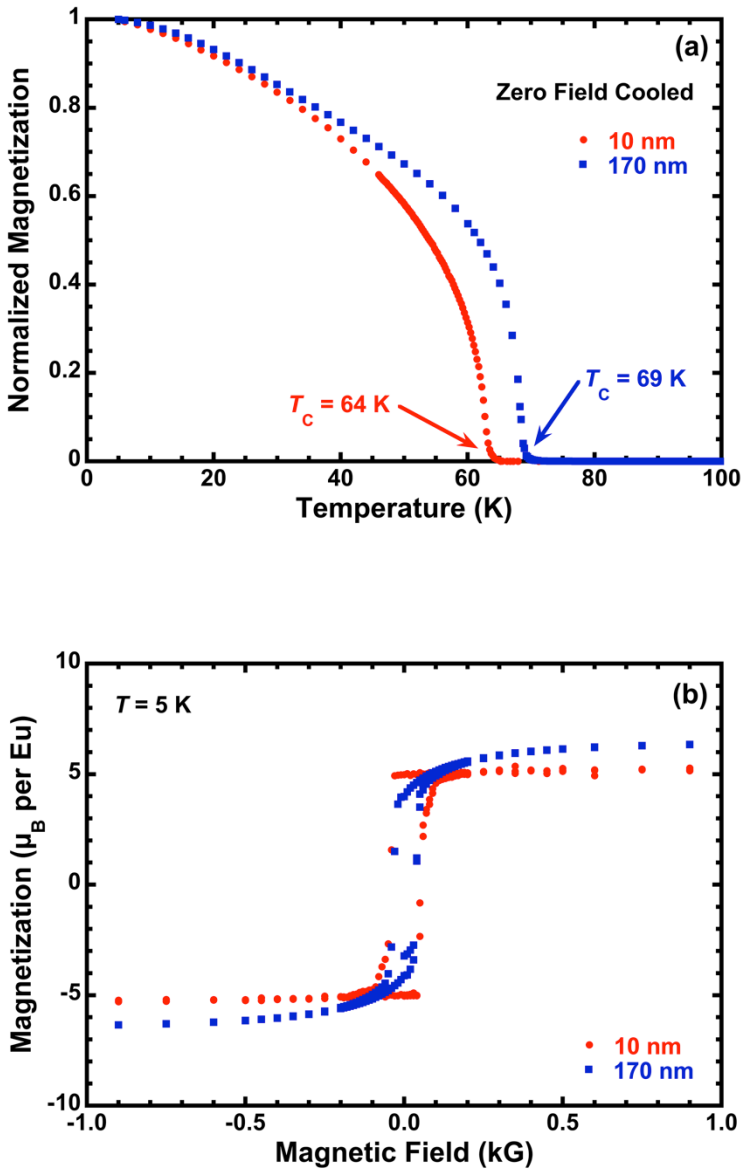

Figure 3-5: (a) Magnetization as a function of temperature measurements indicate a clear onset of magnetization in the absence of an applied magnetic field (Ref. 24)at 64 K in the 10 nm thick film and 69 K in the 170 nm thick film. (b) Magnetic hysteresis curves for the 10 nm and 170 nm thick EuO thin films.

thick film was 64 ± 1 K, and the T_C of the 170 nm thick film was 69 ± 1 K. This matches, within the error, the DFT calculations, which predict a 6% decrease in the T_C for the case of EuO / $LuAlO_3$. Figure 3-5(b) compares the magnetic hysteresis in the same films. The coercive field of the 10 nm thick sample was 55 ± 10 G, and the coercive field of the 170 nm thick sample was 47 ± 10 G. The saturation magnetization was 5.5 ± 0.2 μ_B per europium atom for the 10 nm thick film and 6.6 ± 0.2 μ_B per europium atom for the 170 nm thick film. These are both close to the theoretical maximum of 7 μ_B per europium atom and other reports of EuO thin films.[10,13,23] Though the effect of strain on the coercive field and saturation magnetization is likely non-zero, it is not significant and could not be determined in our experiment.

In conclusion EuO is shown to grow epitaxially on (110) $LuAlO_3$ substrates with an epitaxial orientation relationship of [110](001) EuO || [$1\bar{1}0$](110) $LuAlO_3$ and is commensurate below a critical thickness of 69 nm. The T_C of EuO / YSZ, which shows size effects for films thinner than 10 nm, was compared to the T_C of EuO / $LuAlO_3$. By comparing the T_C vs. thickness of unstrained EuO / YSZ with strained EuO / $LuAlO_3$, a reduction in T_C caused by the biaxial tensile strain is clearly observed, in addition to the reduction in T_C from size effects.

The work at Cornell was supported by the AFOSR (Grant No. FA9550-10-1-0123). The work in Augsburg was supported by the DFG (Grant No. TRR 80). AM gratefully acknowledges support from the NSF IGERT program (NSF Award DGE-0654193) and by the IMI Program of the National Science Foundation under Award No. DMR 0843934. T.B. And C.J.F. were supported by the DOE-BES # DE-SC0002334.

REFERENCES

[1] H. A. Eick, N. C. Baenziger, and L. Eyring, J. Am. Chem. Soc. **78**, 5147–5149 (1956).

[2] T. R. McGuire and M. W. Shafer, J. Appl. Phys. **35**, 984–988 (1964).

[3] G. Petrich, S. Von Molnár, and T. Penney, Phys. Rev. Lett. **26**, 885–888 (1971).

[4] A. Melville, T. Mairoser, A. Schmehl, D. E. Shai, E. J. Monkman, J. W. Harter, T. Heeg, B. Holländer, J. Schubert, K. M. Shen, J. Mannhart, and D. G. Schlom, Appl. Phys. Lett. **100**, 222101 (2012).

[5] S. Von Molnár, IBM J. Res. Dev. **14**, 269–275 (1970).

[6] P. Steeneken, L. Tjeng, I. Elfimov, G. Sawatzky, G. Ghiringhelli, N. Brookes, and D.-J. Huang, Phys. Rev. Lett. **88**, 047201 (2002).

[7] S. Methfessel, Z. Angew. Phys. **18**, 414–432 (1965).

[8] N. Ingle and I. Elfimov, Phys. Rev. B **77**, 121202 (2008).

[9] M. W. Shafer and T. R. McGuire, J. Appl. Phys. **39**, 588–590 (1968).

[10] A. Schmehl, V. Vaithyanathan, A. Herrnberger, S. Thiel, C. Richter, M. Liberati, T. Heeg, M. Röckerath, L. F. Kourkoutis, S. Mühlbauer, P. Böni, D. A. Muller, Y. Barash, J. Schubert, Y. Idzerda, J. Mannhart, and D. G. Schlom, Nat. Mater. **6**, 882–887 (2007).

[11] H. Miyazaki, H. J. Im, K. Terashima, S. Yagi, M. Kato, K. Soda, T. Ito, and S. Kimura, Appl. Phys. Lett. **96**, 232503 (2010).

[12] H. Ott, S. Heise, R. Sutarto, Z. Hu, C. Chang, H. Hsieh, H.-J. Lin, C. Chen, and L. Tjeng, Phys. Rev. B **73**, 094407 (2006).

[13] R. Sutarto, S. Altendorf, B. Coloru, M. Moretti Sala, T. Haupricht, C. Chang, Z. Hu, C. Schüßler-Langeheine, N. Hollmann, H. Kierspel, J. Mydosh, H. Hsieh, H.-J. Lin, C. Chen, and L. Tjeng, Phys. Rev. B **80**, 085308 (2009).

[14] T. Mairoser, A. Schmehl, A. Melville, T. Heeg, L. Canella, P. Böni, W. Zander, J. Schubert, D. Shai, E. Monkman, K. Shen, D. G. Schlom, and J. Mannhart, Phys. Rev. Lett. **105**, 257206 (2010).

[15] T. Mairoser, A. Schmehl, A. Melville, T. Heeg, W. Zander, J. Schubert, D. E. Shai, E. J. Monkman, K. M. Shen, T. Z. Regier, D. G. Schlom, and J. Mannhart, Appl. Phys. Lett. **98**, 102110 (2011).

[16] K. Y. Ahn and M. W. Shafer, J. Appl. Phys. **41**, 1260–1262 (1970).

[17] K. Lee and J. C. Suits, Phys. Lett. **34A**, 141–142 (1971).

[18] Y. Capiomont, N. V. Dang, O. Massenet, and B. K. Chakraverty, Solid State Commun. **10**, 679–683 (1972).

[19] T. R. McGuire, G. F. Petrich, B. L. Olson, V. L. Moruzzi, and K. Y. Ahn, J. Appl. Phys. **42**, 1775–1777 (1971).

[20] R. P. Ingel and D. Lewis III, J. Am. Ceram. Soc. **69**, 325–332 (1986).

[21] P. D. Dernier and R. G. Maines, Mater. Res. Bull. **6**, 433–440 (1971).

[22] R. Sutarto, S. Altendorf, B. Coloru, M. Moretti Sala, T. Haupricht, C. Chang, Z. Hu, C. Schüßler-Langeheine, N. Hollmann, H. Kierspel, H. Hsieh, H.-J. Lin, C. Chen, and L. Tjeng, Phys. Rev. B **79**, 205318 (2009).

[23] R. W. Ulbricht, A. Schmehl, T. Heeg, J. Schubert, and D. G. Schlom, Appl. Phys. Lett. **93**, 102105 (2008).

[24] T. Mairoser, F. Loder, A. Melville, D. G. Schlom, and A. Schmehl, Phys. Rev. B **87**, 014416 (2013).

[25] Vipul Srivastava, Sanjay Bhajanker, and Sankar P. Sanyal, Phys. B Condens. Matter **406**, 2158–2162 (2011).

[26] A. R. Kortan, M. Hong, J. Kwo, J. P. Mannaerts, and N. Kopylov, Phys. Rev. B **60**, 10913–10918 (1999).

[27] C. Kim, I. K. Robinson, T. Spila, and J. E. Greene, J. Appl. Phys. **83**, 7608–7612 (1998).

[28] P. F. Miceli and C. J. Palmstrom, Phys. Rev. B B **51**, 5506–5509 (1995).

[29] R. Schiller and W. Nolting, Solid State Commun. **110**, 121–125 (1999).

[30] M. Müller, G.-X. Miao, and J. S. Moodera, J. Appl. Phys. **105**, 07C917 (2009).

[31] E. Negusse, J. Dvorak, J. S. Holroyd, M. Liberati, T. S. Santos, J. S. Moodera, E. Arenholz, and Y. U. Idzerda, J. Appl. Phys. **105**, 07C930 (2009).

[32] M. Barbagallo, T. Stollenwerk, J. Kroha, N. -J. Steinke, N. Hine, J. Cooper, C. Barnes, A. Ionescu, P. Monteiro, J. -Y. Kim, K. Ziebeck, C. Kinane, R. Dalgliesh, T. Charlton, and S. Langridge, Phys. Rev. B **84**, 075219 (2011).

[33] G. Kresse and J. Furthmüller, Phys. Rev. B **54**, 11169–11186 (1996).

[34] J. P. Perdew, K. Burke, and M. Ernzerhof, Phys. Rev. Lett. **77**, 3865–3868 (1996).

[35] E. Bousquet, N. A. Spaldin, and P. Ghosez, Phys. Rev. Lett. **104**, 037601 (2010).

[36] V. G. Tissen and E. G. Ponyatovskil, JETP Lett. **46**, 361–364 (1987).

[37] N. Souza-Neto, J. Zhao, E. Alp, G. Shen, S. Sinogeikin, G. Lapertot, and D. Haskel, Phys. Rev. Lett. **109**, 026403 (2012).

[38] C. Giacovazzo, H. L. Monaco, G. Artioli, D. Viterbo, G. Ferraric, G. Gilli, G. Zanotti, and M. Catti, *Fundamentals of Crystallography*, 2nd ed. (Oxford University Press, Oxford, 2002), p. 337.

CHAPTER 4

Epitaxial growth of europium monoxide on diamond

Originally submitted to Applied Physics Letters 2013

A. Melville,[1] T. Mairoser,[2] A. Schmehl,[2] M. Fischer,[3] S. Gsell,[3] M. Schreck,[3] D. D. Awschalom,[4] T. Heeg,[1] B. Holländer,[5] J. Schubert,[5] and D.G. Schlom[1,6]

[1]*Department of Materials Science and Engineering, Cornell University, Ithaca, New York 14853, USA*

[2]*Zentrum für elektronische Korrelationen und Magnetismus, Universität Augsburg, Universitätsstraße 1, 86159 Augsburg, Germany*

[3]*Institut für Physik, Universität Augsburg, D-86135 Augsburg, Germany*

[4]*Institute for Molecular Engineering, University of Chicago, Chicago, IL 60637, USA*

[5]*Peter Grünberg Institute, PGI9-IT, JARA-FIT, Research Centre Jülich, D-52425 Jülich, Germany*

[6]*Kavli Institute at Cornell for Nanoscale Science, Ithaca, New York, 14853, USA*

We report the epitaxial integration of phase-pure EuO on both single-crystal diamond and on epitaxial diamond films grown on silicon utilizing reactive molecular-beam epitaxy. The epitaxial orientation relationship is (001) EuO || (001) diamond and [110] EuO || [100] diamond. The EuO layer is nominally unstrained and ferromagnetic with a

transition temperature of 68 ± 2 K and a saturation magnetization of 5.5 ± 0.1 Bohr magnetons per europium ion on the single-crystal diamond, and a transition temperature of 67 ± 2 K and a saturation magnetization of 2.1 ± 0.1 Bohr magnetons per europium ion on the epitaxial diamond film.

Diamond has many desirable properties including high breakdown strength and unparalleled thermal conductivity.[1] This makes it a promising substrate for high power and high frequency applications. Furthermore, diamond doped with nitrogen contains nitrogen-vacancy impurity centers capable of accommodating a long-lived electron spin state, which can be optically excited as well as optically read-out.[2] As a result, diamond is capable of single-photon emissions from a specific spin state, making it a compelling platform for solid-state spin-based electronics at room temperature.[2]

Integrating this multipurpose substrate with functional oxide materials is a natural next step, as it can take advantage of the full range of properties found in oxide materials, e.g., high dielectric constant, ferroelectricity, ferromagnetism, and even oxides that are simultaneously ferroelectric and ferromagnetic.[3] To date oxide materials have been minimally integrated with diamond for use in surface acoustic wave devices,[4–6] or as a buffer layer for other oxide materials.[7] There has only been one report of the epitaxial growth of an oxide on diamond and that is (0001) ZnO on (111) diamond.[4] In this Letter we demonstrate the epitaxial integration of the ferromagnet EuO with (001) diamond single crystals and with epitaxial (001) diamond films on silicon.

Europium oxide (EuO) is a ferromagnetic semiconductor with a spin-polarization of at least 96%,[8,9] giving it the second highest spin-polarization of all known materials after CrO_2.[10] Furthermore, doped EuO has a metal-to-insulator transition (MIT) involving a change in resistivity of up to 13 orders of magnitude[11] and exhibits colossal magneto-resistance (CMR) up to 6 orders of magnitude.[12] The MIT and CMR occur around the

Curie temperature (T_C), which is 69 K in bulk EuO.[13] T_C can be enhanced dramatically by doping with trivalent cations[8,9,14–21] or by introducing oxygen vacancies (EuO_{1-x}).[22–25] Theorists predict that a T_C of ~200 K is possible by combining doping and compressive strain.[26]

The epitaxial integration of EuO with modern semiconductor materials, i.e., Si,[8,27] GaN,[8] and GaAs[28] has already been demonstrated. The lattice mismatch between (001) diamond and (001) EuO (~2%) corresponds to cube-on-cube growth where the EuO grows 45º rotated in-plane compared to the underlying diamond substrate. The diamond surface mesh is illustrated in the top left of Fig. 1, and the arrangement of EuO on diamond resulting in the ~2% lattice mismatch is illustrated in the top right of Fig. 1. This relatively small lattice mismatch compares favorably to the lattice mismatch between EuO and Si, GaN, or GaAs. As the lattice constant of diamond is smaller than that of EuO, a commensurate EuO film on diamond (if it could be achieved) would be in biaxial compression and an enhancement of T_C from 69 K to ~80 K would be expected in undoped EuO from first-principles calculations.[29] Thus, the epitaxial integration of EuO with diamond could potentially result in coherently strained EuO films exhibiting a higher T_C than epitaxial EuO films grown on Si,[8,27] GaN,[8] and GaAs,[28] while still allowing favorable substrate qualities such as long spin lifetimes for injected electrons[30] or a long-lived electron spin state.[2]

10 mm x 10 mm epitaxial (001)-oriented diamond films were grown by CVD on (001) Si utilizing iridium metal and yttria-stabilized zirconia (YSZ) buffer layers;[31]

5 mm × 5 mm × 1 mm diamond single crystals grown by CVD with (001) surfaces were obtained commercially.[32] The EuO thin films on the epitaxial diamond films were grown in a Veeco 930 molecular-beam epitaxy (MBE) system, and the EuO thin films on single-crystal diamond were grown in a Veeco Gen10 MBE system. A cryoshroud cooled with liquid nitrogen was employed in both MBE chambers to reduce the chamber background pressure to less than 1×10^{-8} Torr. EuO films on both types of (001) diamond substrates were grown via reactive oxide MBE in an adsorption-controlled growth regime[33] to ensure high crystalline quality and stoichiometric films. The europium flux, measured by a quartz crystal microbalance, was set to 1.1×10^{14} atoms/ (cm^2•s). This flux was roughly double that of the EuO film growth rate, as determined by measuring the areal density of europium atoms in calibration EuO samples using Rutherford backscattering spectrometry (RBS), ensuring an overabundance of europium during growth. Under such conditions the EuO growth rate is limited by the oxygen flux.[33] The oxygen flux was established by flowing oxygen through a piezoelectric leak valve set at a constant voltage. This resulted in a slight increase in the background pressure during growth that increased gradually over time, but was never more than 1×10^{-8} Torr. After growth the films were capped with ~100 nm of aluminum or ~20 nm of amorphous silicon to prevent further oxidation of the EuO films and enable their *ex situ* characterization. Structural characterization was performed after growth using four-circle X-ray diffraction (XRD) and X-ray reflectivity utilizing Cu K_α radiation. Magnetic properties and the Curie temperature were determined using superconducting quantum interference device (SQUID) magnetometry.

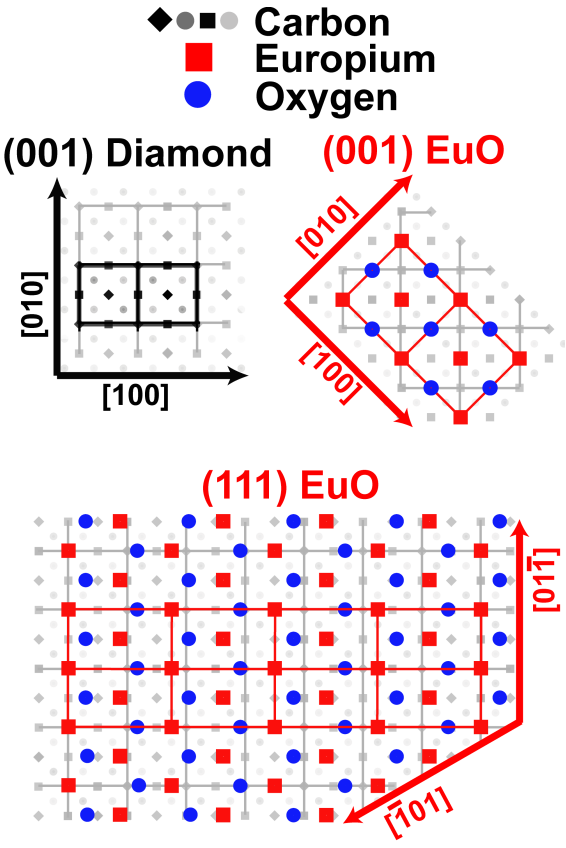

Figure 4-1: Diagram showing the epitaxial orientation relationship between the surface mesh of the (001) EuO film and underlying (001) diamond substrate. The top left image is the diamond surface mesh with two unit cells highlighted. The top right image corresponds to the epitaxial alignment of EuO on diamond corresponding to ~2% lattice mismatch, with two EuO unit cells highlighted. This orientation relationship is (001)[110] EuO || (001)[100] diamond and corresponds to a σ_{EuO} 1 : $\sigma_{diamond}$ 2 interface. The bottom image corresponds to the epitaxial alignment of EuO on diamond with less strain, but with a near-coincident site lattice, with four EuO unit cells highlighted. Here, the epitaxial alignment is (111)[01$\bar{1}$] EuO || (001)[010] diamond. This corresponds to a σ_{EuO} 4 : $\sigma_{diamond}$ 7 interface.

For the growth of EuO on epitaxial diamond films with a diamond surface mesh as shown in the upper left of Figure 4-1, the EuO grew with two epitaxial orientations under growth conditions similar to those used to grow high-quality EuO on $YAlO_3$ (T = 590 ºC).[33] The dominant orientation as determined by XRD measurements was (111) EuO || (001) diamond with [01$\bar{1}$] EuO || [010] diamond as illustrated in the bottom image of Figure 4-1, and the secondary orientation was (001) EuO || (001) diamond also

with [110] EuO || [100] diamond as illustrated in the top right image of Figure 4-1.

The optimal growth conditions for growing (001)-oriented EuO on epitaxial diamond films was achieved by first growing two monolayers to establish the orientation at lower growth temperatures (350 ºC < *T* < 400 ºC). Once the orientation was seeded, the growth temperature was ramped up to 650 ºC (while continuing growth) for better crystallinity. In this case, only the orientation relationship (001)[110] EuO || (001)[100] diamond was found as illustrated in the top right of Figure 4-1. This relatively low starting temperature was established as the lower limit of the adsorption-controlled growth regime by depositing europium in the absence of oxygen on a hot substrate for an hour and confirming absence of an accumulation layer of europium by RBS.

For the growth of EuO on the single-crystal diamond, the EuO also grew with two epitaxial orientations with a dominant orientation as determined by XRD measurements of (111) EuO || (001) diamond with [01$\bar{1}$] EuO || [010] diamond under the adsorption-controlled growth conditions similar to those used to grow high-quality (001) EuO on (110) $YAlO_3$ (*T* = 590 ºC).[33] In contrast to growths on the epitaxial diamond films, however, films grown at lower growth temperatures (*T* < 590 ºC) on single-crystal diamonds were almost exclusively composed of the epitaxial orientation of (111) EuO || (001) diamond with [01$\bar{1}$] EuO || [010] diamond. The optimal growth conditions for growing (001) EuO on single-crystal diamond was to grow at higher growth temperatures (*T* = 760 ºC), where only the orientation relationship (001)[110] EuO || (001)[100] diamond was found.

The difference in EuO growth conditions could be related to differences in structural perfection of the epitaxial diamond film vs. single-crystal diamond (diamond film 004 peak FWHM of 0.2° as compared to the single-crystal diamond 004 peak FWHM of 0.005°) or the difference in surface roughness (R_{RMS}(diamond film) = 13.3 nm as compared to R_{RMS}(single-crystal diamond) = 1 nm).

Epitaxial orientation relationships that change with growth temperature have been seen in other oxide systems, e.g., in the epitaxial growth of $YBa_2Ca_3O_{7-\delta}$ on yttria-stabilized zirconia (YSZ).[34–36] In that system the out-of-plane orientation relationship, (001) $YBa_2Cu_3O_7$ || (001) YSZ, was found to remain constant, while the in-plane orientation relationship was observed to change with growth temperature.[36] At low substrate temperature the dominant in-plane epitaxial orientation relationship observed was [100] $YBa_2Ca_3O_{7-\delta}$ || [100] YSZ while films deposited at high temperature had [110] $YBa_2Ca_3O_{7-\delta}$ || [100] YSZ.[36]

The (111) EuO || (001) diamond orientation has a slightly lower mismatch, +1.8% for $[2\bar{1}\bar{1}]$ EuO || [100] diamond and -2.1% for $[01\bar{1}]$ EuO || [010] diamond, than the expected (001) EuO || (001) diamond orientation, which has a lattice mismatch of -2.1% for both [110] EuO || [100] diamond and $[\bar{1}10]$ EuO || [010] diamond. Although better lattice matched, the (111) EuO || (001) diamond orientation has a larger near-coincident site surface mesh cell corresponding to a Coincident Site Lattice / Displacement Shift Complete (CSL/DSC) model[37] interface of σ_{EuO} 4 : $\sigma_{diamond}$ 7 as shown at the bottom of Figure 4-1. And though films with the better lattice-matched orientation are epitaxial, the

(111) EuO is undesirable, as it contains four distinct in-plane twin variants, resulting in a multitude of twin boundaries. The (001) EuO || (001) diamond orientation is preferred as there is only one in-plane orientation and the films are free of twin boundaries. Furthermore, this latter orientation relationship has a coincident site lattice, corresponding to a CSL/DSC model interface of σ_{EuO} 1 : $\sigma_{diamond}$ 2 as shown at the top right of Figure 4-1.

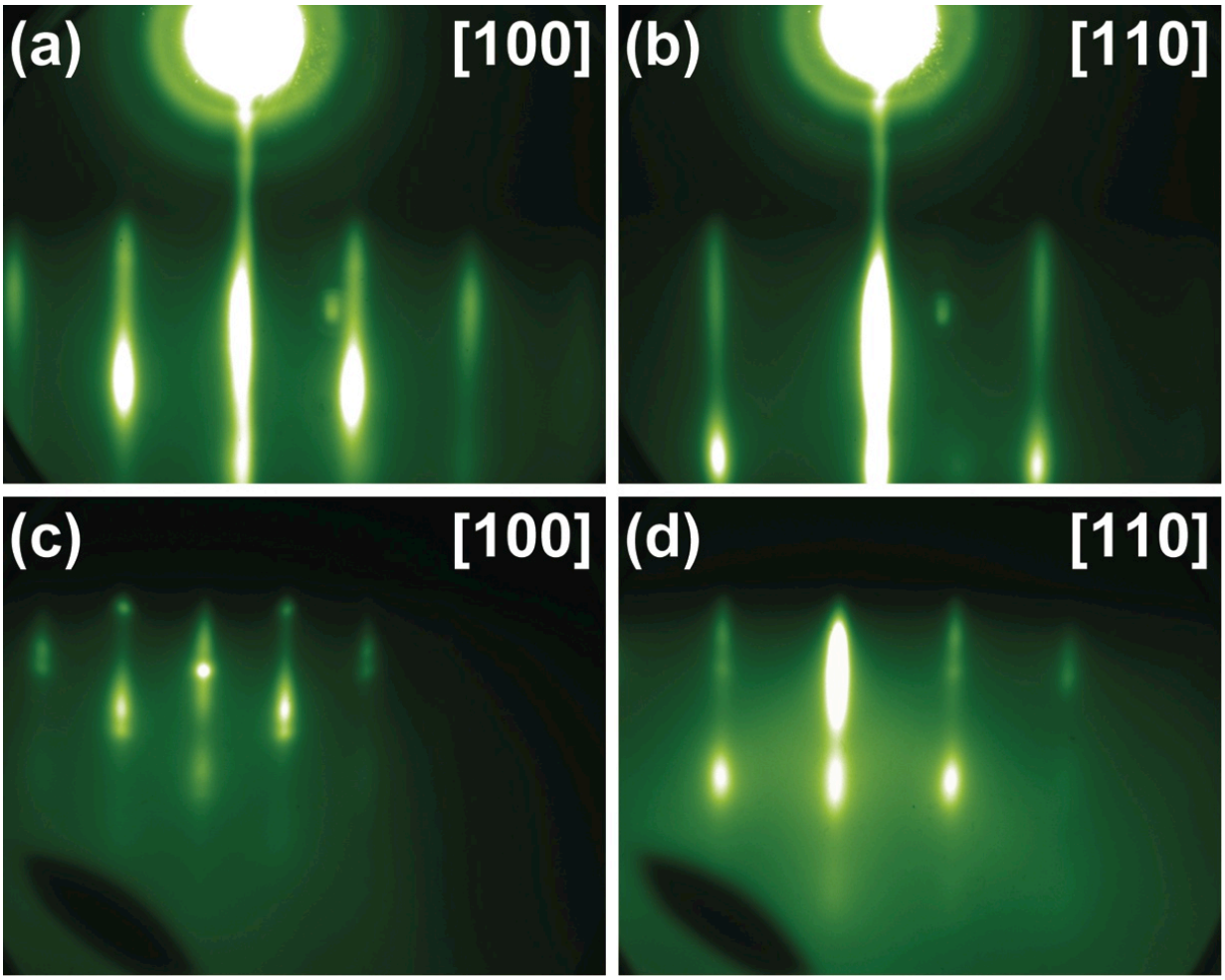

Figure 4-2: RHEED images of a 25 nm thick EuO film grown at 350 ºC < T_{sub} < 400 ºC for two monolayers then ramped to T_{sub} = 650 °C on an epitaxial diamond film along the (a) [100] azimuth and the (b) [110] azimuth. RHEED images of a 37 nm thick EuO film grown at T_{sub} = 760 °C on a single-crystal diamond along the (c) [100] azimuth and the (d) [110] azimuth.

Having established the optimal conditions for the growth of (001) EuO on both single-crystal diamond and on epitaxial diamond films, the remainder of the paper will focus on these (001) EuO films. Reflection high-energy electron diffraction (RHEED) images were taken of both types of EuO films. Figures 4-2(a) and 4-2(b) show the RHEED images with the incident electron beam along the [100] and [110] azimuths, respectively, of (001) EuO on the epitaxial diamond films, and Figures 4-2(c) and 4-2(d) show the RHEED images along the [100] and [110] azimuths, respectively, of (001) EuO on the single-crystal diamond. In all four cases, there is no evidence of other phases or orientations. The transmission diffraction pattern evident in the (001) EuO on single-crystal diamond (Figures 4-2(c) and 4-2(d)) suggest that the film is atomically rough.

The θ-2θ scans in Figures 4-3(a) and 4-3(b) reveal only 00ℓ EuO peaks and capping layer peaks, indicating that the films are single phase with the desired (001) EuO out-of-plane orientation. From calculations of the out-of-plane lattice constant expected for a commensurate (2.1% biaxial compression) EuO film on diamond utilizing the elastic coefficients of EuO,[38] we expected an out-of-plane lattice constant of c = 5.188 Å as compared to the bulk-value of c = 5.141 Å.[39]

Nelson-Riley analysis[40] on the 002, 004, and 006 EuO peaks on the epitaxial diamond film, however, yields c = 5.137 ± 0.001 Å, and Nelson-Riley analysis on the 002, 004, and 006 EuO peaks on single-crystal diamond yields c = 5.135 ± 0.001 Å. Our epitaxial (001) EuO films are clearly not commensurate. The reduced out-of-plane spacing from

Figure 4-3: (a) A θ-2θ scan of the same 25 nm thick EuO film grown on an epitaxial diamond film as shown in Figures 4-2(a) and 4-2(b) reveals phase-pure EuO with only an (001) out-of-plane orientation. (b) A θ-2θ scan of the same 37 nm thick EuO film grown on a single-crystal diamond as shown in Figures 4-2(c) and 4-2(d) reveals phase-pure EuO with only an (001) out-of-plane orientation. There is no indication of europium metal or europium oxides with higher oxygen content in either film. (c) Rocking curve comparison between 002 EuO and 004 diamond of the same EuO film grown on an epitaxial diamond film as shown in Figure 4-3(a). (d) Rocking curve comparison between 002 EuO and 004 diamond of the same EuO film grown on a single-crystal diamond as shown in Figure 4-3(b).

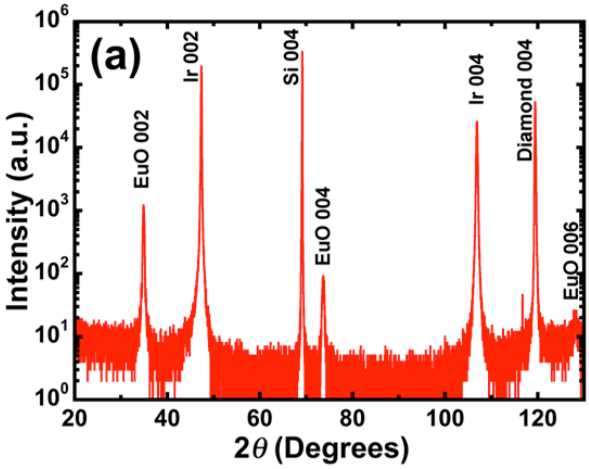
(a)
Intensity (a.u.)
2θ (Degrees)
EuO 002
Ir 002
Si 004
EuO 004
Ir 004
Diamond 004
EuO 006

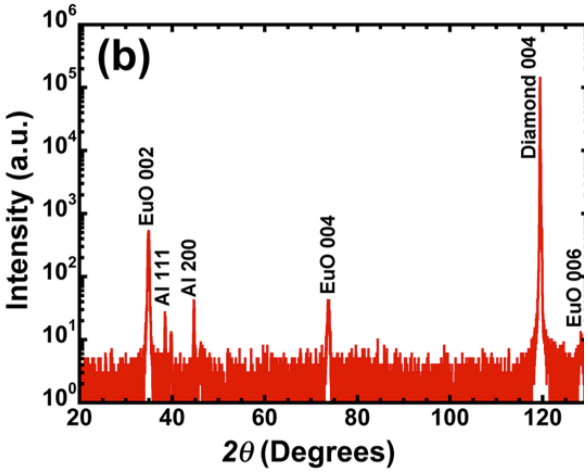
(b)
Intensity (a.u.)
2θ (Degrees)
EuO 002
Al 111
Al 200
EuO 004
Diamond 004
EuO 006

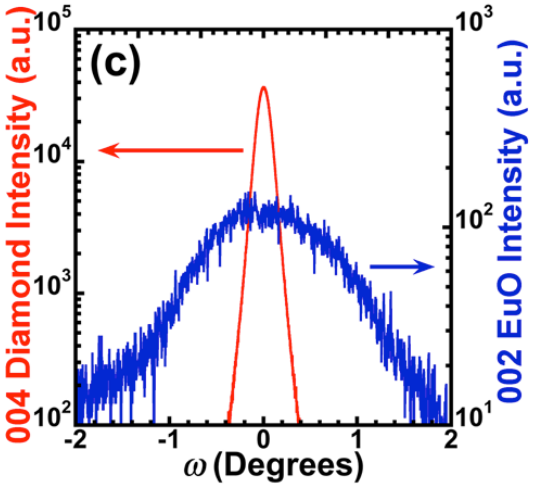
(c)
004 Diamond Intensity (a.u.)
002 EuO Intensity (a.u.)
ω (Degrees)

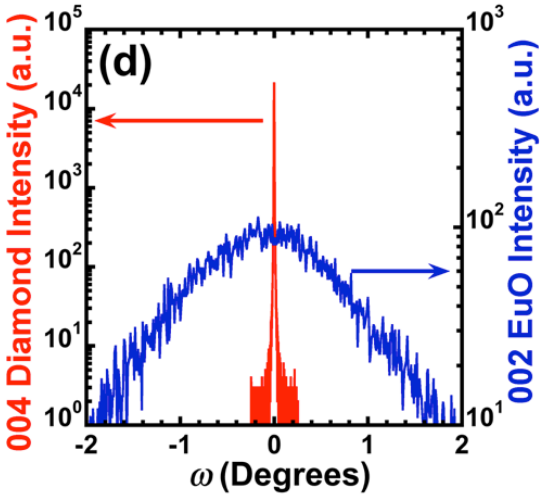
(d)
004 Diamond Intensity (a.u.)
002 EuO Intensity (a.u.)
ω (Degrees)

that of bulk EuO indicates that the films are under slight biaxial tensile strain, likely due to thermal strain imparted during cooling after growth due to the much larger linear thermal expansion coefficient of EuO compared to that of the single-crystal diamond and silicon substrates over relevant temperatures.[41–43]

Rocking curve measurements of the film and underlying substrate were compared using the EuO 002 peak and diamond 004 peak. For the EuO on the epitaxial diamond film, Figure 4-3(c), the EuO 002 peak has a full width at half-maximum (FWHM) of 1.2° in omega compared to the diamond 004 peak FWHM of 0.17°. For the EuO on single-crystal diamond, Figure 4-3(d), the EuO 002 peak has a FWHM of 1.8° in omega compared to the diamond 004 peak FWHM of 0.005°. The large EuO peak FWHM further suggests that the films contain high densities of dislocations and are therefore not commensurate with the underlying substrates. Since the films were not commensurately strained, we could not test the prediction of an enhanced T_C in compressively strained EuO.[26]

Figure 4-4(a) shows ∅-scans of the 111 Si, 111 Ir, 111 diamond, and 222 EuO peaks of the EuO film on the epitaxial diamond film. As expected the diamond, iridium, YSZ, and silicon layers are arranged cube-on-cube with (001)[100] diamond || (001)[100] Ir || (001)[100] YSZ || (001)[100] Si.[31] EuO is also arranged cube-on-cube, but rotated 45° with respect to the underlying diamond film as discussed earlier. The 45° rotation is denoted by the displacement of the four 222 peaks of EuO relative to the four 111 diamond peaks. The YSZ layer could not be resolved by XRD due to its small thickness

Figure 4-4: (a) Azimuthal ∅-scans of the same 25 nm thick EuO film grown on an epitaxial diamond film as shown in Figure 4-3(a) for the 111 Si, 111 Ir, 111 diamond, and 222 EuO diffraction peaks at χ= 54.7°, where χ = 0° aligns the diffraction vector perpendicular to the plane of the substrate. ∅ = 0° corresponds to the in-plane component of the diffraction vector aligned parallel to the [100] direction of the (001) EuO film. The scans are offset for clarity. The positions of the phi peaks indicate that the orientation relationship between the layers is (001)[110] EuO || (001)[100] diamond || (001)[100] Ir || (001)[100] Si. (b) An atomic model illustrates the orientation relationship between all components in the heterostructure. (c) Azimuthal ∅-scans of the same 37 nm thick EuO film grown on a single-crystal diamond as shown in Fig. 3(b) for the 111 diamond and 111 EuO diffraction peaks at χ= 54.7º. The scans are offset for clarity. The positions of the phi peaks indicate that the orientation relationship between the layers is (001)[110] EuO || (001)[100] diamond.

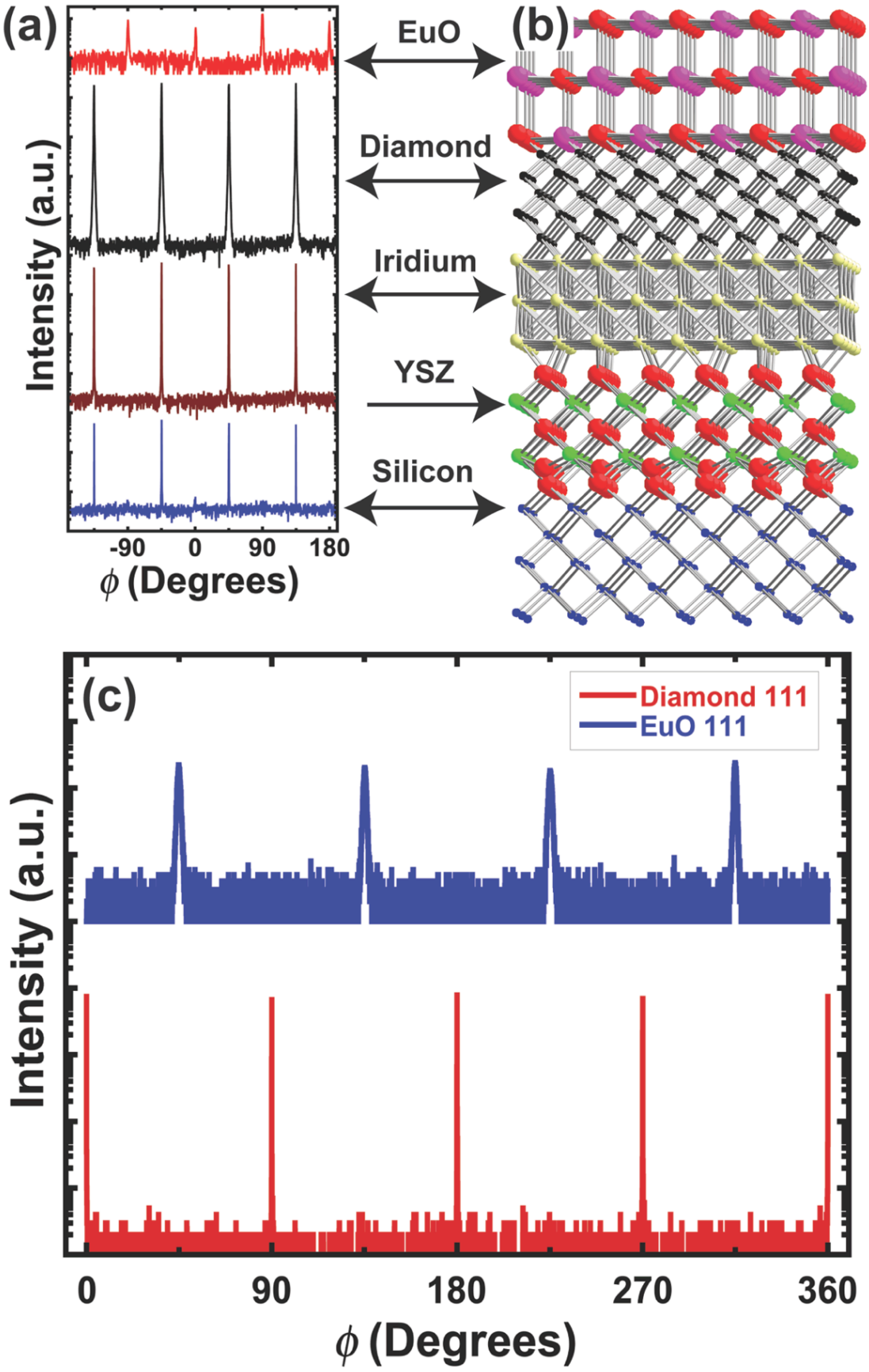
(a)
Intensity (a.u.)
-90
0
90
180
ϕ (Degrees)
EuO
Diamond
Iridium
YSZ
Silicon
(b)
(c)
Diamond 111
EuO 111
Intensity (a.u.)
0
90
180
270
360
ϕ (Degrees)

of just 20 nm. Together the θ-2θ scan and ∅-scans indicate an epitaxial film of EuO on diamond with an orientation relationship of (001)[110] EuO || (001)[100] diamond. A schematic depicting the orientation relationship between the layers in this epitaxial heterostructure is shown in Figure 4-4(b).

Figure 4-4(c) shows ∅-scans of the 111 EuO and 111 diamond reflections of the EuO on single-crystal diamond. EuO is arranged cube-on-cube, again rotated 45° with respect to the underlying diamond. The 45° rotation is denoted by the displacement of the four 111 peaks of EuO relative to the four 111 diamond peaks. Together the θ-2θ scan and ∅-scans indicate an epitaxial film of EuO on diamond with an orientation relationship of (001)[110] EuO || (001)[100] diamond. The d-spacing of the (110) EuO plane was d_{110} = 3.647 ± 0.003 Å, as calculated from the measured θ-2θ positions of multiple reflections from the (111) EuO planes. This value is larger than the bulk value (d_{110} = 3.635 Å),[39] providing further evidence that the film is under tensile strain as a result of the lattice mismatch being relaxed at the high growth temperature. The observed tensile strain, 0.3 ± 0.08 %, is expected to reduce the T_C of EuO by about 1.5 K according to first-principles calculations.[29]

Magnetic measurements were performed in zero applied field and the Curie temperature was determined from the derivative of the magnetization with respect to temperature.[44] The T_C was found to be 67 ± 2 K for EuO grown on the epitaxial diamond film (Figure 4-5(a)) and 68 ± 2 K for EuO grown on the single-crystal diamond (Figure 4-5(b)), which is within experimental error of the expected Curie temperature of EuO given

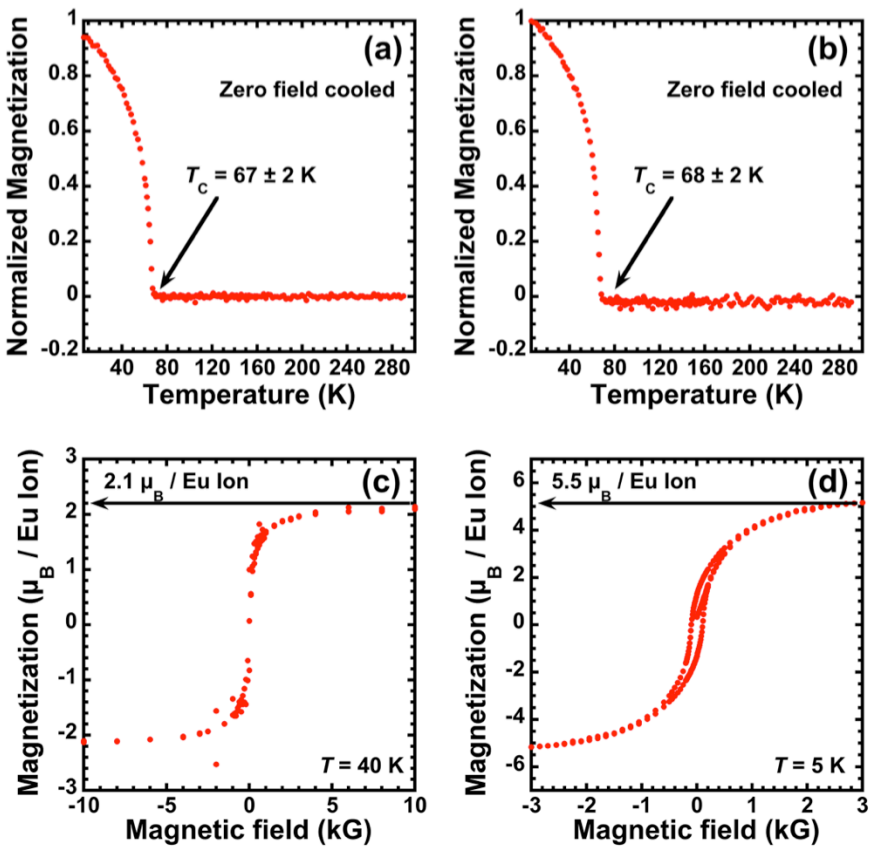

Figure 4-5: Magnetization as a function of temperature of (a) the same 25 nm thick EuO film grown on an epitaxial diamond film as shown in Figure 4-3(a) revealing a T_C of 67 ± 2 K and (b) the same 37 nm thick EuO film grown on a single-crystal diamond as shown in Figure 4-3(b) revealing a T_C of 68 ± 2 K. (c) Magnetic hysteresis measurements show that the same 25 nm thick EuO film grown on epitaxial diamond film as shown in Figure 4-3(a) is ferromagnetic with a coercive field of 50 ± 50 Gauss and a saturation magnetization of 2.1 ± 0.1 Bohr magnetons per europium ion at 40 K. (d) Magnetic hysteresis measurements show that the same 37 nm thick EuO film grown on single-crystal diamond as shown in Figure 4-3(b) is ferromagnetic with a coercive field of 105 ± 10 Gauss and a saturation magnetization of 5.5 ± 0.1 Bohr magnetons per europium ion at 5 K.

the slight T_C shift from the observed tensile strain.[26,29] Magnetic hysteresis of the films reveals a saturation magnetization of 2.1 ± 0.1 μ_B per europium ion and a coercive field of 50 ± 50 G at 40 K for the EuO grown on the epitaxial diamond film (Figure 4-5(c)) and a saturation magnetization of 5.5 ± 0.1 μ_B per europium ion and a coercive field of 105 ± 10 G at 5 K for the EuO grown on single-crystal diamond (Figure 4-5(d)). At 5 K,

the EuO grown on the epitaxial diamond film has a maximum magnetization at 30,000 G of 3.7 ± 0.1 μ_B per europium ion. These values are considerably lower than the 6.9 μ_B per europium ion found in bulk EuO and in high-quality EuO epitaxial films,[8,9,17,28,33,39] and is indicative of our films on diamond not yet being the quality of epitaxial EuO films grown on $YAlO_3$,[8,33] $LuAlO_3$,[29] Si,[8] and GaAs.[28]

In summary, the epitaxial integration of ferromagnetic EuO on epitaxial diamond films and single-crystal diamond was achieved. The epitaxy of the EuO film on (001) diamond exhibited a temperature-dependent orientation as seen in other heteroepitaxy oxide systems. The magnetic hysteresis and Curie temperature of epitaxial EuO films on diamond are comparable to those of bulk EuO.[13] Although the growth conditions used yielded relaxed EuO films, the predicted enhancement of T_C by compressive strain[26] motivates the achievement of commensurate EuO films on diamond – a challenge for future studies.

The work at Cornell and at the Institute for Molecular Engineering at the University of Chicago was supported by the AFOSR (Grant No. FA9550-10-1-0123). The work in Augsburg was supported by the DFG (Grant No. TRR 80) and the EC (oxIDes). AJM gratefully acknowledges support from the NSF IGERT program (NSF Award DGE-0654193). This work was performed in part at the Cornell NanoScale Facility, a member of the National Nanotechnology Infrastructure Network, which is supported by the National Science Foundation (Grant ECCS-0335765).

REFERENCES

[1] Y. Gurbuz, O. Esame, I. Tekin, W. Kang, and J. Davidson, Solid-State Electron. **49**, 1055-1070 (2005).

[2] D. D. Awschalom, R. J. Epstein, and R. Hanson, Sci. Am. **297**, 84-91 (2007).

[3] J. H. Lee, L. Fang, E. Vlahos, X. Ke, Y. W. Jung, L. F. Kourkoutis, J.-W. Kim, P. J. Ryan, T. Heeg, M. Roeckerath, V. Goian, M. Bernhagen, R. Uecker, P. C. Hammel, K. M. Rabe, S. Kamba, J. Schubert, J. W. Freeland, D. A. Muller, C. J. Fennie, P. Schiffer, V. Gopalan, E. Johnston-Halperin, and D. G. Schlom, Nature **466**, 954-958 (2010).

[4] A. Hachigo, H. Nakahata, K. Higaki, S. Fujii, and S.-I. Shikata, Appl. Phys. Lett. **65**, 2556-2558 (1994).

[5] H. Lam, J. Cryst. Growth **268**, 144-148 (2004).

[6] J. J. Chen, F. Zeng, D. M. Li, J. B. Niu, and F. Pan, Thin Solid Films **485**, 257-261 (2005).

[7] S. M. Lee, H. Murakami, and T. Ito, Appl. Surf. Sci. **175-176**, 517-524 (2001).

[8] A. Schmehl, V. Vaithyanathan, A. Herrnberger, S. Thiel, C. Richter, M. Liberati, T. Heeg, M. Röckerath, L. F. Kourkoutis, S. Mühlbauer, P. Böni, D. A. Muller, Y. Barash, J. Schubert, Y. Idzerda, J. Mannhart, and D. G. Schlom, Nat. Mater. **6**, 882-887 (2007).

[9] A. Melville, T. Mairoser, A. Schmehl, D. E. Shai, E. J. Monkman, J. W. Harter, T. Heeg, B. Holländer, J. Schubert, K. M. Shen, J. Mannhart, and D. G. Schlom, Appl. Phys. Lett. **100**, 222101 (2012).

[10] A. Anguelouch, A. Gupta, Gang Xiao, D. Abraham, Y. Ji, S. Ingvarsson, and C. Chien, Phys. Rev. B **64**, 180408 (2001).

[11] G. Petrich, S. von Molnár, and T. Penney, Phys. Rev. Lett. **26**, 885–888 (1971).

[12] Y. Shapira, S. Foner, and T. B. Reed, Phys. Rev. B **8**, 2299 (1973).

[13] T. R. McGuire and M. W. Shafer, J. Appl. Phys. **35**, 984–988 (1964).

[14] K. Y. Ahn, Appl. Phys. Lett. **17**, 347-349 (1970).

[15] K. Lee and J. C. Suits, Phys. Lett. **34A**, 141-142 (1971).

[16] K. Lee and J. C. Suits, IEEE Trans. Magn. **7**, 391 (1971).

[17] R. Sutarto, S. Altendorf, B. Coloru, M. Moretti Sala, T. Haupricht, C. Chang, Z. Hu, C. Schüßler-Langeheine, N. Hollmann, H. Kierspel, J. Mydosh, H. Hsieh, H.-J. Lin, C. Chen, and L. Tjeng, Phys. Rev. B **80**, 085308 (2009).

[18] H. Miyazaki, H. J. Im, K. Terashima, S. Yagi, M. Kato, K. Soda, T. Ito, and S. Kimura, Appl. Phys. Lett. **96**, 232503 (2010).

[19] T. Mairoser, A. Schmehl, A. Melville, T. Heeg, L. Canella, P. Böni, W. Zander, J. Schubert, D. Shai, E. Monkman, K. Shen, D. G. Schlom, and J. Mannhart, Phys. Rev. Lett. **105**, 257206 (2010).

[20] T. Mairoser, A. Schmehl, A. Melville, T. Heeg, W. Zander, J. Schubert, D. E. Shai, E. J. Monkman, K. M. Shen, T. Z. Regier, D. G. Schlom, and J. Mannhart, Appl. Phys. Lett. **98**, 102110 (2011).

[21] P. Liu, J. Tang, J. A. Colón Santana, K. D. Belashchenko, and P. A. Dowben, J. Appl. Phys. **109**, 07C311 (2011).

[22] K. Y. Ahn and M. W. Shafer, J. Appl. Phys. **41**, 1260-1262 (1970).

[23] M. W. Shafer, J. B. Torrance, and T. Penney, J. Phys. Chem. Solids **33**, 2251–2266 (1972).

[24] C. Llinares, J. P. Desfours, J. P. Nadai, C. Godart, A. Percheron, and J. C. Achard, Phys. Status Solidi A **25**, 185-192 (1974).

[25] M. Barbagallo, N. Hine, J. Cooper, N.-J. Steinke, A. Ionescu, C. Barnes, C. Kinane, R. Dalgliesh, T. Charlton, and S. Langridge, Phys. Rev. B **81**, 235216 (2010).

[26] N. Ingle and I. Elfimov, Phys. Rev. B **77**, 121202 (2008).

[27] J. Lettieri, V. Vaithyanathan, S. K. Eah, J. Stephens, V. Sih, D. D. Awschalom, J. Levy, and D. G. Schlom, Appl. Phys. Lett. **83**, 975-977 (2003).

[28] A. G. Swartz, J. Ciraldo, J. J. I. Wong, Y. Li, W. Han, T. Lin, S. Mack, J. Shi, D. D. Awschalom, and R. K. Kawakami, Appl. Phys. Lett. **97**, 112509 (2010).

[29] A. Melville, T. Mairoser, A. Schmehl, T. Birol, T. Heeg, B. Holländer, J. Schubert, C. J. Fennie, and D. G. Schlom, Appl. Phys. Lett. **102**, 062404 (2013).

[30] G. Balasubramanian, P. Neumann, D. Twitchen, M. Markham, R. Kolesov, N. Mizuochi, J. Isoya, J. Achard, J. Beck, J. Tissler, V. Jacques, P. R. Hemmer, F. Jelezko, and J. Wrachtrup, Nat. Mater. **8**, 383–387 (2009).

[31] S. Gsell, T. Bauer, J. Goldfuß, M. Schreck, and B. Stritzker, Appl. Phys. Lett. **84**, 4541-4543 (2004).

[32] Element Six N.V., Cuijk,The Netherlands

[33] R. W. Ulbricht, A. Schmehl, T. Heeg, J. Schubert, and D. G. Schlom, Appl. Phys. Lett. **93**, 102105 (2008).

[34] D. K. Fork, S. M. Garrison, M. Hawley, and T. H. Geballe, J. Mater. Res. **7**, 1641-1651 (1992).

[35] J. A. Alarco, G. Brorsson, G. Ivanov, P. Nilsson, E. Olsson, and M. Löfgren, Appl. Phys. Lett. **61**, 723-725 (1992).

[36] S. M. Garrison, N. Newman, F. Cole, K. Char, and R. W. Barton, Appl. Phys. Lett. **58**, 2168-2170 (1991).

[37] R. W. Balluffi, A. Brokman, and A. H. King, Acta Metall. **30**, 1453-1470 (1982).

[38] Y. Shapira and T. B. Reed, AIP Conf. Proc. **5**, 837-839 (1972).

[39] B. T. Matthias, R. M. Bozorth, and J. H. Van Vleck, Phys. Rev. Lett. **7**, 160–161 (1961).

[40] J. B. Nelson and D. P. Riley, Proc. Phys. Soc. **57**, 160-178 (1945).

[41] G. A. Slack and S. F. Bartram, J. Appl. Phys. **46**, 89-98 (1975).

[42] D. Taylor, Trans. J. Br. Ceram. Soc. **83**, 5-9 (1984).

[43] For the growth of EuO on epitaxial diamond film substrates, the thermal expansion mismatch between EuO and silicon would lead to an in-plane tensile strain of 0.6% and an out-of-plane lattice spacing of 5.127 Å for the 25 ºC XRD measurement, assuming that the EuO film is fully relaxed at growth temperature. Using the same assumptions for the growth of EuO on single crystal diamond substrates, the thermal expansion mismatch between EuO and single-crystal diamond would lead to an in-plane tensile strain of 0.7% and an out-of-plane lattice spacing of 5.123 Å for the 25 ºC XRD measurement. The measured out-of-plane lattice spacings (5.137 Å and 5.135 Å, respectively) implies that the EuO film was not fully relaxed at the growth temperature, but was clamped during cooling. Alternatively, the film was fully relaxed at the growth temperature, but not fully clamped to the substrate during cooling.

[44] T. Mairoser, F. Loder, A. Melville, D. G. Schlom, and A. Schmehl, Phys. Rev. B **87**, 014416 (2013).

CHAPTER 5

PROTECTIVE AMORPHOUS Eu_2O_3 BARRIER FOR EUO THIN FILMS

Originally submitted to Thin Film Science 2014

A. Melville,[1] T. Mairoser,[2] A. Schmehl,[2] J. A. Mundy,[3] D. A. Muller,[3,4] T. Heeg,[1] B. Holländer,[5] J. Schubert,[5] and D.G. Schlom[1,4]

[1]*Department of Materials Science and Engineering, Cornell University, Ithaca, New York 14853, USA*

[2]*Zentrum für elektronische Korrelation und Magnetismus, Universität Augsburg, Universitätsstraße 1, 86159 Augsburg, Germany*

[3]*School of Applied and Engineering Physics, Cornell University, Ithaca, New York 14853, USA*

[4]*Kavli Institute at Cornell for Nanoscale Science, Ithaca, New York, 14853, USA*

[5]*Peter Grünberg Institute, PGI9-IT, JARA-FIT, Research Centre Jülich, Germany*

The efficacy of a Eu_2O_3 capping layer was examined for its ability to protect undoped EuO thin films. After exposing the heterostructure to water under conditions typical for lithographic patterning, the structural, chemical, and magnetic properties of the EuO thin film and Eu_2O_3 capping layer were investigated by structural, chemical, and magnetic techniques. The EuO film remains highly crystalline after the exposure, despite the incomplete conversion of EuO to Eu_2O_3. Importantly, the magnetic properties of EuO

are unaffected by the Eu_2O_3 capping layer, indicating that forming a protective Eu_2O_3 overlayer after growth is effective in maintaining the properties of EuO.

The fantastic and in many ways unparalleled properties of europium oxide (EuO) have been investigated since its discovery as a ferromagnetic semiconductor in 1961 (Ref. 1) with a Curie temperature (T_C) of 69 K.[2] It was found that the T_C can be enhanced by doping with trivalent cations[3–10] or by introducing oxygen vacancies (EuO_{1-x}).[11–14] Theorists predict a maximum T_C of about 200 K by combining doping and compressive strain.[15] In 1971, a metal-to-insulator transition (MIT) was demonstrated in non-stoichiometric or doped EuO to change the resistivity by more than 13 orders of magnitude.[16] The MIT is caused when the EuO becomes ferromagnetic, resulting in the conduction band splitting by 0.6 eV and excess electrons in the system flow into the conduction band.[17] The large spin-splitting of the conduction band means that EuO is nearly fully spin-polarized;[17] transport measurements reveal its spin polarization to be greater than 96%.[18,19] Moreover, epitaxial integration of EuO with modern semiconductor materials has already been demonstrated.[18,20–23]

Unfortunately, the instability of europium monoxide (EuO) has precluded many characterization techniques in EuO thin films, since EuO reacts in air to form the paramagnetic Eu_2O_3 or Eu_3O_4 phases.[24] The reaction proceeds to different depths in different samples consuming several monolayers of EuO,[2,25–27] and in small samples, such as thin films and powder, it could create an oxidized region of Eu^{3+} that could penetrate the entire volume.[28] This is a significant problem for probing the surface of EuO, as it decomposes to Eu_2O_3 or Eu_3O_4 before the EuO can be characterized. Furthermore, several quantitative measurement techniques rely upon a known volume of the EuO layer. Since the extent of decomposition of EuO is unknown, the margin of

error for these calculations is unknown and could vary wildly from sample to sample.

The solution for thin films fabricated in vacuum is either simply to conduct the experiment in vacuum if possible,[17,29–31] or to apply a protective "capping" film on top of the EuO. Eu_2O_3 was an obvious choice since it is a common precursor for the growth of EuO by sputtering or evaporation.[5,11,32] It is, furthermore, not magnetic or conducting, making it useful for both probing the magnetic properties and electronic properties of the underlying EuO film. Although Eu_2O_3 as a deliberate capping layer has been utilized in the past,[25,32–36] a thorough investigation of the structural properties has yet to be performed, and it is uncertain how well this buffer layer protects the underlying EuO films. In one report, films with a buffer layer of Eu_2O_3 degrade over a period of several days.[34] In other reports, the films are stable under "wet air" conditions for more than 20 hours up to 200ºC.[36] These studies did not comment, however, on the durability of these films when exposed to liquid water - a key component to common lithography techniques that are necessary for further characterization and utilization of EuO thin films.[8,9,18,19,37]

Other buffer layers have been explored, often with no comment on their effectiveness at preventing oxidation of the EuO film. Most commonly metals, such as aluminum,[20,38,39] titanium,[18] platinum,[40] , copper,[41] or silver,[41] have been employed, which also act as a convenient top electrode. MgF_2,[42,43] CaF_2,[44] Al_2O_3,[18,45] and silicon[8,9,18,19] have also been used to prevent oxidation, but are not conducting and offer varying degrees of optical transparency. These buffers can also be used, therefore, for

patterning the heterostructures for electronic characterization.[18,44]

In this Letter we characterize the efficacy of applying an Eu_2O_3 cap in the method described by Lee and Suits,[32] which may be able to protect the underlying EuO film from exposure to atmosphere and liquid water. Structural characterization of the Eu_2O_3 cap and determining its penetration depth into the EuO film was performed by four-circle X-ray diffraction (XRD) and X-ray reflectivity (XRR) utilizing Cu K_α radiation, and scanning transmission electron microscopy (STEM) in conjunction with electron energy loss spectroscopy (EELS). Atomic-resolution high angle annular dark field (HAADF) STEM images and EELS line scans were performed on a 200 keV FEI Technai F-20, with a 1.6 Å STEM probe size and an EELS energy resolution of 0.7 eV.

The cap's effectiveness at preventing further oxidation during lithographic processing, e.g., a rinse step used to remove residual photoresist, was simulated by submerging the sample in liquid water for three minutes before performing the structural characterization. No degradation was observed, so the magnetic properties of the films were then measured using superconducting quantum interference device (SQUID) magnetometry. SQUID measurements to determine T_C were made in zero applied field for all samples.[37]

The EuO films were grown in a Veeco Gen10 molecular-beam epitaxy chamber on single-crystalline (110) $YAlO_3$ substrates. The rectilinear surface mesh of $YAlO_3$ is slightly larger than that of EuO and imparts a +2% linear lattice mismatch to EuO, such

that only EuO films under 38 nm can be grown commensurately to the substrate.[46] All films were grown within an adsorption-controlled growth regime. The oxygen partial pressure corresponded to a vacuum chamber pressure of less than 1×10^{-8} Torr. The incident flux of europium atoms was calibrated to 5.5×10^{13} atoms / (cm^2•s) by a quartz crystal microbalance, 20% higher than the EuO growth rate, which had been determined earlier from areal density measurements of europium on calibration samples by Rutherford backscattering spectrometry (RBS). The overabundance of europium atoms prevents the oxidation of Eu^{2+} ions to Eu^{3+}, and the substrate temperature of 400ºC prevents the absorption of Eu metal. Two undoped films, ~30 nm and ~60 nm, were grown. After growth, the Eu_2O_3 cap was introduced by cooling the films in a vacuum chamber pressure of less than 1×10^{-8} Torr to below 200ºC, at which point the oxygen partial pressure was set to 1×10^{-7} Torr for 5 minutes in accordance with Ref. 47. The samples were then removed from the vacuum chamber for *ex situ* characterization.

The θ-2θ scan of the EuO thin films after exposure to water are shown in Figure 5-1(a). The nominally 30 nm and 60 nm thick EuO films exhibit only substrate peaks and 00ℓ EuO peaks, consistent with the phase-pure growth of EuO. There is no evidence of Eu_2O_3 or Eu_3O_4 peaks, suggesting that (a) the Eu_2O_3 cap was amorphous or not present, and (b) the EuO was not completely oxidized in atmospheric conditions or liquid water.

Rocking curves of the EuO 002 peak for the nominally 30 nm and 60 nm thick EuO films are shown in Figures 5-1(b) and (c), respectively, and are compared to the rocking

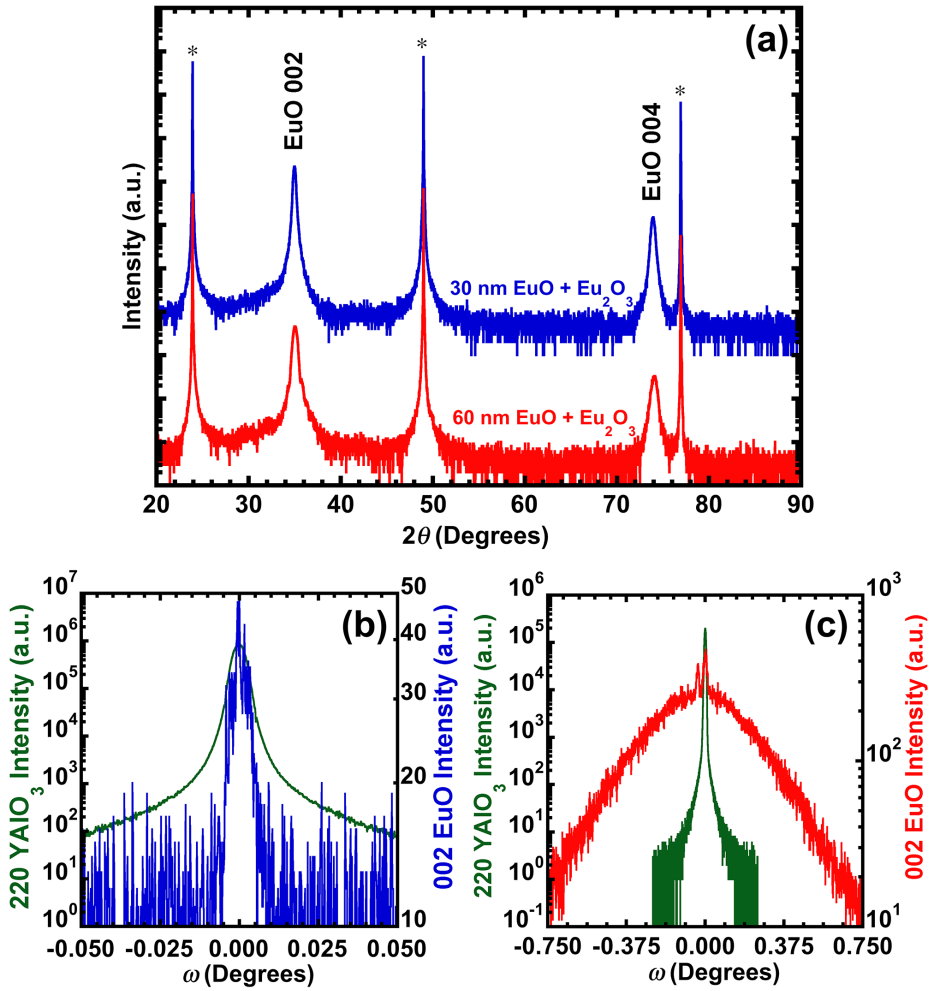

Figure 5-1: (a) XRD scans of the nominally 30 nm thick EuO film (blue) and the nominally 60 nm thick EuO film (red) after exposure to 3 minutes of running water. No Eu_2O_3 peaks or other impurity peaks are visible. (b) Rocking curve comparison between the 220 $YAlO_3$ substrate peak (FWHM = 30 arcseconds) and the 002 EuO peak (FWHM = 34 arcseconds) for the nominally 30 nm thick EuO film. (c) Rocking curve comparison between the 220 $YAlO_3$ substrate peak (FWHM = 30 arcseconds) and the 002 EuO peak (FWHM = 1050 arcseconds) for the nominally 60 nm thick EuO film.

of the corresponding $YAlO_3$ 220 substrate peak. Since the nominally 30 nm thick EuO film is thinner than the critical thickness of 38 nm, it is no surprise that the full-width half maximum (FWHM) of the EuO 002 peak rocking curve is 34 arcseconds, comparable to the 30 arcseconds FWHM of the substrate peak. On the other hand, the nominally 60 nm EuO film is thicker than the critical thickness and has a FWHM of 1050 arcseconds, compared to the 30 arcseconds FWHM of the substrate peak. The

30 nm thick EuO film is commensurate with the substrate, whereas the 60 nm thick EuO film is relaxed due to the formation of line defects to mediate the strain energy in crystals thicker than the critical thickness.[46,48–50] These additional dislocations in the thicker sample could act as fast diffusion channels to enhance oxygen diffusion into the film during the capping process.[51]

The thickness of the films was determined by XRR analysis for the nominally 30 nm thick EuO film and by HAADF-STEM imaging for the nominally 60 nm thick EuO film. XRR of the nominally 30 nm thick EuO film revealed ~15 nm of EuO and ~15 nm of Eu_2O_3. The HAADF images of the nominally 60 nm thick EuO film are shown in Figures 5-2(a) and (b) and show that the bottom ~15 nm of the EuO film is qualitatively different than the top 45 nm. The 15 nm thick bright region near the substrate interface is highly ordered down the zone axis, while the 45 nm dark region is not. Selected area diffraction (not pictured) in each of these regions confirms that the film in the bright region is crystalline, whereas the film in the dark region is amorphous as opposed to ordering along a different zone axis. In consideration of the XRD data, however, the 15 nm thick crystalline region most likely corresponds to the highly crystalline EuO and the 45 nm amorphous region most likely corresponds to the Eu_2O_3. The discrepancy in the thickness of the capping layers (despite identical growth conditions) is attributed to the superior film quality in the thinner film as denoted by the rocking curves.

The abundance of EuO and Eu_2O_3 in these regions could not be determined simply from XRD and HAADF-STEM images alone, so two distinct EELS fingerprints of the Eu-

Figure 5-2: (a) HAADF image of the nominally 60 nm thick EuO film showing the highly crystalline EuO beneath the ~45 nm thick mixed-phase region of amorphous Eu_2O_3 and EuO. (b) Zoomed in image of the same film in Figure 5-2(a) revealing a dark region at the substrate / film interface. An example EELS line map is also drawn on the image for reference. (c) EELS spectra for both the Eu^{2+} and Eu^{3+} signals at several points along the line shown in Figure 5-2(b). (d) Depth profile of the relative abundance of Eu^{2+} and Eu^{3+} cations as a function of position along the line shown in Figure 5-2(b), where 0 nm is within the substrate and 50 nm is within the capped region.

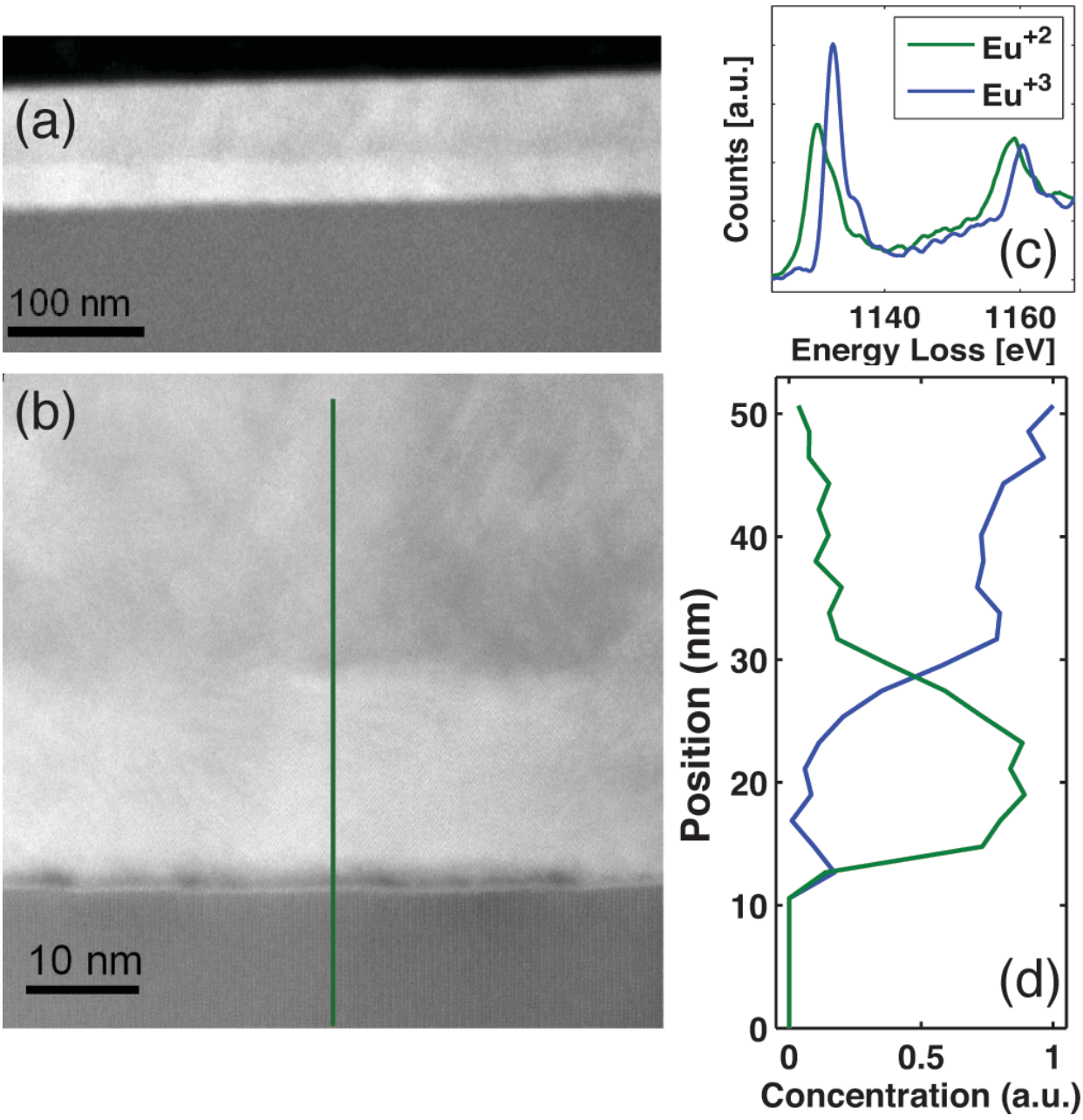
(a)
100 nm
(b)
10 nm
Eu+2
Eu+3
Counts [a.u.]
(c)
1140
1160
Energy Loss [eV]
Position (nm)
50
40
30
20
10
0
(d)
0
0.5
1
Concentration (a.u.)

$N_{4,5}$ edge, corresponding to a valence change in the Eu cation, were taken at several points along a line similar to the one drawn in Fig. 5-2(b). The EELS data are shown in Figures 5-2(c) and (d). These fingerprints were analyzed by multivariate curve resolution to extract the contribution of the Eu^{2+} signal (green) and the Eu^{3+} signal (blue) to determine the relative abundance of each valence, shown in Figure 5-2(d). The line profile denotes a strong Eu^{2+} signal beginning at the $YAlO_3$ interface and continuing ~15 nm along the line scan, whereas the Eu^{3+} signal is negligible (except briefly at the interface). At that point, the Eu^{2+} signal rapidly decreases and the Eu^{3+} signal rapidly increases for the remaining ~45 nm. The presence of Eu^{3+} and the lack of crystalline Eu_2O_3 peaks in the XRD confirm our suspicion that the dark region in HAADF corresponds to amorphous Eu_2O_3. In other words, the post-growth oxidation of EuO was successful in creating a capping layer of Eu_2O_3 at the surface. The concentration of Eu^{2+} does not drop to zero, however, suggesting that the post-growth oxidation did not fully oxidize the EuO, leaving EuO intermixed with the Eu_2O_3 cap.

Another dark region appears at intervals along the substrate interface (Figure 2(b)). Its location corresponds to the small uptick in Eu^{3+} in the EELS data. Unfortunately, the origin of this region of Eu_2O_3 at the interface could not be inferred from the data collected. The Eu_2O_3 may have been caused by a large fluctuation in the oxygen pressure at the surface of the substrate that is common at the beginning of growth. In the adsorption-controlled growth regime, higher oxidation states of Eu will form if the flux of oxygen locally exceeds the flux of Eu. This was not, however, observed in the identically grown (although commensurate) EuO / $YAlO_3$ film imaged in Ref. 52. The

Eu_2O_3 at the interface may also have been caused by a combination of (1) the high dislocation density of an EuO film that is thicker than the critical thickness, and (2) the post-growth oxidation. In this model, the oxygen reacted at the surface of the EuO film, but also diffused down the dislocations. Diffusion along dislocations was demonstrated to be several orders of magnitude faster than single-crystal diffusion in other rocksalt systems.[53–55] Given sufficient time, the oxygen would diffuse entirely down the EuO film, and then diffuse at the interface, which is another fast diffusion pathway.[56–58] The evidence would only appear at the interface boundary, since STEM scans columns of atoms and is insensitive to dislocations whose Berger vectors run parallel to the zone axis (e.g., along the beam direction). Future studies are necessary to determine the origin of the Eu_2O_3 at the substrate interface, and it is beyond the scope of this paper to discuss the possibility of oxygen diffusion along fast diffusion pathways in EuO.

Finally, the magnetic properties of the films were measured. Figure 5-3(a) illustrates that, as expected, both films have a Curie temperature of 69 K, within the error bars. Figure 5-3(b) shows the magnetic hysteresis and saturation magnetization taken at 5 K. Since the conversion of Eu^{2+} to Eu^{3+} appears to be incomplete above the highly crystalline EuO region, the total number of Eu ions in the film was considered, including the nonmagnetic Eu^{3+} within the capping layer. Thus, the saturation magnetization values appear depressed compared to the theoretical maximum of 7 μ_B / Eu ions because there is an uncertain volume of Eu_2O_3 within the capping layer that fails to contribute to the magnetic signal. The saturation magnetization was 4.0 ± 0.1 μ_B / Eu ion for the nominally 30 nm thick EuO film and 3.9 ± 0.1 μ_B / Eu ion for the nominally

60 nm thick EuO film, and the coercive field was 70 ± 10 G for the nominally 30 nm thick EuO film and 110 ± 10 G for the nominally 60 nm thick EuO film. The coercive fields are comparable to those found in other high-quality EuO thin films.[18,39,46,59] By fitting the magnetization to 7 μ_B / Eu ion and assuming that the first 15 nm in both films is 100% EuO, one can extract the percent conversion of magnetic EuO to nonmagnetic Eu_2O_3 in the capping layer. In the nominally 30 nm thick EuO sample, 87% of the EuO in the capping layer converted to Eu_2O_3, and in the nominally 60 nm thick EuO sample, 59% of the EuO in the capping layer converted to Eu_2O_3. The significant pipe diffusion in the thicker sample could be responsible for the limited transformation of EuO to Eu_2O_3 in the capping layer by allowing oxygen to bypass EuO in the capping layer and instead react deeper in the film.

Future work should analyze the effectiveness of the Eu_2O_3 capping layer for doped films, as several questions remain unanswered for that system. Uncertainty exists over whether or not the inclusion of rare-earth dopants would enhance the diffusion of oxygen in the sacrificial region. It is possible that the dopant-induced defects or local strain-fields would enhance oxygen diffusion, similar to the strain-induced line defects found in the incommensurate EuO case. Perhaps a dopant-free sacrificial region on top of the electroactive, doped EuO region is necessary. Furthermore, if there is increased oxygen diffusion near dopants, how would the T_C enhancement or dopant activity be affected?

In conclusion, the robustness of the Eu_2O_3 capping layer was investigated by structural,

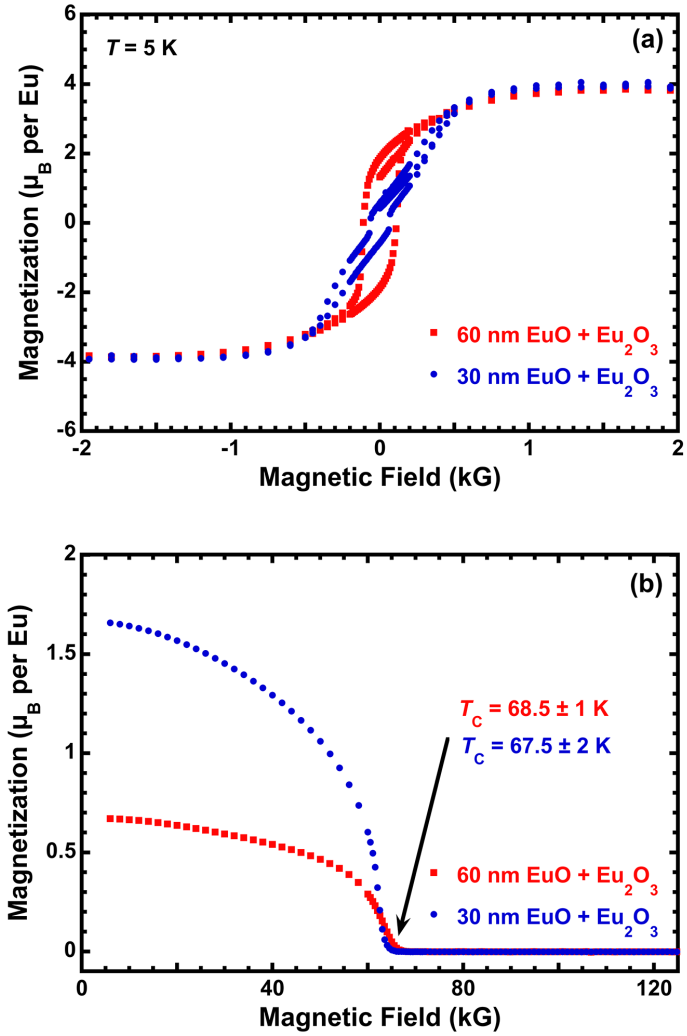

Figure 5-3: (a) Magnetization as a function of temperature of the same films from Figure 5-1 reveals a bulk-like T_C of 68.5 ± 1 K for the nominally 60 nm thick EuO film and 67.5 ± 2 K for the nominally 30 nm thick EuO film. (b) Magnetic hysteresis measurements at 5 K show that the same EuO films are ferromagnetic with a saturation magnetization of 3.9 ± 0.1 μ_B / Eu ion and a coercive field strength of 110 ± 10 Gauss for the nominally 60 nm thick EuO film and a saturation magnetization of 4.0 ± 0.1 μ_B / Eu ion and a coercive field strength of 70 ± 10 Gauss for the nominally 30 nm thick EuO film.

chemical, and magnetic analysis. Although the Eu_2O_3 layer was incomplete and amorphous, it was sufficient for protecting the underlying EuO film from exposure to liquid water under similar conditions to lithography processes. The magnetic data further confirms the incomplete Eu_2O_3 layer and the preservation of the EuO. Utilization of this

capping layer in thin films may be a poor choice for magnetic and electronic characterization, since unreacted EuO in the sacrificial layer interferes with the characterization of the EuO in the non-sacrificial layer. The problem is significantly reduced for bulk samples, where the passivation layer represents a small percentage of the overall sample volume.

The work at Cornell was supported by the AFOSR (Grant No. FA9550-10-1-0123). The work in Augsburg was supported by the DFG (Grant No. TRR 80) and the EC (oxIDes). This work made use of the electron microscopy facility of the Cornell Center for Materials Research (CCMR) with support from the National Science Foundation Materials Research Science and Engineering Centers (MRSEC) program (DMR 1120296) and NSF IMR-0417392. AJM gratefully acknowledges support from the NSF IGERT program (NSF Award DGE-0654193). J.A.M. acknowledges financial support from the Army Research Office in the form of a National Defense Science & Engineering Graduate Fellowship and from the National Science Foundation in the form of a graduate research fellowship. This work was performed in part at the Cornell NanoScale Facility, a member of the National Nanotechnology Infrastructure Network, which is supported by the National Science Foundation (Grant ECCS-0335765).

REFERENCES

[1] B. T. Matthias, R. M. Bozorth, and J. H. Van Vleck, Phys. Rev. Lett. **7**, 160–161 (1961).

[2] T. R. McGuire and M. W. Shafer, J. Appl. Phys. **35**, 984–988 (1964).

[3] K. Y. Ahn, Appl. Phys. Lett. **17**, 347–349 (1970).

[4] K. Lee and J. C. Suits, Phys. Lett. **34A**, 141–142 (1971).

[5] K. Lee and J. C. Suits, IEEE Trans. Magn. **7**, 391 (1971).

[6] R. Sutarto, S. Altendorf, B. Coloru, M. Moretti Sala, T. Haupricht, C. Chang, Z. Hu, C. Schüßler-Langeheine, N. Hollmann, H. Kierspel, J. Mydosh, H. Hsieh, H.-J. Lin, C. Chen, and L. Tjeng, Phys. Rev. B **80**, 085308 (2009).

[7] H. Miyazaki, H. J. Im, K. Terashima, S. Yagi, M. Kato, K. Soda, T. Ito, and S. Kimura, Appl. Phys. Lett. **96**, 232503 (2010).

[8] T. Mairoser, A. Schmehl, A. Melville, T. Heeg, L. Canella, P. Böni, W. Zander, J. Schubert, D. Shai, E. Monkman, K. Shen, D. G. Schlom, and J. Mannhart, Phys. Rev. Lett. **105**, 257206 (2010).

[9] T. Mairoser, A. Schmehl, A. Melville, T. Heeg, W. Zander, J. Schubert, D. E. Shai, E. J. Monkman, K. M. Shen, T. Z. Regier, D. G. Schlom, and J. Mannhart, Appl. Phys. Lett. **98**, 102110 (2011).

[10] P. Liu, J. Tang, J. A. Colón Santana, K. D. Belashchenko, and P. A. Dowben, J. Appl. Phys. **109**, 07C311 (2011).

[11] K. Y. Ahn and M. W. Shafer, J. Appl. Phys. **41**, 1260–1262 (1970).

[12] M. W. Shafer, J. B. Torrance, and T. Penney, J. Phys. Chem. Solids **33**, 2251–2266 (1972).

[13] C. Llinares, J. P. Desfours, J. P. Nadai, C. Godart, A. Percheron, and J. C. Achard, Phys. Status Solidi **25**, 185–192 (1974).

[14] M. Barbagallo, N. Hine, J. Cooper, N.-J. Steinke, A. Ionescu, C. Barnes, C. Kinane, R. Dalgliesh, T. Charlton, and S. Langridge, Phys. Rev. B **81**, 235216 (2010).

[15] N. Ingle and I. Elfimov, Phys. Rev. B **77**, 121202 (2008).

[16] G. Petrich, S. Von Molnár, and T. Penney, Phys. Rev. Lett. **26**, 885–888 (1971).

[17] P. Steeneken, L. Tjeng, I. Elfimov, G. Sawatzky, G. Ghiringhelli, N. Brookes, and D.-J. Huang, Phys. Rev. Lett. **88**, 047201 (2002).

[18] A. Schmehl, V. Vaithyanathan, A. Herrnberger, S. Thiel, C. Richter, M. Liberati, T. Heeg, M. Röckerath, L. F. Kourkoutis, S. Mühlbauer, P. Böni, D. A. Muller, Y. Barash, J. Schubert, Y. Idzerda, J. Mannhart, and D. G. Schlom, Nat. Mater. **6**, 882–887 (2007).

[19] A. Melville, T. Mairoser, A. Schmehl, D. E. Shai, E. J. Monkman, J. W. Harter, T. Heeg, B. Holländer, J. Schubert, K. M. Shen, J. Mannhart, and D. G. Schlom, Appl. Phys. Lett. **100**, 222101 (2012).

[20] J. Lettieri, V. Vaithyanathan, S. K. Eah, J. Stephens, V. Sih, D. D. Awschalom, J. Levy, and D. G. Schlom, Appl. Phys. Lett. **83**, 975–977 (2003).

[21] A. G. Swartz, J. Ciraldo, J. J. I. Wong, Y. Li, W. Han, T. Lin, S. Mack, J. Shi, D. D. Awschalom, and R. K. Kawakami, Appl. Phys. Lett. **97**, 112509 (2010).

[22] Adrian G Swartz, Patrick M Odenthal, Yufeng Hao, Rodney S Ruoff, and Roland K Kawakami, ACS Nano **6**, 10063–9 (2012).

[23] A. Melville, T. Mairoser, A. Schmehl, M. Fischer, S. Gsell, M. Schreck, D. D. Awschalom, T. Heeg, B. Holländer, J. Schubert, and D. G. Schlom, Appl. Phys. Lett. **103**, 222402 (2013).

[24] G. J. McCarthy, J. Am. Ceram. Soc. **57**, 502 (1974).

[25] K. Y. Ahn and J. C. Suits, IEEE Trans. Magn. **3**, 453–455 (1967).

[26] J. O. Dimmock, C. E. Hurwitz, and T. B. Reed, Appl. Phys. Lett. **14**, 49–51 (1969).

[27] K. Lee and J. C. Suits, J. Appl. Phys. **41**, 954–956 (1970).

[28] JW Coburn and K. Lee, J. Appl. Phys. **42**, 5903–5905 (1971).

[29] J. C. Suits and K. Y. Ahn, J. Appl. Phys. **39**, 570 (1968).

[30] H. Ott, S. Heise, R. Sutarto, Z. Hu, C. Chang, H. Hsieh, H.-J. Lin, C. Chen, and L. Tjeng, Phys. Rev. B **73**, 094407 (2006).

[31] D. E. Shai, A. Melville, J. W. Harter, E. J. Monkman, D. Shen, A. Schmehl, D. G. Schlom, and K. M. Shen, Phys. Rev. Lett. **108**, 267003 (2012).

[32] K. Lee and J. C. Suits, IBM Tech. Discl. Bull. **71**, 2337 (1971).

[33] K. Y. Ahn and G. S. Almasi, IEEE Trans. Magn. **5**, 944–949 (1969).

[34] K. Y. Ahn, J. Appl. Phys. **40**, 3193–3195 (1969).

[35] G. S. Almasi and K. Y. Ahn, J. Appl. Phys. **41**, 1258–1259 (1970).

[36] G. Street, IEEE Trans. Magn. **8**, 45–47 (1972).

[37] T. Mairoser, F. Loder, A. Melville, D. G. Schlom, and A. Schmehl, Phys. Rev. B **87**, 014416 (2013).

[38] M. Müller, G.-X. Miao, and J. S. Moodera, J. Appl. Phys. **105**, 07C917 (2009).

[39] R. Sutarto, S. Altendorf, B. Coloru, M. Moretti Sala, T. Haupricht, C. Chang, Z. Hu, C. Schüßler-Langeheine, N. Hollmann, H. Kierspel, H. Hsieh, H.-J. Lin, C. Chen, and L. Tjeng, Phys. Rev. B **79**, 205318 (2009).

[40] M. Barbagallo, T. Stollenwerk, J. Kroha, N.-J. Steinke, N. Hine, J. Cooper, C. Barnes, A. Ionescu, P. Monteiro, J.-Y. Kim, K. Ziebeck, C. Kinane, R. Dalgliesh, T. Charlton, and S. Langridge, Phys. Rev. B **84**, 075219 (2011).

[41] N. Iwata, G. Pindoria, T. Morishita, and K. Kohn, J. Phys. Soc. Japan **69**, 230–236 (2000).

[42] C. Paparoditis, R. Suryanarayanan, C. Llinares, E. Monteil, and G. Bordure, Solid State Commun. **9**, 1871–1876 (1971).

[43] O. Massenet, Y. Capiomont, and N. Van Dang, J. Appl. Phys. **45**, 3593–3599 (1974).

[44] Tetsuro Matsumoto, Katsuhiko Yamaguchi, Masatada Yuri, Kenji Kawaguchi, Naoto Koshizaki, and Koji Yamada, J. Phys. Condens. Matter **16**, 6017–6028 (2004).

[45] Tiffany Santos and Jagadeesh Moodera, Phys. Rev. B **69**, 241203 (2004).

[46] R. W. Ulbricht, a. Schmehl, T. Heeg, J. Schubert, and D. G. Schlom, Appl. Phys. Lett. **93**, 102105 (2008).

[47] S. M. Lee, H. Murakami, and T. Ito, Appl. Surf. Sci. **175-176**, 517–524 (2001).

[48] A. R. Kortan, M. Hong, J. Kwo, J. P. Mannaerts, and N. Kopylov, Phys. Rev. B **60**, 10913–10918 (1999).

[49] C. Kim, I. K. Robinson, T. Spila, and J. E. Greene, J. Appl. Phys. **83**, 7608–7612 (1998).

[50] P. F. Miceli and C. J. Palmstrom, Phys. Rev. B B **51**, 5506–5509 (1995).

[51] G. R. Love, Acta Met. **12**, 731–737 (1964).

[52] J. A. Mundy, D. Hodash, A. Melville, R. Held, T. Mairoser, D. A. Muller, L. F. Kourkoutis, A. Schmehl, and D. G. Schlom, Arxiv arXiv:1308.0967 (2013).

[53] A. Atkinson and R. I. Taylor, Philos. Mag. A **39**, 581–595 (1979).

[54] I. Sakaguchi, H. Yurimoto, and S. Sueno, Solid State Commun. **84**, 889–893 (1992).

[55] M. Legros, G. Dehm, E. Arzt, and T. J. Balk, Science (80-.). **319**, 1646–1649 (2008).

[56] M. Liberatore and B. J. Wuensch, Mater. Res. Soc. Symp. Proc. **357**, 357–393 (1995).

[57] Y. Oishi, K. Ando, H. Kurokawa, and Y. Hiro, J. Am. Ceram. Soc. Ceram. Soc. C60–C62 (1983).

[58] A. Atkinson and R. I. Taylor, J. Mater. Sci. **13**, 427–432 (1978).

[59] A. Melville, T. Mairoser, A. Schmehl, T. Birol, T. Heeg, B. Holländer, J. Schubert, C. J. Fennie, and D. G. Schlom, Appl. Phys. Lett. **102**, 062404 (2013).

CHAPTER 6

CONCLUSIONS AND FUTURE DIRECTIONS

6.1 SUMMARY

This thesis has presented research findings investigating the relationship between the structure and composition of EuO and its magnetic and electronic properties. It utilizes an adsorption-controlled growth method to fabricate ultra-high quality EuO samples by molecular-beam epitaxy. The aims of this thesis are three-fold. First, it looks at and compares the effect on the electronic and magnetic properties of EuO using magnetic and non-magnetic trivalent cations. Second, it explores the effect of biaxial strain on the magnetic properties of EuO, experimenting with tensile strain via $LuAlO_3$ substrates and with compressive strain via diamond substrates. Finally, a capping method that utilizes a sacrificial EuO layer in order to form a protective Eu_2O_3 capping layer was examined for its effectiveness at protecting the underlying EuO thin film from water and atmosphere.

In Chapter 2, the addition of a novel dopant cation, Lu^{3+}, was examined for its role in enhancing the T_C and altering the electronic properties of EuO. In a film with 5% Lu-doping, the T_C was found to be 119 K. The MIT occurred across the elevated T_C, but the resistivity changed only by a single order of magnitude. These effects were similar to the effects of doping EuO by 5% with Gd^{3+} or La^{3+}. Despite the lack of magnetism in the Lu^{3+} dopant, the 5% Lu-doped EuO thin film had a spin-polarization of 96%, the highest value reported for EuO.

In Chapter 3, the effect of biaxial tensile strain imparted from a novel substrate, $LuAlO_3$, was examined for its role in reducing the T_C of EuO as predicted by theoretical calculations. This experiment removed all other possible sources of a reduced T_C (e.g., size effects) by comparing a series of identical EuO thin films with varying thickness for both unstrained EuO, grown on YSZ substrates (0.0% strain), and inhomogeneously strained EuO, grown on $LuAlO_3$ substrates (+1.0% strain). The reduction in T_C for inhomogeneous strain was also calculated for EuO. A reduced T_C was observed for unstrained EuO / YSZ thinner than 10 nm, corresponding to the reduced magnetism expected in such ultrathin ferromagnetic samples. A greater reduction in T_C was observed for strained EuO / $LuAlO_3$ thinner than 20 nm, indicating that the difference in T_C must have been caused by the imparted biaxial strain. Furthermore, the reduction in T_C matched the calculated value. This experiment additionally discovered that the critical thickness for EuO / $LuAlO_3$ was 69 nm, and that relaxation for these films occurs simultaneously in both directions, despite the difference in strain along perpendicular directions.

In Chapter 4, this thesis attempted to elucidate the effect of biaxial compressive strain on the magnetic properties of EuO. Epitaxial EuO films were grown for the first time on both single-crystal diamond substrates and diamond films on silicon. The orientation of the EuO crystal on diamond depended heavily on substrate temperature during growth, and differed between the single-crystal diamond and the thin film diamond. The (001) orientation was stabilized and its growth optimized for both substrates. The rocking

curves and in-plane lattice constants of the EuO on both types of substrates indicated that the EuO was not compressively strained, most likely due to a combination of defects in the film and a large thermal expansion coefficient mismatch between EuO and these substrates. The T_C of EuO was unaffected by the substrates, remaining, within error, the bulk value of 69 K. The saturation magnetization, however, was affected by film quality, being reduced in both the EuO grown on single-crystal diamonds and also the EuO grown on diamond films.

In Chapter 5, a procedure for transforming the upper monolayers of EuO into a protective Eu_2O_3 capping layer was optimized and examined. The Eu_2O_3-capped EuO thin films endured exposure of the heterostructure to both water and atmosphere to confirm the effectiveness of the capping layer. Following these tests, the thin films were examined by STEM and XRD to confirm that EuO remained. Significant differences were discovered in the diffusion depth of oxygen into the EuO during the Eu_2O_3 capping procedure between commensurate thin films and relaxed thin films. The oxygen diffused deeper in relaxed thin films, conceivably along the stress-related defects that were present in much higher concentration than in the commensurate thin films. As a result, the conversion of EuO to Eu_2O_3 at the surface of the thin films was lower in the relaxed films. In both cases, the Eu_2O_3 capping layer was rather effective at preventing the annihilation of EuO via oxidation or hydroxylation, and magnetic measurements of both cases confirmed the presence of high quality EuO. The lack of a thorough conversion and absence of an abrupt EuO / Eu_2O_3 interface may, however, pose a challenge for effectively analyzing the magnetic properties, given the presence of EuO in the capping

layer and an uncertainty in the EuO thin film volume.

6.2 Future Directions

The future direction for research investigating EuO is clear. Although this work made significant progress in the field of EuO, it generated more questions than it answered.

Though the choice of dopant ions was investigated, more work remains. For example, there is insufficient knowledge of the solubility limits for different dopants, or the optimal dopant material and doping level. The existence of inactive dopants has been discovered, but its origins remains a mystery. Solving this mystery requires the same high-quality EuO found in this thesis, as well as a significant devotion of resources toward identifying the physical origin of the inactive dopants (e.g., defects, dopant segregation). Moreover, only rare-earth dopants were explored in this thesis, but trivalent cations exist in the transition metals and the other elements. How do these dopants, with huge variations in ionic size and electronic structure, affect the magnetic and electronic properties of EuO?

In the work on straining EuO, the obvious future direction is successfully applying compressive biaxial strain to EuO. One may consider using an as-of-yet undiscovered substrate that imparts less strain than the diamond substrates used in this thesis. Also, choosing an oxide substrate would effectively remove the disparity in thermal expansion coefficients, as well as provide an ionic surface for improved chemical compatibility at the surface. Another direction to explore is pushing the strain to higher values, such as

the +5% strain or -4% strain predicted to generate ferroelectricity in EuO.[1] Thus far, preliminary evidence suggests that radical changes in growth dynamics may be necessary to impart such large strains in EuO, but the existence of a ferromagnetic ferroelectric rocksalt is tremendously alluring and well-worth the effort.

Finally, the effect of simultaneously doping and straining EuO has neither been explored nor optimized. The combination will most likely enhance the T_C to values even higher than by any single method. Is it even possible to impart such large strains while simultaneously doping up to 16%? This is one of the most exciting future directions for EuO, as it is the most likely to thrust EuO into the realm of practical application.

REFERENCES

[1] E. Bousquet, N. A. Spaldin, and P. Ghosez, Phys. Rev. Lett. **104**, 037601 (2010).